ผลของพอลิออกซิล 40 ไฮโดรเจเนเทดคาสเตอร์ออยล์ต่อการก่อรูปเพลเลตที่ใช้ซิลิคอนไดออกไซด์เป็นสารช่วยอัดรีดและทำให้เป็นทรงกลม

นายสรรเพชญ ลิมปโกมล

วิทยานิพนธ์นี้เป็นส่วนหนึ่งของการศึกษาตามหลักสูตรปริญญาเภสัชศาสตรดุษฎีบัณฑิต
สาขาวิชาเภสัชกรรม ภาควิชาวิทยาการเภสัชกรรมและเภสัชอุตสาหกรรม
คณะเภสัชศาสตร์ จุฬาลงกรณ์มหาวิทยาลัย
ปีการศึกษา 2559

EFFECT OF POLYOXYL 40 HYDROGENATED CASTOR OIL ON PELLET FORMATION USING SILICON DIOXIDE AS AN EXTRUSION-SPHERONIZATION AID

Mr. Sanpeth Limpakomon

A Dissertation Submitted in Partial Fulfillment of the Requirements
for the Degree of Doctor of Philosophy Program in Pharmaceutics
Department of Pharmaceutics and Industrial Pharmacy
Faculty of Pharmaceutical Sciences
Chulalongkorn University
Academic Year 2016

Thesis Title	EFFECT OF POLYOXYL 40 HYDROGENATED CASTOR OIL ON PELLET FORMATION USING SILICON DIOXIDE AS AN EXTRUSION-SPHERONIZATION AID
By	Mr. Sanpeth Limpakomon
Field of Study	Pharmaceutics
Thesis Advisor	Jittima Chatchawalsaisin, Ph.D.
Thesis Co-Advisor	Associate Professor Poj Kulvanich, Ph.D.

Accepted by the Faculty of Pharmaceutical Sciences, Chulalongkorn University in Partial Fulfillment of the Requirements for the Doctoral Degree

.....Dean of the Faculty of Pharmaceutical Sciences
(Assistant Professor Rungpetch Sakulbumrungsil, Ph.D.)

THESIS COMMITTEE

.....Chairman
(Associate Professor Parkpoom Tengamnuay, Ph.D.)

.....Thesis Advisor
(Jittima Chatchawalsaisin, Ph.D.)

.....Thesis Co-Advisor
(Associate Professor Poj Kulvanich, Ph.D.)

.....Examiner
(Assistant Professor Nontima Vardhanabhuti, Ph.D.)

.....Examiner
(Narueporn Sutanthavibul, Ph.D.)

.....External Examiner
(Associate Professor Tanasait Ngawhirunpat, Ph.D.)

สรรเพชญ ลิมปโกมล : ผลของพอลิออกซิล 40 ไฮโดรเจเนเทดคาสเตอร์ออยล์ต่อการก่อรูปเพลเลตที่ใช้ซิลิคอนไดออกไซด์เป็นสารช่วยอัดรีดและทำให้เป็นทรงกลม (EFFECT OF POLYOXYL 40 HYDROGENATED CASTOR OIL ON PELLET FORMATION USING SILICON DIOXIDE AS AN EXTRUSION-SPHERONIZATION AID) อ.ที่ปรึกษาวิทยานิพนธ์หลัก: อ. ภญ. ดร.จิตติมา ชัชวาลย์สายสินธ์, อ.ที่ปรึกษาวิทยานิพนธ์ร่วม: รศ. ภก. ดร.พจน์ กุลวานิช, 141 หน้า.

ซิลิคอนไดออกไซด์มีศักยภาพที่จะใช้เป็นสารช่วยอัดรีดและทำให้เป็นทรงกลม อย่างไรก็ตามจำเป็นต้องมีสารละลายของสารลดแรงตึงผิวเพื่อเป็นของเหลวยึดเกาะอยู่ในสูตรตำรับ ผลของสารลดแรงตึงผิวต่อการก่อรูปเพลเลตยังไม่เคยมีรายงานการศึกษามาก่อน วัตถุประสงค์ของการศึกษานี้คือเพื่อตรวจสอบผลของความเข้มข้นของพอลิออกซิล 40 ไฮโดรเจเนเทดคาสเตอร์ออยล์ซึ่งใช้เป็นสารลดแรงตึงผิวในสูตรตำรับเพลเลตของซิลิคอนไดออกไซด์ชนิดชอบน้ำ สูตรตำรับประกอบด้วยซิลิคอนไดออกไซด์และสารละลายของสารลดแรงตึงผิวในอัตราส่วน 1 ต่อ 2 โดยน้ำหนัก ศึกษาสมบัติของสารที่ใช้ในสูตรตำรับ เช่น ความตึงผิวและความหนืดของของเหลวยึดเกาะ ความสามารถของซิลิคอนไดออกไซด์ในการดูดและการยึดเกาะของเหลวรวมทั้งวิทยากระแสของมวลเปียก เป็นต้น และนำข้อมูลที่ได้ไปใช้ในการอธิบายพฤติกรรมการก่อรูปเพลเลต ผลการศึกษาพบว่าสูตรตำรับที่ใช้สารละลายของสารลดแรงตึงผิวความเข้มข้นร้อยละ 2.5 ให้เพลเลตที่มีรูปร่างกลมและมีปริมาณผลได้ของเพลเลตในขนาดเป้าหมาย (0.71 – 1.4 มิลลิเมตร) ซึ่งทำซ้ำได้ ความเข้มข้นของสารลดแรงตึงผิวที่ต่ำกว่าให้เพลเลตขนาดโตหรือรวมกันเป็นกลุ่ม ในขณะที่ความเข้มข้นของสารลดแรงตึงผิวที่สูงกว่าให้เพลเลตที่มีรูปร่างเป็นท่อน พฤติกรรมดังกล่าวสามารถอธิบายได้ด้วยอันตรกิริยาระหว่างน้ำและหมู่ไซลานอลซึ่งมีความสำคัญในมวลเปียกที่มีความเข้มข้นของสารลดแรงตึงผิวต่ำ โดยแสดงให้เห็นได้ด้วยอุณหภูมิที่ทำให้สูญเสียน้ำเพิ่มขึ้น เมื่อความเข้มข้นของสารลดแรงตึงผิวสูงอันตรกิริยานี้จะลดลง ทำให้เกิดโครงสร้างที่เป็นของแข็งมากขึ้นจากอันตรกิริยาระหว่างหมู่ไซลานอลซึ่งสังเกตได้จากสมบัติหยุ่นหนืดและแรงอัดรีด ความสมดุลของอันตรกิริยาทั้งสองส่วนจะทำให้เกิดการเปลี่ยนรูปร่างอย่างเหมาะสมของมวลเปียก

ภาควิชา วิทยาการเภสัชกรรมและเภสัชอุตสาหกรรม
สาขาวิชา เภสัชกรรม
ปีการศึกษา 2559

ลายมือชื่อนิสิต .....
ลายมือชื่อ อ.ที่ปรึกษาหลัก .....
ลายมือชื่อ อ.ที่ปรึกษาร่วม .....

5376959133 : MAJOR PHARMACEUTICS

KEYWORDS: EXTRUSION-SPHERONIZATION / PELLETS / SILICON DIOXIDE / SURFACTANT

SANPETH LIMPAKOMON: EFFECT OF POLYOXYL 40 HYDROGENATED CASTOR OIL ON PELLET FORMATION USING SILICON DIOXIDE AS AN EXTRUSION-SPHERONIZATION AID. ADVISOR: JITTIMA CHATCHAWALSAISIN, Ph.D., CO-ADVISOR: ASSOC. PROF. POJ KULVANICH, Ph.D., 141 pp.

Colloidal silicon dioxide (CSD) has been shown to be a potential extrusion-spheronization aid. A surfactant solution is, however, necessary to be incorporated in formulation as a binding liquid. The effects of surfactant on pellet formation have not been reported. The objectives of this study were to investigate the effect of surfactant, polyoxyl 40 hydrogenated castor oil (HCO-40), concentrations in the formulation of fumed hydrophilic silicon dioxide pellets. The formulations were composed of CSD to HCO-40 solution at a ratio of 1 to 2 by weight. Properties of materials, such as surface tension and viscosity of binding liquids, liquid uptake and binding ability of CSD as well as rheology of wet masses were characterized and information obtained was used to explain behavior of pellet formation. The results showed that rounded pellets and reproducibility of yield in target size (0.71 – 1.4 mm) were obtained from the formulation containing 2.5% w/w surfactant. The lower surfactant concentrations gave bigger pellets or agglomeration, while the higher surfactant concentrations produced rod shaped pellets. This could be explained that interaction between water-silanol groups was significant in the wet mass with the low concentrations of surfactant, evidenced by an increase in desorption temperature. At the high concentrations of surfactant, this interaction was reduced leading to more solid structure caused by interaction of silanol-silanol groups as observed in viscoelastic properties and extrusion forces. The balance between these interactions would induce an appropriate deformability of wet masses.

Department: Pharmaceutics and Industrial Pharmacy Student's Signature .....
Advisor's Signature .....
Field of Study: Pharmaceutics Co-Advisor's Signature .....
Academic Year: 2016

ACKNOWLEDGEMENTS

I would like to take this opportunity to express my immense gratitude to my family who has given their support and assistance.

The scholarship from the Graduate School, Chulalongkorn University to commemorate the 72nd anniversary of his Majesty King Bhumibala Aduladeja is gratefully acknowledged.

I am grateful to Chulalongkorn University Drugs and Health Product Innovation Promotion Center established with the seeding support from Chulalongkorn University Centenary Academic Development Project for providing research facilities.

I am also grateful to the Faculty of Pharmaceutical Sciences, Chulalongkorn University (Grant number Phar2557-RG07) for partial support.

I would like to thank Synchrotron Light Research Institute which gave the opportunity for using of the Small Angle X-ray Scattering (SAXS) and also provided useful knowledge and support.

I would like to thank BASF (Thai) Limited for providing polyoxyl 40 hydrogenated castor oil.

I wish to acknowledge the helpful suggestion given by Professor Fridrun Podczeck for the application of Enslin apparatus and rheometer in studying behavior of silicon dioxide wet mass.

I gratefully thank my advisor, Dr. Jittima Chatchawalsaisin, and my co-advisor, Associate Professor Poj Kulvanich, who spent their valuable time and knowledge for me to complete this thesis.

CONTENTS

Page

Page

Page

LIST OF TABLES

Page

LIST OF FIGURES

Page

Page

Page

Page

CHAPTER I
INTRODUCTIONS

Quality attributes of pharmaceutical product can be influenced by input materials attributes and process parameters. Pellets prepared by extrusion-spheronization always require appropriate properties of wet mass which can be obtained by using extrusion-spheronization aid. Microcrystalline cellulose (MCC) is the most favorable extrusion-spheronization aid but some drawbacks of this material have been found e.g. MCC pellet may not disintegrate [1], may give incomplete drug release [2] and is incompatible with ranitidine [3]. Many materials have been investigated for MCC replacement. A key of success in findings is often involved with role of water in the wet mass.

Recently, the material which has been proved to be an extrusion-spheronization aid is colloidal silicon dioxide (CSD) with addition of surfactant solution in the formulation instead of water as binding liquid [4].

CSD is an inorganic material which is used as a glidant in tablet formulations [5, 6]. It is also be used as thickening agent in suspensions [5] or emulsion stabilizer [7]. Because of high surface area of CSD, it can be used as an adsorbent [8-11]. CSD as an extrusion-spheronization aid can produce acceptable pellets with water soluble and water insoluble excipients [4]. It is postulated that CSD can overcome the drawbacks of MCC. CSD pellets have been shown to disintegrate rapidly and provide completely drug release [4]. However, how CSD can form pellets and the role surfactant solution in the formulation has not been investigated. It is possible that mechanism of pellet formation may be different from other materials

CSD surface contains the silanol groups which can react with other materials via hydrogen bond, also siloxanes which can react with other materials via hydrophobic interaction. Water and surfactant in the wet mass could therefore interact with CSD

surface through these interactions which may be investigated by thermogravimetric analysis [12, 13] and the atomic force microscope [14]. The existing interaction in the wet masses may influence their properties such as viscoelastic properties and may help in explanation pellet formation.

In addition, the properties of water retention can be measured by using centrifugal force. The water that cannot be retained would be squeezed out [15-17]. Deformation behavior is investigated by several types of rheometer. The rheological properties give useful information about formulation which can produce pellet with desired properties [18-20].

Understanding of input materials for pellet formulation is necessary for controlling their properties in order to produce pellets of consistent quality. This may be also useful to understand the behavior of the pelletization process. Therefore, the objectives of the present study were (1) to evaluate the effect of concentrations of the surfactant, polyoxyl 40 hydrogenated castor oil (HCO-40), on CSD pellet formation by extrusion-spheronization; (2) to investigate the role of HCO-40 in the formulation of pellets. The characteristics of a fume hydrophilic silicon dioxide (Aerosil® 200) used as extrusion-spheronization aid, HCO-40 solution and their mixtures were studied. The potential interaction in the mixture was explored.

CHAPTER II

LITERATURE REVIEW

1. Pelletization by extrusion-spheronization

Pharmaceutical pellets are spherical particles with 0.5 – 2.0 mm diameter having high density and narrow in size distribution. Pellets are applied in multiple unit solid formulations by compression into tablets or filling into capsules. Dose dumping and local irritation could be avoided for modified released dosage forms [21]. Large scale of pellets production in pharmaceutical relies on two major pelletization processes i.e. drug layering and extrusion-spheronization. Drug layering process produces pellets by spraying drug and binding solution on non-pareils. Extrusion-spheonization process produces pellets by mechanical force in two pieces of equipment, extruder and spheronizer. The latter technique requires an appropriate formulation and/or a specific extrusion-spheronization aid in order to obtain pellets with desired properties.

2. Extrusion-spheronization aid

Wet mass used in extrusion-spheronization process should contain some specific properties. In extrusion process, wet mass must be forced through a narrow cross-section of the die. So, it required self-lubricating property that was often obtained from squeezed out binding liquid [22-24]. The binding liquid lubricates the die wall in order to reduce friction but the liquid should be absorbed back to the wet mass. Under the extrusion force, it was possible that poor formulations (i.e. unsuitable extrusion aid) would lead to liquid migration. In this case, the liquid content in the extrudate is inconsistent, influencing ability to form pellets during spheronization. Variation in extrudate may fail in spheronization or result in wide size distribution of pellets [24].

During spheronization, extrudates or particles are subjected to centrifugal force from which liquid may migrate to the surface of particles. The too wet surface would induce agglomeration of the particles.

For this reason, formulation of pellets must possess self-lubrication and water retention properties. In addition, it should have plasticity properties so that the wet mass can be deformed to be cylindrical extrudate, which subsequently be deformed to spherical particles.

Microcrystalline cellulose (MCC) is the most common extrusion-spheronization aid because it has the essential properties. Water is often used as binding liquid and help to modify plasticity. MCC could behave like a sponge [25, 26]. Binding liquid in MCC wet mass could be squeezed out to lubricate the die wall and reabsorbed back after passing through the die. It was also explained by crystallite gel model that particles of MCC were in colloidal size. These particles were linked together by the hydrogen bond and hence trapped some water in the gel network. The gel network might be destructed by force e.g. extrusion force. MCC particles without gel structure might be easily deformed by applying shear force and plastic deformation was obtained. The network could be deformed more easily with increasing water in the gel network [27].

Some drawbacks of using MCC in pellet formulation have been reported. MCC pellets may not disintegrate [1]. MCC may adsorb some drug resulting in incomplete drug release [2]. Using organic solvent with MCC may cause high porous and friable pellets [28]. Some drug i.e. ranitidine, was degraded quickly when formulating pellets with MCC [3].

Accordingly, alternate extrusion-spheronization aids have been investigated. These include polysaccharides, synthetic polymers, wax like substances and silicon dioxide. Powdered cellulose which was found to have low binding properties than other celluloses, so it needed sodium carboxymethylcellulose (SCMC) in the

formulations [29]. In addition, poor water retention property of powdered cellulose allowed high water migration during extrusion process resulting in wide size distribution of pellets [30]. Low range of water could be applied as binding liquid with powdered cellulose that made difficult to formulation [29-31].

Hydroxypropyl methylcellulose (HPMC) and hydroxyethylcellulose (HEC) could be used as extrusion-spheronization aid when hydroxylpropylcellulose (HPC) in isopropyl alcohol was used as binding liquid. HPMC pellets had better size distribution and shape than HEC pellets [32, 33].

Chitosan required a diluted acid solution as a binding liquid. The formulation could load only small amount of drug [34]. κ-carrageenan produced pellets with acceptable shape factor but rough surface [2, 17, 35-37]. Pectin and its derivatives needed Ca^{2+} ion for crosslinking when they were used as extrusion-spheronization aid. The formulation gave wide size distribution and rod shape pellets [38, 39].

Fine grade of crospovidone was also investigated and it could produce pellets of narrow size distribution and acceptable aspect ratio [40]. Glyceryl monostearate was also reported the possibility to form pellets with required small amount of water in the formulation [41]. Recently, colloidal silicon dioxide (CSD) had been investigated as extrusion-spheronization aid which could produce acceptable pellets with narrow size distribution [4]. The formulation was successful when 5% Cremophor® ELP solution was used as binding liquid.

3. Silicon dioxide

Silicon dioxide can be classified based on method of preparation as the following:

(1) Precipitated silicon dioxide (Precipitated silica)

Precipitated silicon dioxide is produced by wet process [42]. Sodium silicate is mixed with sulfuric acid from which silicon dioxide will precipitate. Precipitated silicon dioxide will be ground into micrometer size. Silanol groups are found as

functional groups in precipitated silicon dioxide with higher quantity than in the fume silicon dioxide. However, more impurity may be found in precipitated silicon dioxide. Precipitated silicon dioxide used in pharmaceutical formulations such as Syloid® 244 [43].

(2) Fume silicon dioxide (Fume silica, pyrogenic silica)

Fume silicon dioxide can be prepared from silicon tetrachloride that is sprayed through the flame. After that, fume of silicon dioxide, having size in nanometer range, is obtained [44]. The surface area of particle is very high. Because of silanol groups exist on the silicon dioxide surface, nanoparticles of fume silicon dioxide aggregate or agglomerate by hydrogen bond and form bigger size. Fume silicon dioxide used in pharmaceutical manufacturing are commercial available such as Aerosil®, Cab-O-sil® and Wacker®.

In addition, silicon dioxide can be classified based on porosity. Aerosil® is the non-porous fume silicon dioxide. It has true density of 2.2 g/cm^3 and specific surface area of 200±25 m^2/g [44]. Silanol group density of Aerosil® was 1.8-2.16 SiOH/nm^2 measured using lithium alanate method [45]. Surface area of Aerosil® primary particle calculated from average primary particle size (12 nm) [44]

A compacted grade of Aerosil®, Aeroperl® is mesoporous and macro porous silicon dioxide. Aeroperl® is produced from fume silicon dioxide by compaction in order to reduce dust in the process. Moreover, more porous structure make Aeroperl® showing better adsorption property than the Aerosil® [46]. The other mesoporous silicon dioxide is Syloid® FP silica that have network of mesopore.

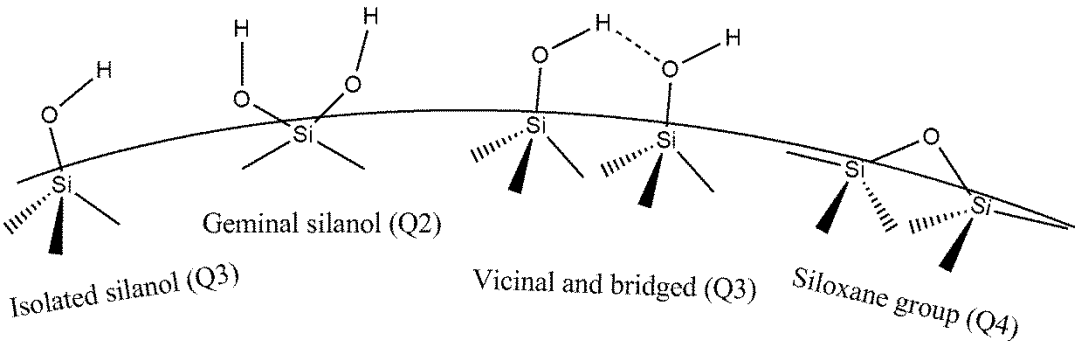

Figure 1 Surface chemistry of Aerosil® 200 (CSD) modified from Zhuravlev , 2000 [47], the Q value was from ^{29}Si NMR characterization

The character of silicon dioxide can be both hydrophilic and hydrophobic. Hydrophilic silicon dioxide surface contains hydroxyl group called silanol groups as shown in Figure 1. Silanol group can interact with water via hydrogen bond that makes silicon dioxide hydrophilic. Hydrophilic silicon dioxide improved wettability of drug particle [48]. Moisture content of hydrophilic grade was increased with relative humidity but hydrophobic grade was not affected by the humidity [6, 49].

Hydrophobic silicon dioxide is made by modification of silanol groups on hydrophilic silicon dioxide. Alkyl groups or other hydrophobic groups are used for silanol substitution [6]. Absence of the silanol group, the modified silanol group cannot interact with the water via hydrogen bond then the surface is hydrophobic. One grade of hydrophobic silicon dioxide, Aerosil® R974, showed an increase in contact angle of water from 0 to 143 degree, while contact angle of water on hydrophilic silicon dioxide (Aerosil® 200, Aerosil® 50) is zero [50]. Hydrophobic silicon dioxide may not be agglomerated because of low inter-molecular interaction from silanol on their surface.

4. Applications of silicon dioxide

Silicon dioxide is applied to pharmaceutical formulations. In tablet formulation, silicon dioxide has been used as a glidant to improve flowability of material. With

small particle size and high specific surface area of fume silicon dioxide, silicon dioxide can be adsorbed on the granule surface. Van de Waal force decreases by increasing distance between granules. Therefore, granules can flow freely without attraction from others [51]. Hydrophobic silicon dioxide was the better glidant than the hydrophilic one [6]. Hydrophilic type may adsorb water from environment and loss of glidant properties but hydrophobic type cannot interact with water. Both types of silicon dioxide, however, may decrease tablet hardness. Decreasing of tablet hardness was less found for hydrophilic silicon dioxide because it can adsorb some moisture on its surface. The moisture acts as the plasticizer that increases compressibility of the silicon dioxide [50].

Large surface area of fume silicon dioxide is also beneficial for using silicon dioxide as carrier. Aerosil® 200 was used as a carrier of self-micro emulsion drug delivery system (SMEDDS). It could change the liquid formulation to solid formulation without changing emulsion droplet size. Adsorbed with Aerosil® 200 made the formulation increasing the dissolved drug and in-vivo pharmacokinetic parameters [8].

Fume silicon dioxide has polar groups and non-polar area on their surface. It makes silicon dioxide behaving like surfactant. Both hydrophilic and hydrophobic silicon dioxides were used as the surfactant in solid-lipid nanoparticles (SLN) [52]. Aerosil® R972, a hydrophobic grade fume silicon dioxide could be incorporated in the oil phase of the SLN because of their hydrophobic surface [52]. Particle of fume silicon dioxide can also be used as emulsion stabilizer. Silicon dioxide particles were adsorbed on the oil droplet to protect the droplet from coalescence. Using of Aerosil® 200 grade which was compatible with water and oil gave benefit to this function [7].

As silicon dioxide is a good glidant, co-process of silicon dioxide and other excipients may improve gliding property of the material. Silicified microcrystalline

cellulose composed of 2% colloidal silicon dioxide and MCC showed the superior compressibility and flowability [5]. Co-precipitation is another method for improving the properties of materials. Silicon dioxide dispersed in water was mixed with starch which was swelled in alkaline solution. Precipitated rice starch was obtained after pH adjusted and dried of that suspension. Precipitated rice starch aided flow and compact properties of tablet formulation [53]. Rice starch and colloidal silicon dioxide were also co-spray dried. Friction force between spray-dried particles was reduced and flowability was improved [54].

Silicon dioxide with or without lactose or magnesium carbonate were mixed with non-ionic surfactant, Cremophor® ELP. The mixture could be extruded with a screen extruder and formed pellets in a spheronizer [4]. Silicon dioxide is a potential extrusion-spheronization aid and it was proved to give more uniform pellets when extrusion was carried out using long die extruder [55]. The pellets of silicon dioxide quickly disintegrated and showed rapid release.

5. Surfactant

Surfactant is a surface active agent that can reduce the surface tension of liquid. It contains amphiphilic properties because it consists of hydrophilic and hydrophobic regions. Therefore it can be dispersed in both water and oil. Surfactant is wildly used in many industries such as paint, petrochemicals and pharmaceuticals. In pharmaceutical applications, surfactants are wildly used because it can improve wetting property of the material. The surfactant in tablet formulation increases wettability of hydrophobic drug and hence increases dissolution via micellar solubilization. Other uses of surfactant can be found in emulsions which contain water soluble phase and oil soluble phase. The role of surfactant in emulsion is to decrease the surface tension of water and stabilize the oil droplet.

The surfactant which contains head and tail structure can form into micelles. The tail is the hydrocarbon part of surfactant that can miscible with the oil. The

head was the polar part of surfactant that shows the hydrophilic property. However the head of the surfactant can be divided into 4 groups based on their charge. Cationic and anionic surfactants comprise positive charge and negative charge functional group, respectively. Amphoteric surfactants contain both positive and negative charge functional groups. Nonionic surfactants contain only polar group without any charge.

The surfactant can be used as an emulsifier because of their amphiphilic properties. The polar group or ionic charge dissolves in aqueous phase while the hydrocarbon chain dissolves in the oil phase. Hence, the surfactant can be adsorbed around the oil droplet and prevents oil droplet from coalescence.

The surfactant reduces surface tension of liquid leading to reduction of contact angle between solid-liquid interface. The solid surface can be easily wet by aid of the surfactant. Types of surfactant for wetting effect are important for hydrophobic drug. Charged surfactant may form ion pair with the ionic drug and show lower diffusion and dissolution. Nonionic surfactant may increase dissolution without ion pair forming [56]. Concentration of surfactant used as wetting agent should be lower than critical micelle concentration. The concentration that higher than critical micelle concentration shows an effect in improved solubility via micellar solubilization [57]. Allaboun et al. found that the ratio of total solubility/intrinsic solubility of benzocaine was increased when sodium lauryl sulfate was added in the solution medium [58]. Cationic and anionic surfactants in the dissolution medium showed superior solubility enhancement but nonionic surfactant showed a little improvement [59, 60]. Moreover, Alkhamis et al. found that dissolution of gliclazide was increased with chain length of the cationic surfactant but it was decreased when chain length of anionic surfactant was increasing [59].

Alternatively, solid dispersion in which the surfactant is used as a carrier is a technique for solubility improvement. The solid dispersion can be prepared in by

means of melting [61, 62] and freeze drying method [63]. The surfactant such as poloxamer interacted with the active drug via hydrogen bond can stabilize drug in the amorphous form [62]. Sometime, surfactant used in solid dispersion may not help increaseing the dissolution. Mah et al. found that Tween® 80 or poloxamer 407 in ternary solid dispersion with indomethacin and polymer decreased the dissolution [57].

In pellet formulation, a surfactant may be added to increase drug dissolution via micellar solubilization. Podczeck et al. found that single surfactant at the concentration of 25% in binding liquid increased the drug dissolution more than the mixed surfactant [64]. However, the surfactant may reduce the dissolution by obstructing the pore of the pellets. Levis and Deasy used co-processed MCC with sodium lauryl sulfate in extrusion-spheronization and found that pellets showed low dissolution. It was possible that low dissolution was due to the amount of surfactant being lower than critical micelle concentration then enhancing solubility by micellar solubilization did not happen [65].

The surfactant may also aid the extrusion process via lubrication. Podczeck et al. found that pellet formulation which contained low water content in the wet mass resulted in forced flow curve in extrusion profile. Using of the small amount of the surfactant changed the extrusion profile to a steadier curve. Nevertheless, the increased surfactant concentration in the binding liquid may increase the extrusion force because of increased viscosity of that liquid [64]. Podczeck et al. also found that incorporation of surfactant provided rounder pellets [66]. Nevertheless, Newton et al. showed that the wet mass containing 92% of surfactant in the binding liquid could be extruded; while, the wet mass with mono-di glyceride over than 46% in the binding liquid could not be extruded [67].

In addition, the surfactant has been found in the pellets as a component as self-emulsifying (SE) system [68, 69]. The formulation of pellets containing surfactant was extensively studied.

Newton et al. found that the extrusion force was increased when content of SE system in the binding liquid was increased [70]. The SE system made the pellets of lower strength and more friable because it reduced interparticular bonding of MCC [69]. Crushing load of pellets was reduced with oil/surfactant ratio so that the pellet was deformed easily [68]. Nikolakakis et al. found that the size of pellets produced with the SE system containing a surfactant of high hydrophilicity was small because the pellets were shrunk during drying process [69]. In addition, high hydrophilicity or high HLB surfactant required more water in extrusion-spheronization process [68, 69].

Capillary rheometer was used in evaluating the wet mass which contained non-ionic surfactants. Podczeck et at., found that wet masses of MCC and surfactant used in pellet formulation showed non-Newtonian flow. They showed shear thinning property by power law index values that lower than 1.0 [64]. Similarly, the SE system that was consisted of mono-di glyceride and polysorbate surfactant in wet mass showed non-Newtonian flow of wet mass. Newton et al. found that increasing of SE system in the wet mass may change shear resistance and increase elasticity of wet mass. Moreover, the increased concentration of SE system in binding liquid changed the rheology of binding liquid from Newtonian to non-Newtonian flow. However, it did not change the flow behavior of the wet mass. The researchers concluded that rheological properties of the wet mass resulted from interaction between MCC and the binding liquid; and the viscosity of binding liquid was not related with the wet mass rheology [71].

6. Characterization of wet mass for extrusion-spheronization

In extrusion-spheronization process, round pellets with narrow size distribution are desired. The wet mass for extrusion-spheronization should possess the ability of

water retention, self-lubrication and plastic deformation. Characterization of wet mass may give information about feasibility of the process. Pellet properties may also be predictable or controlled by understanding the properties of wet mass. Many tools are proposed here for wet mass characterization.

6.1. Extrusion profile

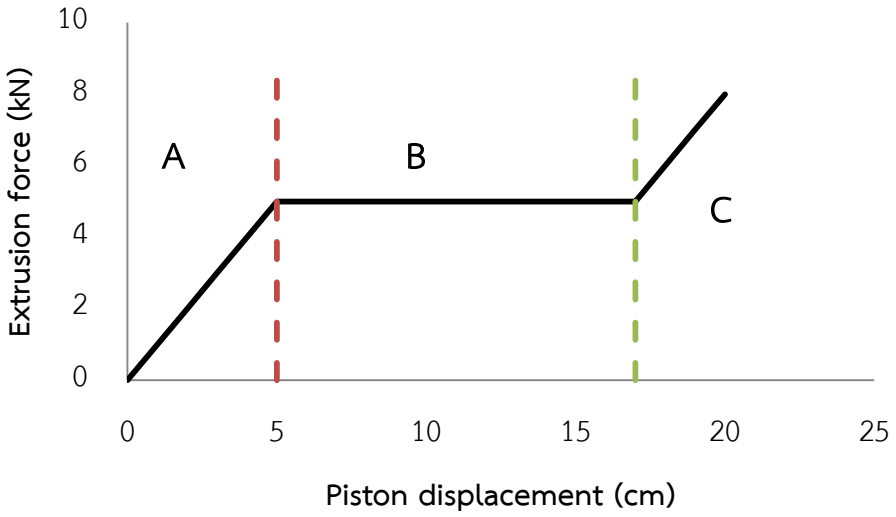

Figure 2 Extrusion profile consisting of 3 stages, compression stage (A), steady state flow stage (B) and forced flow stage (C)

Extrusion force measured versus piston displacement of ram extruder is present in the form of an extrusion profile. Harrison et al. demonstrated that the extrusion profile comprised 3 stages, as shown in Figure 2. During stage A or compression stage, wet mass was packed before flow through the die orifice. In this stage, the void space in the wet mass was eliminated and apparent density of the wet mass in the barrel was increased. After the compression stage, the wet mass was flown through the die. The extrusion force remained constant as shown in a steady state flow stage (B). The last stage (C) was a forced flow stage in which the piston approached to the die and the extrusion force was increased [72].

In the steady state flow stage, different of final and initial force less than 5% was acceptable and the large difference showed the water movement in the extrusion [64]. Podczeck et al. found 5 patterns of the flow which occurred during extrusion of wet mass containing non-ionic surfactants [66]. The forced flow pattern was found in formulation with low water content. The surfactant amount over 80% in formulations gave the initial peaks in the extrusion profile [66]. Irregular profile of extrusion from non-uniform content of water in extrusion was due to water movement [22, 24].

Water movement in extrusion was cause by formulation [24, 73, 74] and setting of the instrument [18, 24, 75]. Formulation consisted of particles which were different in size and shape altered the behavior of water movement. Milling of acetyl salicylic acid in the extrusion prevented water from migration because of arrangement of small particle size [76]. A high extrusion rate also reduced water movement because water has not enough time to move, and hence the surface of extrudate was uniform because water content in the extrudate was consistent [18]. With high extrusion rate, the fracture of the extrudate may also be found [18, 75]. Although, an increase in die length of the ram extruder resulted in increased steady state extrusion force, the die length did not influence water migration in extrusion process [18].

6.2. Water retention property

Optimum water content in wet mass and extrudate is important for production pellets. Loss of water from the wet mass and extrudate may be due to evaporation or squeezing out by force. Water retention in the wet mass can be evaluated by various techniques.

Direct measurement

Water retention in the extrudate can be directly measured during extrusion by collecting extrudate at time intervals and determining its water content. The

inconsistent water content in the extrudate suggested water movement occurring in the process. The wet mass with water retention ability should be extruded with a constant force. It was found that loss of water in the extrudate caused an increase in the extrusion force [24].

Thermal analysis

Fielden et al. used thermogravimetric analysis (TGA) to evaluate the MCC wet mass. They found that detected water content was close to the added water. With lactose in formulation, the median temperature of water loss increased about 10°C in extrudate sample. The result suggested only little water was absorbed by MCC as structured water [26].

Moreover, TGA can be applied to gain information about adsorption of materials on substrate. The works have been carried out by many researchers. Wang and Wunder determined the content of water and octadecyl trichlorosilane which were adsorbed on silica by using TGA [77]. Kinetic of material desorption was also investigated with aid of TGA [78-80]. Maretto et al. determined regenerating temperature of mesoporous silica alumina after adsorbed hydrocarbon waste by TGA [78]. Increasing thermal stability of organobentonite may be detected by TGA. Desorption temperature was increased via co-adsorption of anionic and non-ionic surfactant on the bentonite which was useful for pentachlorophenol elimination [79]. Capillary force increased desorption temperature of ibuprofen which was adsorbed in the pore of upsalite. It raised the desorption temperature that was recorded by the TGA [80].

Centrifugation

Centrifugal force was applied for determination of squeezed out water that cannot be retained in the wet mass. Thommes and Kleinebudde applied the amount of left water in the wet mass after centrifugation which was adsorbed by one unit of material weight to indicate water retention volume (WRV) [17]. In addition,

Tomer and Newton and Tomer et al. used a ratio of water in the wet mass before and after centrifugation to determine the moisture retention capacity (MRC) [15, 16]. Non-extruded wet mass had low WRV. But, highly plastic deformation was found in high WRV wet mass [17]. As same as WRV, poor extrudablity of wet mass had low MRC [16].

Enslin apparatus

Rate and content of water uptake or penetration can be measured by Enslin apparatus [81-83]. Packed particles absorbed water by two mechanisms i.e. swell and capillary rise. Wettability in term of contact angle could be tested with non-swell material and calculated from water penetration rate. It has been reported that rate and content of water uptake in pasta powder depended on their particle size [81]. Decreasing rate and content of water uptake may show the porosity decreasing by compression forces [83]. This informed that uniform packed of material was required when Enslin apparatus was used. Moreover, penetration rate and wettability could indicate behavior of liquid on solid surface. Micelle aggregation made the penetration rate change due to polarity of micelle [84]. Chemical structure of ingredient in liquid also affected the rate of penetration [85].

6.3. Deformability of wet mass

Deformability of wet mass and extrudate is essential character for extrusion-spheronization. The wet mass must be pushed through die hole with increasing its density. Extrudate must be broken to smaller pieces and rounded into spherical pellets. Deformability may be evaluated by determining some parameters e.g. yield point, viscoelasticity or required torque during mixing process.

Yield point informs plastic deformation and can be determined using penetration tool. Pelletization process required not too low yield point of wet mass to deform into pellets. The low yield point indicated too plastic deformation leading to uncontrollable agglomeration [17].

Viscoelastic properties inform flow and deformability of wet mass in the process. Control stress rheometer was often used in viscoelastic evaluation. Suitable wet mass that produced round pellets may show constant storage modulus or constant loss modulus with increase binding liquid content [20]. Wet mass used in extrusion-spheronization processes was dominated by elastic modulus [18, 20].

Torque required during mixing was related with some physical properties of pellets. For example, the maximum torque had some relations with density and friability of pellets, but could not be related to shape and size with this torque value [86]. Alvarez et al. found that wet masses from different grade of MCC gave same torque values by measured from mixer torque rheometer. However, these wet masses could not produce pellets which had same size and shape [87].

Capillary rheometer informs flow of wet mass used in extrusion-spheronization. Because of high shear rate from this instrument, rheology from capillary rheometer may be close to real extrusion process. Power model gave power index value to inform Newtonian like flow behavior. Otherwise, Herschel-Bulkley model may inform the yield value of wet mass [18].

To evaluate deformability of wet mass, using of single technique may not differentiate wet mass characteristics. Data from more than one technique may be used to understand about quality attributes of the wet mass that can form pellets by extrusion-spheronization.

6.4. Self-lubrication

Lubrication is necessary when wet mass has to flow through small die holes. Sufficient lubrication reduces extrusion pressure. Increasing binding liquid content may decrease extrusion pressure but it may not produce a good quality pellets. Some extrusion-spheronization aid which contains self-lubrication property is therefore needed. Self-lubrication may be complicated to measure and direct measurement has not been found yet. The extrudate with smooth surface may be

because lubrication layer existed [75]. However, water content in the formulation or extrusion rate may possibly produce extrudate surface smooth.

6.5. Other characterization

Other characteristics of wet mass which are not described above such as interaction between excipients in the wet mass may also be related to pellet formation and quality of pellets. Several techniques may be used to study the behavior of excipients in pellet formation.

Atomic force microscope (AFM)

A contact mode AFM can be used to measure surface topology of substrate from which image of materials and friction between AFM tip and the surface can be explored. This function is beneficial to investigation of aggregated or adsorbed structure on the surface. The contact mode AFM can also measure force at the distance that the tip jumps in or pulls off. The force-distance curve shows repulsive or attractive force between the tip and sample. The attractive force exists when the tip jumps in to contact to the substrate. It shows attractive force before the tip contact to the substrate that causes the tip to deflect. After that, the force that pulls the AFM tip when its leaves the substrate is adhesion force. Characteristic of adsorption layer can be determined from the force distance curve.

McNamee et al. reported that friction on surface measured by contact mode AFM was decreased when the surfactant, sodium dodecyl sulfate, was present. It may be because the negative charge of anionic surfactant increased repulsive force [88].

Lüderitz and Klitzing found that increased concentration of cationic surfactant, hexadecyltrimethylammonium bromide (CTAB), which was adsorbed on silica particle, changed the attractive force to repulsive force. It may be resulted from micelle arrangement on the particle [89]. In their experiment, the colloidal probe

was attached with other substrates. Therefore, the benefit of this application was determination of inter-particular force.

Another function of the AFM is a tapping mode. The tapping tip oscillates over but do not touch a measured substrate. This mode also provide surface topology like the contact mode, but the phase image provides better contrast [90]. This tapping mode could show the effect of adsorption by phase angle. Surface topology of micelle [10] and characteristics of surfactant aggregates [91, 92] could be observed by the tapping mode AFM. In addition, direction of phase shift possibly informs the stiffness of material. The positive phase shift was found in greater stiffness material [93]. Positive phase shift was found on glycerin droplet more than that found on graphite [94]. Different in sharpness of the tip could also give an opposite phase shift on the same samples [95]. Therefore, it may be complicated to distinguish the mechanical properties of material by using only the phase shift result.

Infrared spectroscopy (IR)

Infrared spectroscopy is used for functional group characterization. Moreover, the interaction between chemical compounds may be detected. CSD has silanol group (Si-OH) on the surface which can be detected by IR.

Basically, surface silanols are divided into 3 types. Isolated single silanol and geminal silanol are silanol groups that are not interacted with the other groups. Vicinal silanols are the silanol group which is interacted with another silanol group by hydrogen bonding. The surface silanol groups can interact with other silanol or other functional groups of water or other molecules by hydrogen bonding from which the molecules are adsorbed on CSD surface.

Silanol peak intensity which was detected by IR may be decreased with increasing storage time. IR spectra of the samples treated under vacuum showed silanol peak more clearly [77]. Van Roosmalen and Mol showed that only one peak positioning at 3748 cm^{-1} after vacuum treatment of silicon dioxide powder (Cab-o-sil®

and Aerosil®) [96]. Subsequently, they found OH stretching of both isolated and germinal silanols at 3749 and 3742 cm^{-1}, respectively in the IR spectra of silica gel surface [97]. Tripp and Hair also found a sharp peak of isolated and germinal silanol in the IR spectra of fume silica (Aerosil® 380) at 3747 cm^{-1} [98]. Wang and Wunder demonstrated that the IR spectra of silicon dioxide showed broad peak around 3400 – 3500 cm^{-1} due to physically adsorbed water; the peak of hydrogen bonded silanol group shown at 3520 cm^{-1} was overlapped with this broad peak [77].

Solid-state nuclear magnetic resonance spectroscopy

Nuclear magnetic resonance spectroscopy (NMR) technique has been used for in chemical structure characterization. Similar to IR technique, the solid state NMR can differentiate the silanol groups in to 3 types. ^{1}H-^{29}Si CP/MAS NMR spectra showed peaks of isolate single silanol and vicinal silanol at -100 ppm (Q3) and that of geminal silanol was found at -90 ppm (Q2). Bulk silicon dioxide or silicon dioxide on which the hydrogen atom in the silanol group has been substituted by silicon atom were found at -110 ppm in the ^{1}H-^{29}Si CP/MAS NMR spectra; and this was called as bulk siloxane silicon [99]. The hydrogen atom in the silanol groups was also detected by ^{1}H HR MAS NMR. It showed chemical shift around 3 ppm that indicated adsorbed water and surface silanol group [100].

Small angle X-ray scattering (SAXS)

Nanostructure of materials and interaction with a substrate can be revealed by SAXS technique. Scattering pattern i.e. scattering intensity versus scattering vector (q) of X-ray on the detector is dependent on crystallized or repeated structure of materials.

Size and dimensionality of particle is obtained by using model independence i.e. Guinier plot and Porod's law plot. The Guinier plot is plotting of intensity in log scale against q^2. Then, radius of gyration (R_g) is obtained from the Guinier plot in low q-range. The R_g value is valid when the calculated R_g value multiplied with the

maximum q in fitting is lower than 1.0 [101]. The R_g value can inform the size of nanostructure. For spherical structure, radius of the structure can be calculated by Equation 1 [102].

$$R=R_g/(3/5)^{1/2} \qquad \text{Equation 1}$$

Where, R_g is the radius of gyration from Guinier plot; R is the radius of the structure

For cylindrical shape, the cross section radius (R_C) can be calculated by Equation 2 [102].

$$R_C=R_{gC}(2)^{1/2} \qquad \text{Equation 2}$$

Where, R_{gC} is the cross-sectional radius of gyration; R_C is the cross section radius

For flat particle, the thickness radius of gyration (R_{gt}) which is correlated with the thickness of particle (T) can be calculated by Equation 3 [102].

$$T= R_{gt}(12)1/2 \qquad \text{Equation 3}$$

Where, R_{gt} is the thickness radius of gyration; T is the thickness of particle

The slope from intensity scattering suggests dimensionality of the sample structure. The x-ray scattering intensity (I) is related to particle number according to the inverse of the power law state in Equation 4.

$$I=B/q^{dm} \qquad \text{Equation 4}$$

Where, I is the scattering intensity; B is the constant; q is the scattering vector; dm is the particle dimension or mass fractal dimension

This equation is valid for sample with 1 and 2 dimensions. The value of dm is 1 and 2 for the system that contains 1 and 2 dimension samples, respectively. The value of dm is between 2 and 3 for the non-smooth planar system [102]. In 3D system (dm=3), there are surface fractal dimension (ds) in Equation 5.

$$I=B/q^{2dm-ds}=B/q^{6-ds} \qquad \text{Equation 5}$$

For smooth particles, ds value is 2 and for non-smooth particles the ds value is 2 – 3 [102].

Another model independence informs dimensionality of the sample structure. The slope in high q range of the plot between intensity versus q in log-log scale is determined and the value is justified as the dimensionality of particles based on Porod's law as shown Table 1.

Table 1 Slope value from Porod's law

Slope	Dimensionality of particles
-1	1-dimensional system (line)
-2	2-dimensional system (plane)
-2 to -3	non-smooth 2-dimensional system (non-smooth planar system)
-3 to -4	non-smooth 3-dimensional system (clusters of nanoparticles with non-smooth surface)
-4	Smooth surface 3-dimensional system (well dilute dispersed nanoparticles)

Particle size and size polydispersity of silica nanoparticles were evaluated using SAXS [103-105]. Sarkar et al. compared particle size obtained from SAXS and SEM image which estimated the size from surface area. The result from two evaluation technique was not much different [103]. Bharti et al. measured size of lysine adsorbed silica particle and found that Guinier intensity was not different when increased temperatures [104]. Balmer et al. characterized core-shell structure of surfactant-silica nanoparticle and found that SAXS technique was suitable for samples contained high electron density contrast like surfactant and silica particle. Low polydispersity of particle size is another factor that increases advantage of SAXS [105]. Brambilla et al. using Porod's plot to evaluate hybrid silica morphology. It

was found that structure of silica changed from sphere to lamellar when increasing of octadecylsilane [106]

CHAPTER III

MATERIALS AND METHODS

1. Materials

1.1. Colloidal silicon dioxide (CSD, hydrophilic fume silica, Aerosil® 200, true density of 2.2 g/mL, specific surface area approximately 200 m^2/g , Batch No. 153011014, 3152051414, 153050314, 154090714, Evonik Industries, Rheinfelden, Germany)

1.2. Microcrystalline cellulose (MCC, Avicel® PH101, Lot No. C1110059, FMC Corporation, Philadelphia, Pennsylvania, USA)

1.3. Polyoxyl 40 hydrogenated castor oil (HCO-40, Kolliphor® RH40, Lot No. 32177616K0, 14275475L0, BASF, Lampertheim, Germany)

1.4. Hexane of reagent plus grade (Lot No. OA4G2A, Honeywell Burdick & Jackson™, Gyeonggi-do, Korea).

2. Equipment

2.1. Atomic force microscope (Model SPA 400, Seiko Instrument Inc., Chiba, Japan) with scanning probe microscope (SPM) probe (Model SHOCON, AppNano, Mountain View, California, USA) and force modulation probe (Model Etalon HA_HR, NT-MDT, Moscow, Russia) and Nanonavi software version 5.0 (SII Nanotechnology, Inc., Chiba, Japan)

2.2. Balance with 0.01 mg resolution (Model XP205, Mettler Toledo, Greifensee, Zürich, Switzerland)

2.3. Balance with 1 mg resolution (Model ML303, Mettler Toledo, Greifensee, Zürich, Switzerland)

2.4. Balance with 10 mg resolution (Model PB3002, Mettler Toledo, Greifensee, Zürich, Switzerland)

2.5. Gas (helium) pycnometer (Model Ultrapycnometer 1000, Quantachrome, Boynton Beach, Florida, USA)

2.6. Hot air oven (Capacity 100 kg, Charatchai Machinery, Limited Partnership, Bangkok, Thailand)

2.7. Infrared spectrometer (Model Nicolet iS10, Thermo Scientific Instrument, Waltham, Massachusetts, USA) with Omnic software version 8.2.0.387 (Thermo Fisher Scientific Inc., Waltham, Massachusetts, USA)

2.8. Planetary mixer (Model AR400, Erweka, Heusenstamm, Germany)

2.9. Plate-plate rotational rheometer (Model Gemini 200HR^{Nano} Rotonetic^{TM} Drive2, Malvern–Bohlin Instruments, Malvern, Worcestershire, UK) with Bohlin software version R6.51.0.3 (Malvern–Bohlin Instruments, Malvern, Worcestershire, UK) and water bath temperature controller (Julabo F12-ED, Julabo GmbH, Seelbach, Germany)

2.10. Small Angle X-ray Scattering (SAXS) (Beam line 1.3W (Small/ Wide Angle X-ray Scattering) with SAXSIT software version 3.69 (Synchrotron Light Research Institute, Nakhon Ratchasima, Thailand)

2.11. Scanning electron microscope (Model 6610LV, Jeol, Tokyo, Japan)

2.12. Sieve shaker (Model O: FT-200M, Filtra, Barcelona, Spain)

2.13. Solid state nuclear magnetic resonance spectrometer (Model Ascend 400WB, Bruker, Bruker Corporation, Billerica, Massachusetts, USA) with Bruker Topspin software version 3.2 (Bruker Corporation, Billerica, Massachusetts, USA)

2.14. Spheronizer (Model S320, Aeromatic Fielder, Eastleigh, Hampshire, England)

2.15. Stereo microscope (Model SMZ 745T, Nikon Corporation, Tokyo, Japan) with NIS element basic research software version 3.2002.710.0 (Nikon Corporation, Tokyo, Japan)

2.16. Tensiometer, (Model DCAT 11EC, Data Physics Corporation, Filderstadt, Germany) with SCAT software version 2.8.1.77 (Data Physics Corporation, Filderstadt,

Germany) and water bath temperature controller (Thermo Neslab, Thermo Electron, Newington, Connecticut, USA)

2.17. Texture analyzer (Model TA-XT plus, Stable Micro Systems, Godalming, Surrey, UK) with Exponent software version 6.1.8.0 (Stable Micro Systems, Godalming, Surrey, UK)

2.18. Thermo gravimetric analyzer (Model TGA/SDTA851^{e}, Mettler Toledo, Greifensee, Zürich, Switzerland) with STARe software version 13.00 (Mettler Toledo, Greifensee, Zürich, Switzerland)

2.19. Universal testing machine (Model LR50K Plus, Lloyd Instrument, Bognor Regis, West Sussex, UK) with Nexygen Plus software version 3.0 (Lloyd Instrument, Bognor Regis, West Sussex, UK)

2.20. Viscometer (Model DV II+, Brookfield Engineering Laboratories, Inc., Middleboro, Massachusetts, USA) with water bath temperature controller (Thermo Neslab, Thermo Electron, Newington, Connecticut, USA)

2.21. Liquid pycnometer (witeg liquid pycnometer, 10.220 mL, witeg Labortechnik GmbH, Wertheim, Germany).

3. Methods

3.1. Characterization of input materials

Input materials, i.e. CSD, HCO-40 solutions and dispersions/ wet masses of CSD with HCO-40 solutions were characterized.

3.1.1. Binding liquid characterization

Surface tension of binding liquids

Surface tension of binding liquids used in pellet formation was measured by tensiometer (Model DCAT 11EC, Data Physics Corporation, Filderstadt, Germany) operated with SCAT software version 2.8.1.77 (Data Physics Corporation, Filderstadt, Germany) using 10 x 19.9 x 0.2 mm^{3} Wilhelmy plate (Data Physics Corporation, Filderstadt, Germany). An amount (50 g) of the liquid sample (as tabulated in Table

2) was filled in a sample cup. Temperature of the binding liquids was controlled at 25° C by water bath temperature controller (Thermo Neslab, Thermo Electron, Newington, Connecticut, USA). The motor speed was 1.00 mm/s. Liquid surface detection was set at 8.00 mg and immersion depth was set at 3.00 mm after surface detection. Data was recorded at rate 5 points per second. Measurement was ended when the standard deviation of the last 30 points was not larger than 0.030 mN/m. The Wilhelmy plate was burned with flame from alcohol burner after each test. Each binding liquid, the measurement was repeated three times and average was reported.

Table 2 Composition of binding liquids

No.	HCO-40 (g)	Water (g)	Concentrations of binding liquid (% w/w)
1	0.3	299.7	0.1
2	1.5	298.5	0.5
3	3	297	1
4	4.5	295.5	1.5
5	6	294	2
6	7.5	292.5	2.5
7	9	291	3
8	15	285	5
9	22.5	277.5	7.5
10	30	270	10
11	37.5	262.5	12.5

Viscosity of binding liquids

Viscosity of binding liquids as shown in Table 2 was measured by viscometer (Model DV II+, Brookfield Engineering Laboratories, Inc., Middleboro, Massachusetts,

USA). An amount (20 g) of binding liquid was filled in a sample chamber assembled water flow jacket (Model Brookfield UL adaptor, Brookfield Engineering Laboratories, Inc., Middleboro, Massachusetts, USA). With this chamber, viscosity as low as 1 mPas could be measured. Testing speed was selected to 100 rpm for required torque (10–100%) [107]. Temperature was controlled at 25° C by water bath temperature controller (Thermo Neslab, Thermo Electron, Newington, Connecticut, USA) that connected to UL adaptor via water flow jacket. For each liquid, the viscosity was measured three times.

Density of binding liquids

Density of binding liquids was measured by witeg liquid pycnometer which is 10.220 mL in volume (witeg Labortechnik GmbH, Wertheim, Germany). Density of binding liquid was measured in duplicate.

Micelle formation and characterization

In this study, Small Angle X-ray Scattering (SAXS) technique was used to determine size and shape of micelles formed in the binding liquid. In addition, it was used to investigate behavior of micelle when CSD was present in the binding liquid as 1% suspension, wet mass containing weight ratio of CSD to binding liquid at 1: 2 and dried CSD pellets made from the wet mass.

The study was carried out by setting distances between sample and the detector at 960 mm and 4800 mm. The actual distance was calibrated with sodium behenate and styrene ethylene butylene styrene (SEBS) to be 963.77 mm and 4833.8 mm, respectively. The calibrated values were used in calculating valid range of scattering vector q (q-range) by SAXSIT software.

The calculated q-range of this experiment was 0.09 – 4.10 nm^{-1}, allowing the particle in the size range of 1.53 – 70.10 nm to be measured. The X-ray radiation was obtained from synchrotron light source at beam line 1.3W (Small/ Wide Angle X-ray Scattering, Synchrotron Light Research Institute, Nakhon Ratchasima, Thailand).

The X-ray at 9.5 keV passed through the sample and scattered. Scattering patterns were collected by charge-coupled device detector (Model Rayonix SX165, Rayonix, LLC, Evanston, Illinois, USA) with an 18 mm beam stopper.

Each liquid sample, i.e. solution and suspension, was filled in a liquid cell holder using 100 µL micropipette. DI water and the empty liquid cell were used as a blank and reference, respectively. For the wet mass, a small amount of sample was attached to the Kapton tape and placed in the sample holder. For dried pellets, the samples were ground and attached to the Kapton tape before placing in the sample holder. The Kapton tape was used as a blank for the wet mass and pellet samples.

Scattering patterns were processed by SAXSIT software version 3.69 (Synchrotron Light Research Institute, Nakhon Ratchasima, Thailand). Micelle shape (based on dimensional structure) and size could be determined by using of SAXSIT software.

To determine particle shape, the scattering intensity (I) was plotted against q values in ln-ln scale. The intensity data at a fixed calculated q-range from 0.7 to 1.4 were used for calculation of slope which indicates dimensionality of structures, stated in Table 1, (Chapter II).

In addition, scattering intensity was plotted against q^2 in ln-linear scale (i.e. Guinier plot) by SAXSIT software. The Guinier fitting was carried out using a range of data starting from the lowest calculated q value to obtain the value of radius of gyration (R_g). The valid R_g was determined when the fitted R_g multiplied by maximum q value used in the fitting was not more than 1.0. The valid R_g value was then used to calculate the micelle size (geometrical radius of the spherical particle, R) via Equation 1 as the following:

$$R=R_g/(3/5)^{1/2}$$

where, R_g was the radius of gyration from Guinier plot; R was the geometrical radius of the particle.

Interaction between HCO-40 and CSD surface

Interaction between HCO-40 and CSD surface was investigated by atomic force microscopic (AFM) method. The AFM experiment gave information about topological image, friction image, force-distance profile, and phase image.

CSD particles were attached onto a 10 x 10 mm glass slide using acrylic polymer. The slide was then placed in an AFM liquid cell. Binding liquids as shown in Table 2 and water were used as the medium in this experiment. The medium was dropped into the liquid cell by using micropipette. The AFM was controlled via Nanonavi software version 5.0 (SII Nanotechnology, Inc., Chiba, Japan).

Topological and friction graphics CSD particles attached on the glass slide in the area of 1 x 1 μm^2 were studied by AFM Model SPA 400 (Seiko Instrument Inc., Chiba, Japan) with contact mode using scanning probe microscope (SPM) probe (Model SHOCON, AppNano, Mountain View, California, USA) made up of silicon (Si). The topological graphics show surface of CSD particle and friction graphic show friction of the CSD surface that the SPM probe was dragged through.

To obtain a force-distance profile, the experiment was performed by pressing the SPM probe on the observed CSD particle surface. The probe was moved from the starting position downward to particles in distance of 210 nm. Then, the SPM probe was moved backward to the starting position. An adhesion (pull-off) force which was the force that pulled the SPM probe back from the CSD surface was measured. For each sample, the force-distance profile was measured for 20 points on the CSD surface.

The phase image was observed by tapping mode of AFM. The samples were prepared as above described. The experiment was performed in the area of 5 x 5 μm^2 on CSD attached glass slide in the liquid cell using force modulation probe (Model Etalon, NT-MDT, Moscow, Russia) made up of silicon (Si). Topological and phase graphics were obtained. Phase shift on CSD particle or CSD cluster was

observed by comparing their phase angle with the phase angle on acrylic surface. The observed phase shift for all binding liquid concentrations was compared.

3.1.2. CSD characterization

Liquid uptake ability of CSD

Liquid penetration or uptake rate can be evaluated by capillary method. In this study, the liquid penetration rate of binding liquids, as shown in Table 2, into CSD was measured using modified Enslin apparatus [82, 108]. The apparatus was set up with a glass funnel with 60 mm diameter connecting with 5 mL pipette as shown in Figure 3. A weighing balance with 1 mg resolution (Model ML303, Mettler Toledo, Greifensee, Zürich, Switzerland) was used for determination of liquid weight decrease on the pipette side. Liquid penetration rate of water and binding liquids into MCC, a common extrusion-spheronization aid was also measured for comparison, respectively.

First, liquid levels in both sides were equally adjusted before the test. Then, CSD about 0.6 g was manually packed into a plastic tube having a number of 1 mm pores and laid with No.1 filter paper (Whatman International, Limited., Maidstone, England) to avoid silica particle from leakage. Due to aggregation of CSD, CSD was passing through a sieve No.20 before packed. The filled tube was gently tapped against the table for 5 times before placing on the funnel. After that, the liquid in the pipette was allowed to flow and penetrate into pack CSD in the tube. The weight decrease was measured every 1 s by the weighing balance and data was sent to a computer connected via RS-232 port. The data points included in the slope calculation varied between 8-125 points depending on liquid penetration rate. The fast penetration gave a low number of data points in this experiment i.e. penetration of hexane or the experiments of MCC. This should be noted that the calculated slope was obtained from the profile where the linearity was observed with R^2>0.98. The end of this experiment was considered when constant weight was observed or

the water in the pipette was exhausted. The experiment was repeated 8 times for each liquid sample.

A liquid penetration rate was the weight decrease of liquid determined on the pipette side per unit time. Presumably, the weight decrease was due to that the liquid was adsorbed by CSD. The slope of the plot between square of weight decrease against time was calculated as the value of $\frac{C\rho^2\sigma_s \cos\phi}{\eta}$ according to modified Washburn equation (Equation 6).

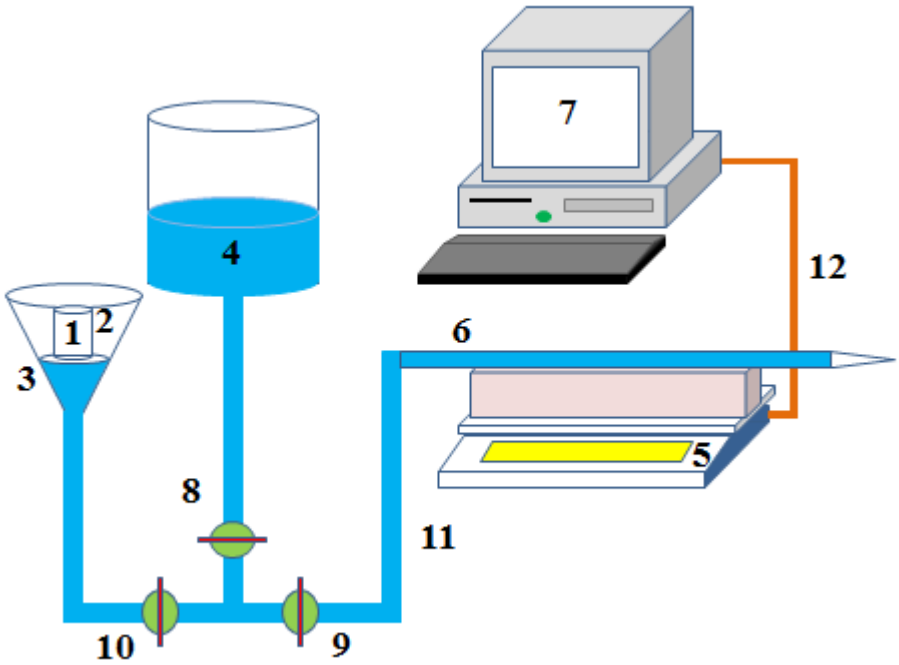

Figure 3 Schematic diagram of Enslin apparatus modified from Caprez et al. [82] and Ferrari et al. [108]: 1) Perforated tube, 2) Funnel, 3) Supporting screen, 4) Liquid reservoir, 5) Balance (d=0.001 g), 6) Pipette, 7) Computer, 8, 9, 10) Valve , 11) Silicone tube, and 12) RS-232-Serial cable

From the modified Washburn equation, contact angle between liquid and solid could be calculated. Hexane (0.31 mPas of viscosity [109], 0.6594 g/mL of density [109] and 18.43 mN/m of surface tension [110]) is considered as the liquid which can

completely wet the substrate [111, 112]. Hence phi (ϕ) is zero and cos phi is 1. Therefore C, material constant could be calculated [111]. Contact angle between liquid and solid samples could be calculated.

$$m^2 = (\frac{C\rho^2\sigma_s \cos\phi}{\eta})t \qquad \text{Equation 6}$$

Where m mass of liquid uptake (g)

ρ density of liquid (g/cm^3)

C material constant (cm^5)

σ_s liquid surface tension (mN/m)

ϕ contact angle (degree)

η liquid viscosity (mPa·s, mNs/m^2)

t contact time (s)

Liquid binding ability of CSD

Desorption of water and surfactant from wet mass was studied via thermo gravimetric analysis. Accurately weighed amount of 30 mg of wet mass containing 1: 2 of CSD: binding liquids, which shown in Table 2, was placed in the 40 µL alumina crucible. Then, it was heated from 50 to 600° C with 10° C/min heating rate using thermo gravimetric analyzer (Model TGA/SDTA851^e, Mettler Toledo, Greifensee, Zürich, Switzerland) with STARe software version 13.00 (Mettler Toledo, Greifensee, Zürich, Switzerland). Nitrogen gas was flushed at 40 mL/min during experiment. The thermograms were normalized before doing first derivatization because the sample weight was not constant. Maximum rates of weight decrease were identified. Temperature at the maximum weight decrease rate is justified as desorption temperature (T_{desorp}) [78, 113, 114].

In addition, the experiment was carried out for MCC wet mass containing 1: 1.2 of MCC: binding liquids as shown in Table 2, 1: 2 of CSD: water, 2.2 mg untreated CSD powder and 10 mg HCO-40.

The experiments were performed in triplicate. If T_{desorp} was shifted, it may indicate interaction between silicon dioxide and other molecules [13, 114, 115]; between surfactant and substrate [79] .

3.1.3. Wet mass characterization

Rheology of wet mass

It has been reported that there was some relation between MCC wet mass rheology and pelletization by extrusion-spheronization [18, 20]. In the present study, CSD wet mass for pellet preparation could not be tested using the plate-plate rheometer because sample was broken and slipped in preliminary test. With this limitation, instead of wet mass, CSD pastes prepared by dispersion of CSD in HCO-40 solutions were used. Solid content of the CSD paste was maximized at 15% w/w. The compositions of the paste are shown in Table 3. Rheology was tested with the plate-plate rotational rheometer (Model Gemini 200HR^{Nano} Rotonetic^{TM} Drive2, Malvern–Bohlin Instruments, Malvern, Worcestershire, UK). This rheometer was controlled by Bohlin software version R6.51.0.3 (Malvern–Bohlin Instruments, Malvern, Worcestershire, UK).

A 25 mm serrated plate–plate (Malvern–Bohlin Instruments, Malvern, Worcestershire, UK) was used in viscoelastic measurements to prevent sample from slippery. The paste of approximately 2 g was placed on the lower plate. After that, the upper plate was moved downward until the distance between the plates was 2 mm. The excess paste was trimmed out. During the experiment, temperature was controlled at 25°C by water bath temperature controller (Julabo F12-ED, Julabo GmbH, Seelbach, Germany). All samples were equilibrated on the plate at 25 °C for 2 min before testing was started.

Table 3 CSD pastes rheological studied

Dispersing liquid concentration (% w/w)	Stock solution (12.5% w/w HCO-40), g	Water q.s. (g)	CSD (g)
Water	0	50	8.8
0.1	0.4	50	8.8
0.5	2	50	8.8
1	4	50	8.8
1.5	6	50	8.8
2	8	50	8.8
2.5	10	50	8.8
3	12	50	8.8
5	20	50	8.8
7.5	30	50	8.8
10	40	50	8.8
12.5	50	NA	8.8

The dispersing liquid was prepared by dilution of stock solution i.e. 12.5% w/w HCO-40 to the desired concentration. The CSD powder was mixed with 50 g of dispersing liquid using mortar and pestle for about 2 min. Then, the paste was packed in the airtight glass containers before the test.

To evaluate strength of paste structure, amplitude sweep was tested with deformation range from 0.01% to 100% strain. The test was repeated three times for each sample. An appropriate stress for frequency sweep test was selected from the amplitude sweep test. Relatively low range of stress in linear viscoelastic range (LVR) or linear storage modulus (G') was considered for selection of stress value.

Frequency sweep test was performed with selected stress value. The totals of 41 points of frequency sweep from 0.1 to 100 rad/s range were recorded. Storage or

elastic modulus (G'), and loss or viscous modulus (G'') at each shear rate were obtained. Complex modulus and damping factor were calculated simultaneously, via Equation 7 and Equation 8, respectively, with the G' and G'' value. An impact of change in viscoelastic properties of the paste due to varied HCO-40 concentrations were discussed in regarded to processability.

$$\vec{G}^* = \vec{G}' + \vec{G}'' \qquad \text{Equation 7}$$

$$\textit{Damping factor} = G''/G' \qquad \text{Equation 8}$$

3.2. Pellet preparation and characterization

3.2.1. Pellet formulations

For each formulation, 150 g of colloidal silicon dioxide (CSD) was used as an extrusion-spheronization aid. Binding liquids were polyoxyl 40 hydrogenated castor oil (HCO-40) solutions in deionized (DI) water with varied concentrations as shown in Table 4. An amount of the binding liquid was two times the CSD weight in the formulations.

3.2.2. Pellet preparation

Pellets were prepared by extrusion-spheronization process. HCO-40 and water were weighed and mixed in a 500 mL beaker in order to prepare the binding liquid. CSD and the binding liquid were mixed in a planetary mixer (Model AR400, Erweka, Heusenstamm, Germany) for 20 min. During the first 10 min, mixing was performed at 6 rpm speed. After that, mixing speed was increased to 30 rpm for further 10 min. The process was stopped and scratched with the spatula, if need.

Table 4 Pellet formulations studied

Formulation No.	Concentration of HCO-40 in binding liquid (% w/w)	CSD (g)	Binding liquid (g)
1	0.1	150	300
2	0.5	150	300
3	1	150	300
4	1.5	150	300
5	2	150	300
6	2.5	150	300
7	3	150	300
8	5	150	300
9	7.5	150	300
10	10	150	300
11	12.5	150	300

Extrusion

Wet mass was extruded using ram extruder. The wet mass about 55 g was manually packed into a 25.4 mm internal diameter and 200 mm height barrel assembled with a 1 mm diameter and 4 mm length die. A piston was forced to move downward in the barrel by a crosshead of a universal testing machine (Model LR50K plus, Lloyd Instrument, Bognor Regis, West Sussex, UK) with Nexygen plus software version 3.0 (Lloyd Instrument, Bognor Regis, West Sussex, UK). The moving speed for contact the wet mass was 100 mm/min. Then the extrusion force was begun to record, after 5 N of preload was detected. Extrusion process was performed at a piston speed of 200 mm/min. Extrusion forces as force-displacement profiles were recorded via computer which was connected to the 50 kN load cell of the universal testing machine. The piston displacement was set at 150 mm with about 155 mm height of packed wet mass in the barrel. After extrusion, about 5 mm

of plug remained. From the force-displacement profile, each extrusion force was calculated by average force data from peak to the end of the extrusion process. For each batch, 8 extrusions were carried out. An average of extrusion force data from 24 extrusions for 3 batches was reported.

Spheronization

About 380–400 g of extrudate was collected and placed onto a 320 mm radial cut plate spheronizer (Model S320, Aeromatic Fielder, Eastleigh, Hampshire, England). Spheronization was operated at 225 rpm for 10 min. Then, pellets were dried in a hot air oven (Capacity 100 kg, Charatchai Machinery, Limited Partnership, Bangkok, Thailand) at 50° C for 12 hours. Experiments were repeated in triplicate. Pellets were kept in polyethylene bag before further characterization.

3.2.3. Pellet characterizations

Pellet size and size distribution evaluation

Size and size distribution of dried pellets were analyzed using sieve method. The experiment was carried out using 80 g of pellets placed on a sieve set with $\sqrt{2}$ progression i.e. 0.35, 0.50, 0.71, 1.0, 1.4, 2.0 mm (mesh No. 45, 35, 25, 18, 14, 10). The sieve set was shaken on a sieve shaker (Model O: FT-200M, Filtra, Barcelona, Spain) for 10 min. Percent under size was calculated and plotted on probability-log scale against the sieve size. Geometric mean and standard deviation were determined and reported for pellet size and size distribution, respectively. Geometric standard deviation was calculated from pellet size at 16% of probability scale.

Pellet yield

Pellet yield was obtained from two consecutive sieves i.e. sieve No. 18 and 25. The pellet size range 0.71-1.4 mm was included in yield calculation, each batch. The weight of pellets in two main consecutive sieve size was also reported.

Pellet shape

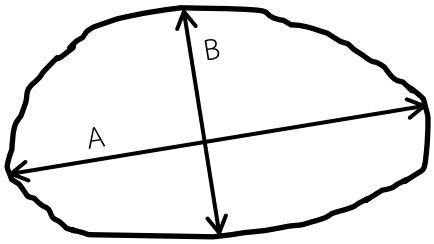

Figure 4 Maximum Feret diameter of particle (A) and Feret diameter at 90 degree to the maximum Feret diameter (B)

Images of 500 pellets from the modal size range of each batch were projected by stereo microscope (Model SMZ 745T, Nikon Corporation, Tokyo, Japan). The maximum of value of Feret diameter (maximum Feret diameter) and the length that projected 90 degree across the maximum Feret diameter (Feret diameter at 90 degree) were measured by using NIS element basic research software version 3.2 (Nikon Corporation, Tokyo, Japan). Aspect ratio was calculated by dividing maximum Feret diameter by Feret diameter at 90 degree according to equation 9.

Aspect ratio = Maximum Feret diameter (A)/ Feret diameter at 90 degree (B)

Equation 9

Pellet morphology

Image of pellets in modal size was captured by stereo microscope (Model SMZ 745T, Nikon Corporation, Tokyo, Japan) with magnification of 0.67x.

Morphology of pellet samples in the size range of 0.71 – 1.0 mm were investigated using scanning electron microscopy (Model 6610LV, Jeol, Tokyo, Japan). Surface morphology of pellets was investigated at 70x and 20000x; and their cross-section were observed at 20000x. Prior to investigation, the samples were fixed on brass stub using the carbon paste then sent for gold sputter coating. For additional information, CSD was also observed at 20000x.

Pellet mechanical strength

Pellet mechanical strength was tested by texture analyzer (Model TA-XT plus, Stable Micro Systems, Godalming, Surrey, UK) using 5 kg load cell. This equipment was operated using Exponent software version 6.1.8.0 (Stable Micro Systems, Godalming, Surrey, UK). For each batch, 30 pellet samples in the size range of 0.71 – 1.0 mm were investigated. The 6 mm cylindrical stainless steel plunger (P/6 probe, Stable Micro Systems, Godalming, Surrey, UK) was moved down with a speed of 0.10 mm/s. The trigger force for detecting pellets was set to 0.1 g. After pellet detection, the diameter of tested pellet was recorded as strain height. Then, the plunger was moved down for a certain distance, i.e. 10% strain of the pellet. After that, the plunger was returned to the starting position. Force-time profiles were recorded after pellet detection until plunger was returned to the starting position. The fracture force of pellet was determined based on the first peak with peak threshold which was set to 1 g. The pellet tensile strength (σ) was calculated by Exponent software using equation 10 [116] in which the pellet size was taken into account. The mechanical strength of 30 pellets per batch was then averaged.

$$\sigma = 1.6F/\pi D^2 \qquad \text{Equation 10}$$

σ = tensile strength (MPa)

F = fracture force (N)

D = pellet diameter (strain height, mm)

Pellet true density

True density of pellets was determined with samples in the modal size range of the third batch depending on the formulation. The pellets about 3–5 g were placed in the oven at 100°C until constant weight was obtained. The pellets true density was evaluated by gas (helium) pycnometer (Model Ultrapycnometer 1000, Quantachrome, Boynton Beach, Florida, USA).

3.3. Interaction between CSD and surfactant in pellets

3.3.1. Infrared spectroscopy

Pellets were ground using a porcelain mortar and pestle. A small amount of ground pellets was mixed with potassium bromide (KBr). The mixture was pressed into a disc by hydraulic pressing machine at 8 ton force. A compressed disc was placed in sample holder and investigated by infrared spectrometer (Model Nicolet iS10, Thermo Scientific Instrument, Waltham, Massachusetts, USA) with Omnic software version 8.2.0.387 (Thermo Fisher Scientific Inc., Waltham, Massachusetts, USA). After background collection, 32 scans of infrared spectra of each sample were collected with 4 cm^{-1} resolution. Each sample was investigated in triplicate. CSD as received and CSD which was mixed with water and dried in oven at 50°C for 2 h, and HCO-40 were used as references.

3.3.2. Solid state nuclear magnetic resonance spectroscopy

Pellets were ground by porcelain mortar. Ground pellets were investigated using solid state nuclear magnetic resonance spectroscopy (Model Ascend 400WB, Bruker Corporation, Billerica, Massachusetts, USA) operated via Bruker Topspin software version 3.2 (Bruker Corporation, Billerica, Massachusetts, USA). Pellets from all formulations were subjected to the proton magic angle spinning NMR (^{1}H MAS NMR) and silicon cross-polarization magic angle spinning NMR (^{29}Si CP MAS NMR) via solid state nuclear magnetic resonance spectroscopy. CSD as received and CSD which was mixed with water and dried in oven at 50°C for 2 h, were used as references.

For ^{1}H MAS NMR, magic angle spinning technique was used with a transmitting frequency of 400 MHz. A sample was placed in 4 mm zirconia rotor with Kel-F cap. A chemical shift was calibrated using adamantane amount of 1.87 ppm. The experiment was performed with a spinning rate of 10000 Hz.

For ^{29}Si CP MAS NMR, the experiment was performed with cross polarization/magic angle spinning technique at a transmitting frequency 79.5 MHz. A

sample was placed in 7 mm zirconia rotor with Kel-F cap. An amount of dimethyl-5-silapentane sulfonate of 1.87 ppm was used in chemical shift calibration. A spinning rate was set at 5000 Hz with 4000 μs of contact time

CHAPTER IV
RESULTS AND DISCUSSIONS

1. Characterization of input materials

Input materials i.e. HCO-40 solutions, CSD and dispersions or wet masses were characterized in order to understand and identify attributes of materials that were critical to formation of CSD pellets by extrusion-spheronization.

1.1. Binding liquid characterizations

The viscosities, surface tension and density of solution are shown in Table 5. Viscosities of the solutions were slightly increased with increasing HCO-40 concentrations. However, their surface tension was rather constant because the concentration of HCO-40 solutions used in this experiment was higher than its measured critical micelle concentration of 0.036% w/w and reported value of 0.039% [5].

Table 5 Surface tension, viscosity and density of HCO-40 solutions

HCO-40 Concentration (% w/w)	Surface tension, mN/m Mean (SD), n=3	Viscosity, mPas Mean (SD), n=3	Density (g/mL), n=2
water	72.587 (0.046)	1.98 (0.02)	0.996
0.1	44.177 (0.115)	2.04 (0.01)	0.996
0.5	42.884 (0.116)	2.04 (0.01)	0.996
1	43.064 (0.031)	2.09 (0.01)	0.997
1.5	42.878 (0.058)	2.12 (0.02)	0.997
2	42.936 (0.035)	2.18 (0.02)	0.998
2.5	42.882 (0.006)	2.21 (0.02)	0.998
3	42.789 (0.057)	2.23 (0.01)	0.998
5	42.693 (0.007)	2.43 (0.02)	1.000
7.5	42.548 (0.050)	2.54 (0.02)	1.003
10	42.434 (0.026)	2.71 (0.01)	1.005
12.5	42.063 (0.054)	2.75 (0.00)	1.007

Small-angle X-ray scattering (SAXS) patterns are shown in Figure 5-Figure 8. The scattering pattern of solution samples showed oscillation with low intensity. The oscillating characters depend on particle size and size distribution. The profiles of 0.5 – 12.5% w/w HCO-40 solutions showed similar pattern of poly-disperse nanoparticles, while there was no characteristic scattering pattern for 0.1% w/w.

For suspensions, wet masses and dried pellets, the oscillating character was not found, perhaps because the q-range i.e. the sample to detector distance was not suitable for the particle size of the measured systems which contained CSD particle. In addition, very wide size distribution of particles in the measured system could smear the scattering profile [102].

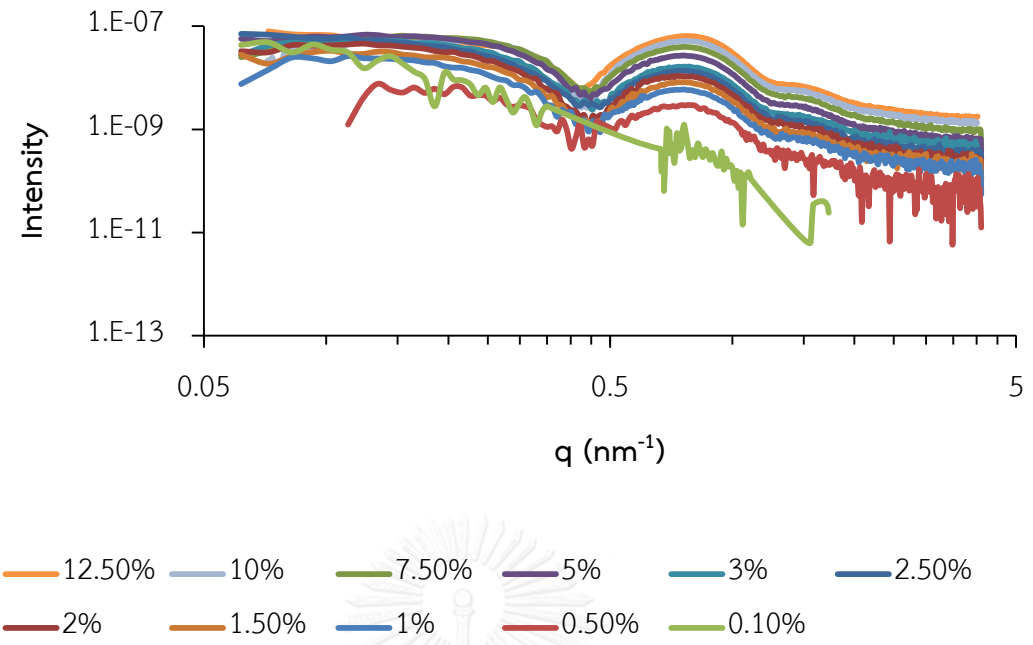

Figure 5 SAXS patterns of the HCO-40 solution of varied concentrations

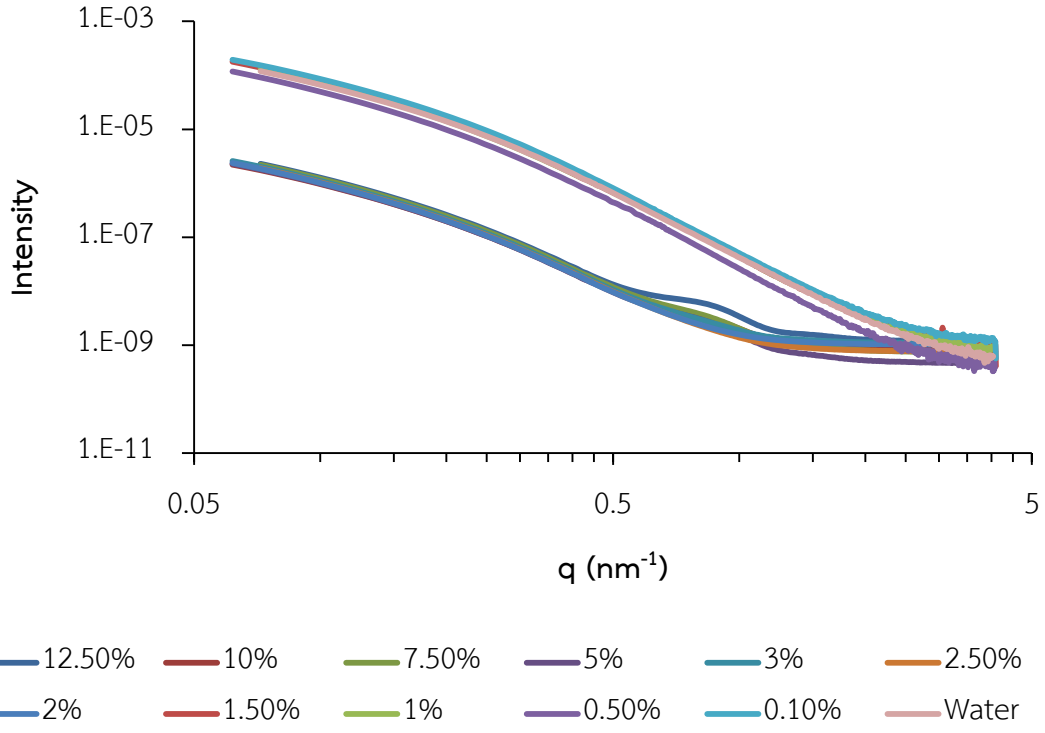

Figure 6 SAXS patterns of suspensions of 1% w/w CSD in the HCO-40 solution of varied concentrations

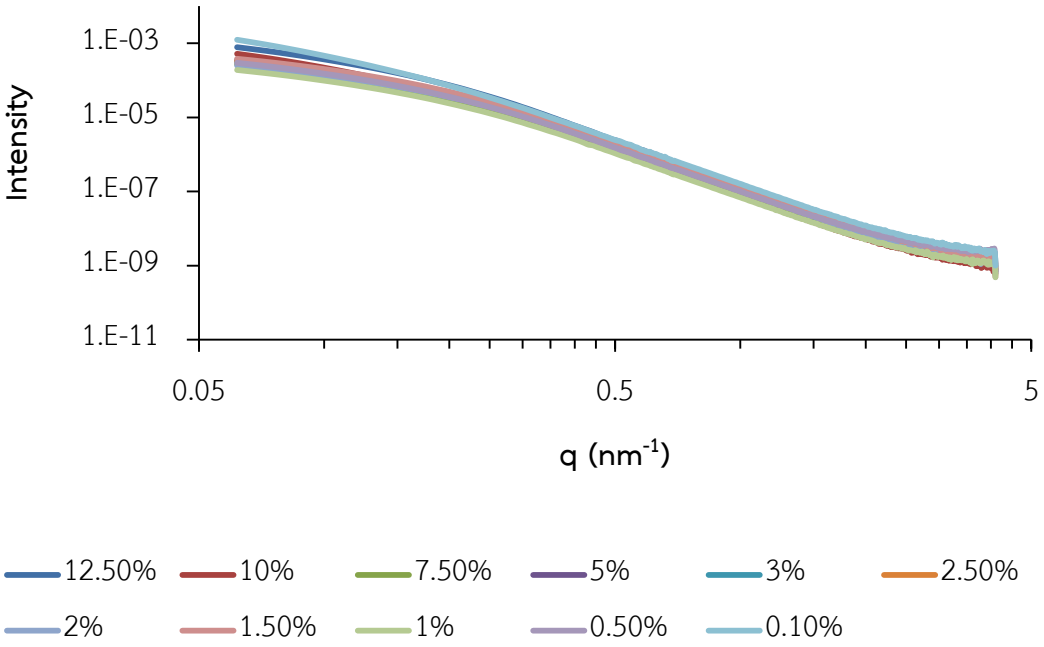

Figure 7 SAXS patterns of wet mass prepared from CSD and the HCO-40 solution of varied concentrations

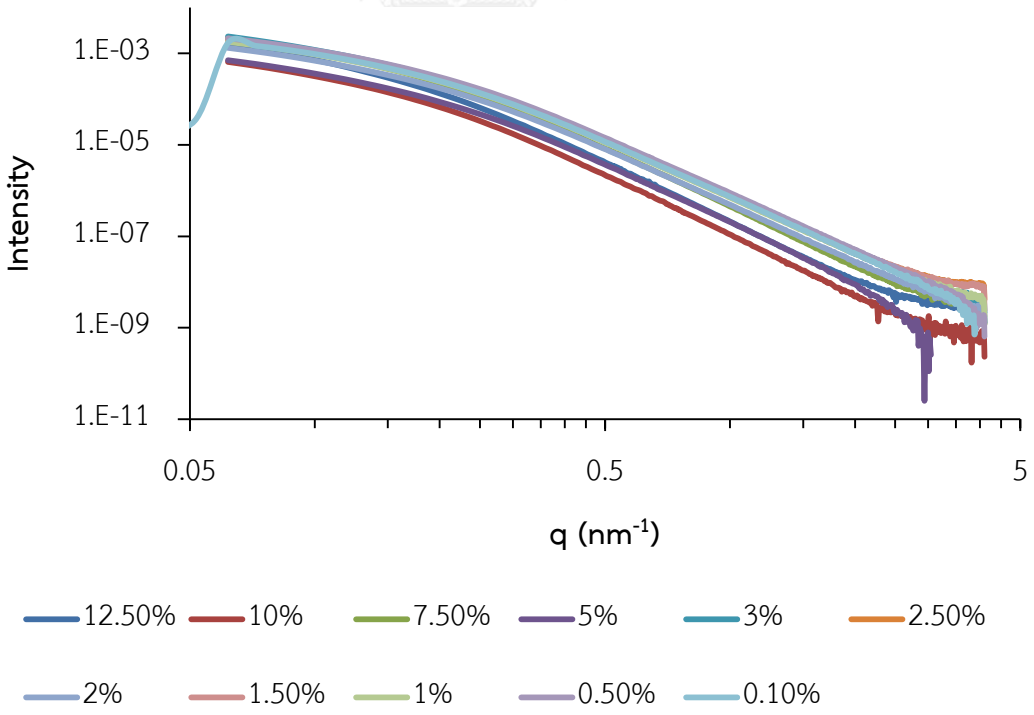

Figure 8 SAXS patterns of dried CSD pellets with varied concentrations of binding liquid

Table 6 Dimensionality of particles from according to Porod's law

HCO-40 concentration (% w/w)	Slope from Porod's law			
	Solution	Suspension (1% CSD)	Wet mass (33% CSD)	Dried pellets
0.1	-5.2	-3.9	-3.9	-4.1
0.5	-3.4	-4.1	-3.9	-4.1
1	-4.1	-4.1	-3.9	-4.1
1.5	-4.4	-4.1	-4.0	-4.1
2	-4.2	-1.3	-4.0	-4.1
2.5	-4.3	-1.7	-3.9	-4.1
3	-4.3	-1.6	-3.9	-4.2
5	-4.3	-2.9	-4.0	-4.3
7.5	-4.3	-2.5	-4.0	-4.4
10	-4.5	-2.3	-4.0	-4.5
12.5	-4.1	-2.7	-4.1	-4.4

Table 7 Radius of gyration (R_g) and geometrical radius (R) of the particle in HCO-40 solutions

HCO-40 Concentration (% w/w)	R_g from Guinier fit (nm), n=1	Geometrical radius of micelles (micelles size, nm)
0.1	NA	NA
0.5	5.9	7.6
1	5.0	6.5
1.5	5.3	6.9
2	5.9	7.6
2.5	6.4	8.3
3	4.8	6.2
5	4.6	5.9
7.5	3.9	5.1
10	4.0	5.1
12.5	5.0	6.5

NA: none of valid R_g

The slope of the plot between ln (I) versus ln (q) for q value of 0.7 – 1.4 nm^{-1} was varied for solution (-3.4 to -5.2), suspensions (-1.3 to -4.1), wet masses (-3.8 to -4.0) and dried pellets (-4.0 to -4.4), shown in Table 6. This indicated that for the solutions containing 1.0 – 12.5% w/w HCO-40, the structure of particles were smooth surface nanoparticles of micelles while in the solution containing 0.5% w/w HCO-40, the particles were in clusters with non-smooth surface. At the very low concentration, the slope could not be explained by Porod's law.

When there was CSD particles in the samples i.e. suspensions in HCO-40 solution of low concentration, wet masses and dried pellets, the slope was around -4 suggesting the smooth surface nanoparticles in the samples. It could be resulted

from dimensionality of CSD particles having colloidal size (7 – 16 nm [5]), rather than the dimensionality of micelles which scattered with low intensity. For the suspensions with 2.0% w/w and higher HCO-40, the slope varying around -1 to -3 might be explained by complex structures present in the samples. It was likely that the structures in these samples were in 1-dimensional (line) or 2-dimensional (planar) system. The oscillating pattern observed in the solution samples containing micelles was markedly observed for the suspension with 12.5% w/w HCO-40, shown in Figure 6.

Brambilla et al. reported a slope as a coefficient value which showed in the form of positive value to indicate the hybrid silica structure. The coefficient value of 1 to 2 indicated fern-like structure and that of 2 to 3 indicated rough surface structure of silica. The coefficient value of 4 showed dense and uniformed particles [106]. Therefore, CSD particles in suspension which were dispersed at 2.0% w/w and higher concentration may be arranged their structure similar to what has been described earlier.

The micelle size in term of geometrical radius of the spherical particle, R, determined in the solution samples was in the nanometer-size of 5.0 – 8.2 nm, as shown in Table 7, and wide size distribution, regardless of HCO-40 concentration.

Generally, it was unclear from SAXS data that whether or not the dimensionality and the size of micelles with or without CSD in the systems would affect the formation of CSD pellets by varying concentration of HCO-40.

Interaction between HCO-40 and CSD surface

Image of CSD surface on glass slide in the HCO-40 solutions obtained from contact mode and tapping mode, are shown in Figure 9 and Figure 12, respectively.

The image of CSD clusters from contact mode (Figure 9) and tapping mode (Figure 12) AFM were not different whether they were in the water or in the HCO-40 solutions. Surface roughness was observed in all samples.

The image area and resolution was limited by roughness of the sample's surface. The CSD powders appeared to form clusters on the glass slide. In contact mode AFM topology, the lighter colored area was a CSD cluster. The varied color present on the contact mode AFM-friction image indicated different friction. In tapping mode AFM-phase image, the darker color was the CSD cluster.

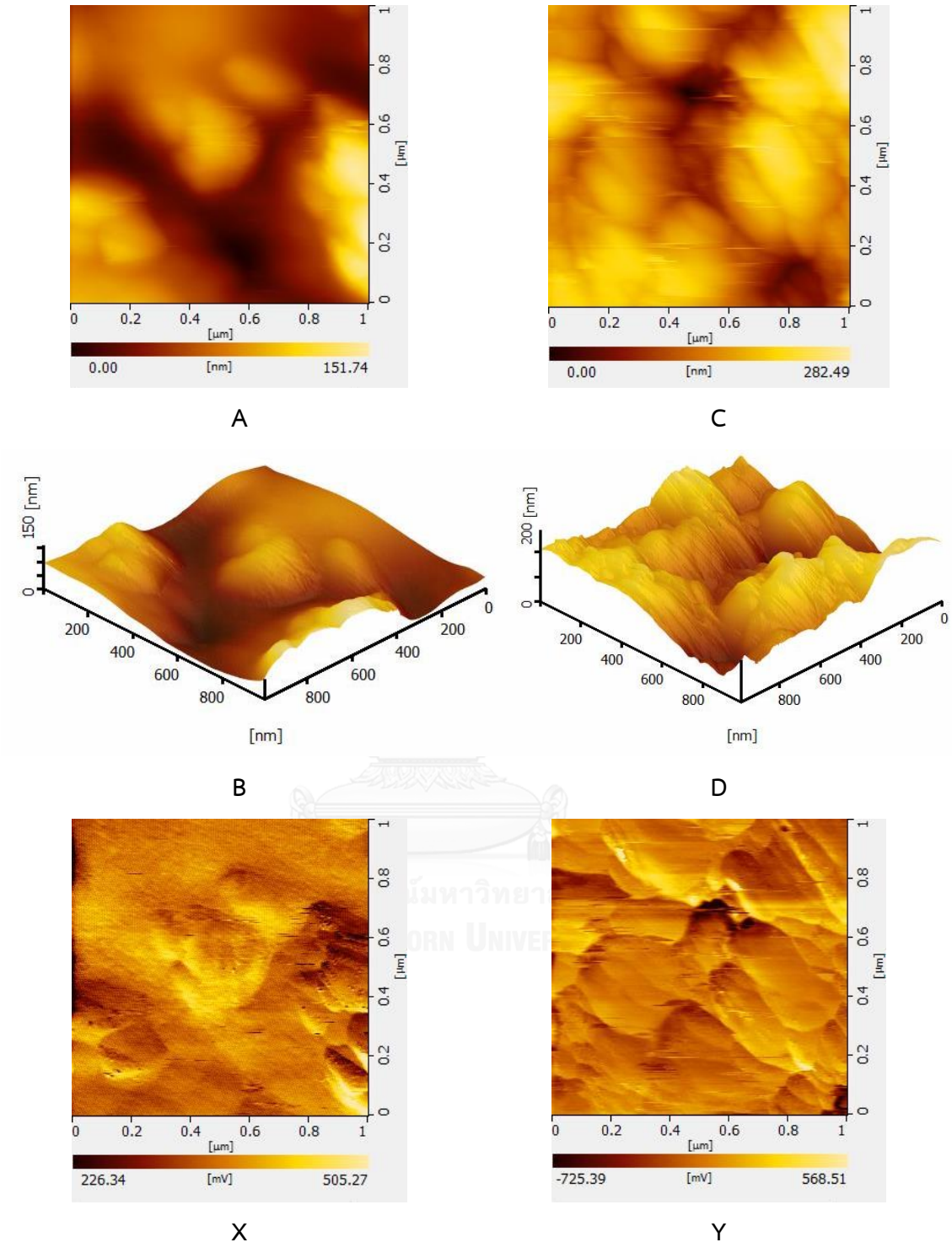

Figure 9 Contact mode AFM-topological images of CSD surface: 2-dimention (A), 3-dimension (B) in water; 2-dimention (C), 3-dimention (D) in 2.5% w/w HCO-40 solution and friction image in water (X); friction image in 2.5% w/w HCO-40 solution (Y)

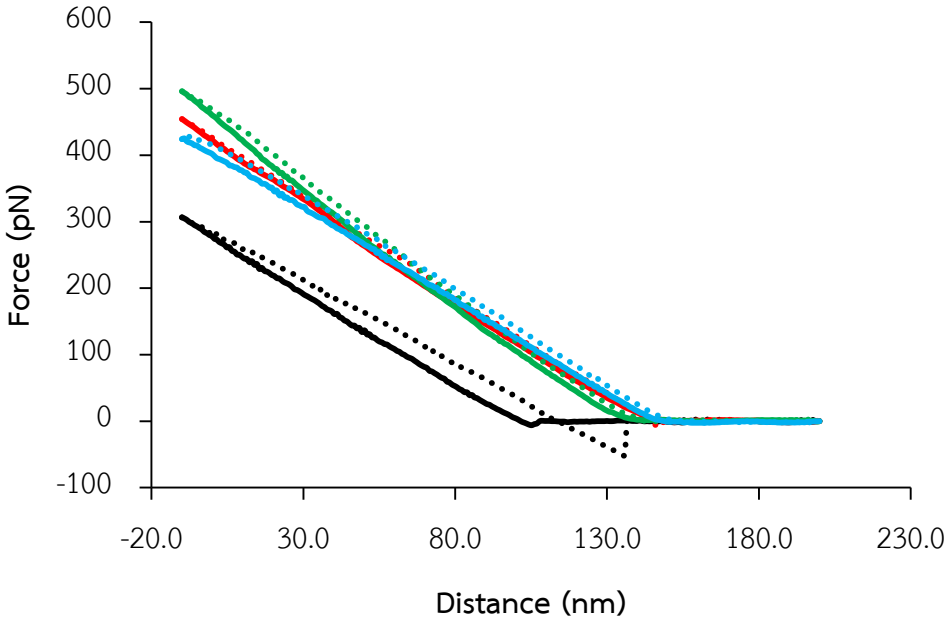

Figure 10 Force-distance profile obtained from contact mode AFM, during approach (solid line) and retraction (dot), in liquid media which were water (black) and HCO-40 solutions at concentration 0.1% w/w (red), 2.5% w/w (green), 12.5% w/w (light blue)

Table 8 Force measured in AFM force-distance experiments

HCO-40 concentration (% w/w)	Attractive (Snap-in) force, pN Mean (SD), n=20	Adhesive (pull-off) force, pN Mean (SD), n=20
water	-6.19 (4.07)	-36.75 (15.72)
0.1	-1.27 (1.15)	-8.50 (13.11)
0.5	-1.24 (0.86)	-5.32 (4.36)
1	-1.34 (0.97)	-1.27 (1.41)
1.5	-1.80 (0.85)	-2.88 (2.34)
2	-1.37 (0.93)	-1.98 (2.52)
2.5	-1.36 (1.23)	-1.59 (3.33)
3	-2.23 (1.26)	-1.63 (1.63)
5	-2.06 (1.28)	-2.53 (2.16)
7.5	-0.43 (0.50)	-4.97 (3.10)
10	-0.53 (0.44)	-1.17 (1.72)
12.5	-0.67 (0.80)	-0.88 (1.73)

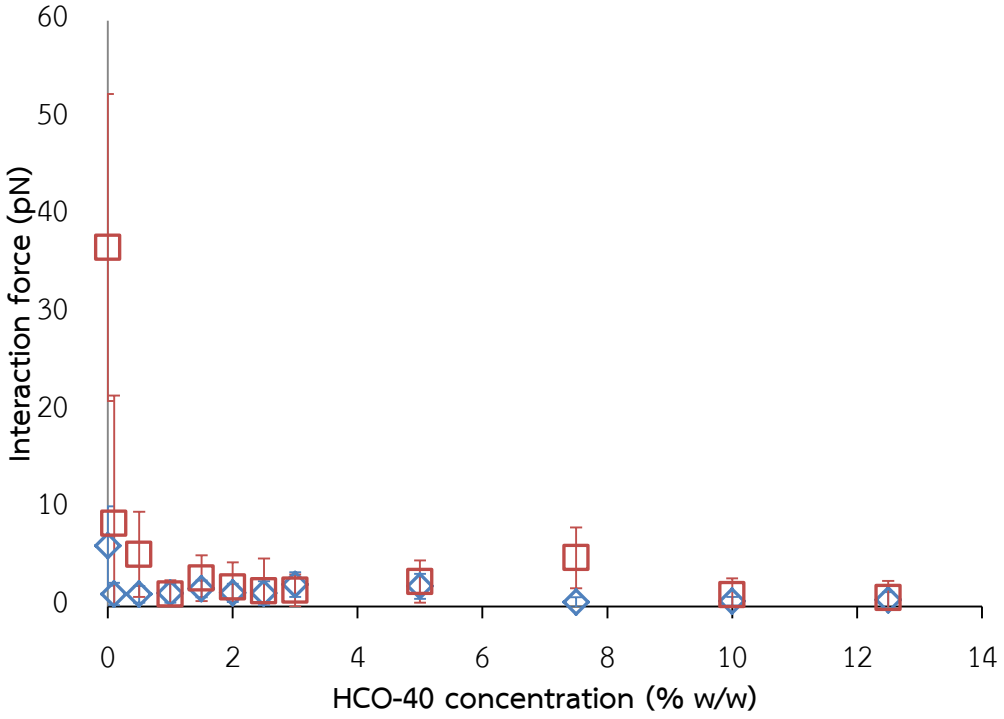

Figure 11 Force measured in AFM force-distance experiments, attractive force (◇), adhesive force (□)

The force-displacement profile (Figure 10) resulted from the AFM tip during approach to (jump-in) the CSD surface and retraction (pull-off) in the liquid medium. When the tip was deflected on the surface, the measured force was called attractive force or jump-in force. The tip remained moving upon predetermined distance. After that, the probe was pulled-off. The force that required for separating the tip from substrate was called adhesive force or pull-off force. The measured force, as shown in Table 8, is in negative value due to its direction.

High attractive and adhesive forces were observed in water. In addition, the adhesive force was higher than jump-in force and it had approximately 30 – 40 nm longer length of separation in water. The jump-in and pull-off force were markedly decreased with the presence of HCO-40 in the media. It was possible due to accumulation of HCO-40 on the CSD surface.

The tapping mode AFM-phase image, as shown in Figure 12, was of CSD cluster in water and 2.5% w/w HCO-40 solution. In the image, positive phase shift is the darker contrast with higher phase angle (z value). The analysis of phase image is demonstrated in Figure 13. The ΔZ value showed phase difference between CSD surface and acrylic polymer surface. It was observed that phase angle on CSD was higher than on acrylic surface. However, the variation was not systematically related to HCO-40 concentrations. This because micelles of HCO-40 randomly aggregate on the CSD surface or stay in the bulk solution. From this result, the tapping mode AFM phase image could not differentiate the effect of the HCO-40 concentrations.

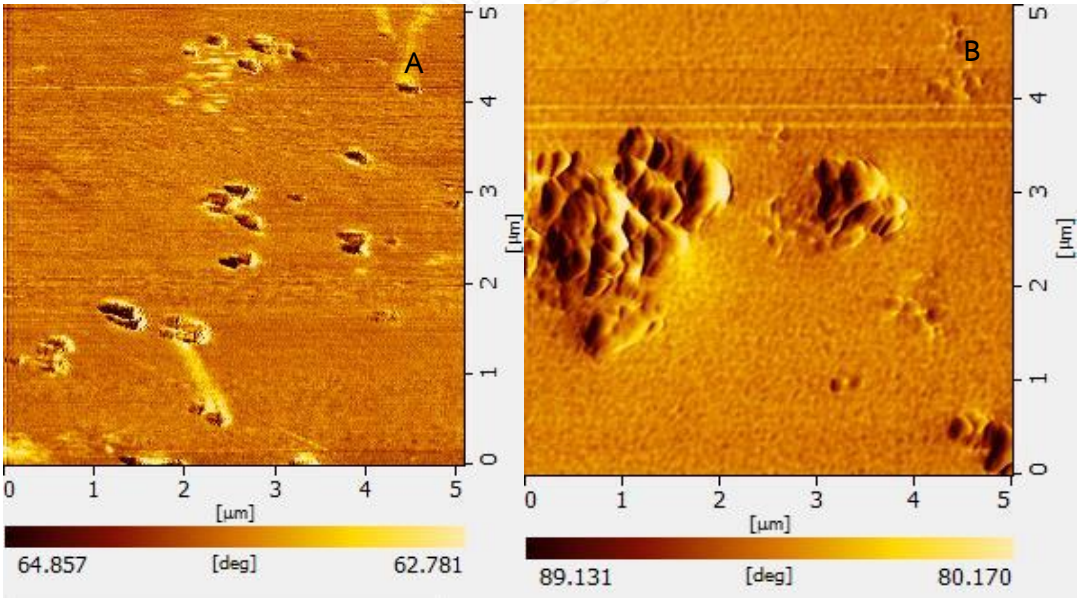

Figure 12 Tapping mode AFM-phase image of CSD sample in water (A) and 2.5% w/w HCO-40 solution (B)

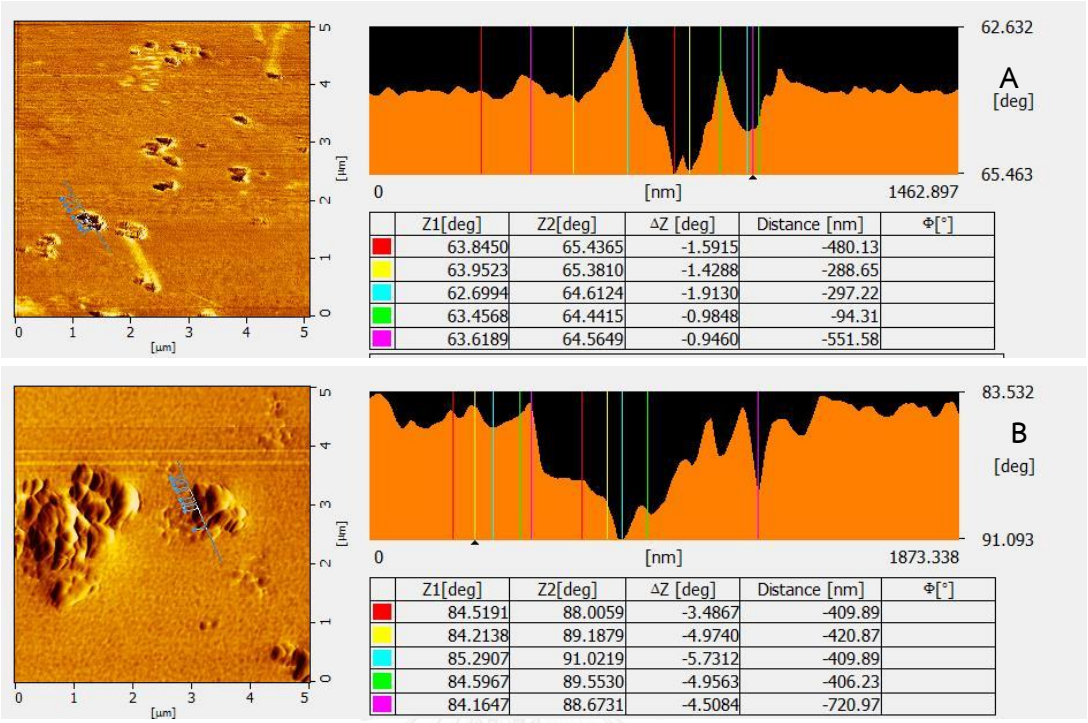

Figure 13 Tapping mode AFM-phase analysis of CSD sample in water (A) and 2.5% w/w HCO-40 solution (B)

1.2. CSD characterization

Liquid penetration properties of CSD

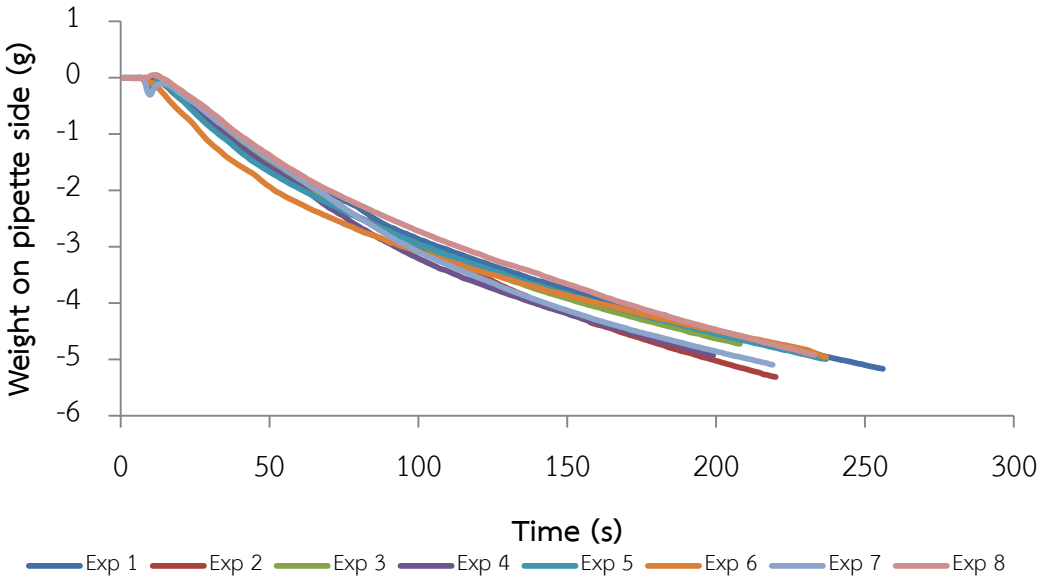

Figure 14 Weight on pipette side while liquid penetration was progressed by CSD with 2.5% HCO-40 solution; the measurement was repeated eight times

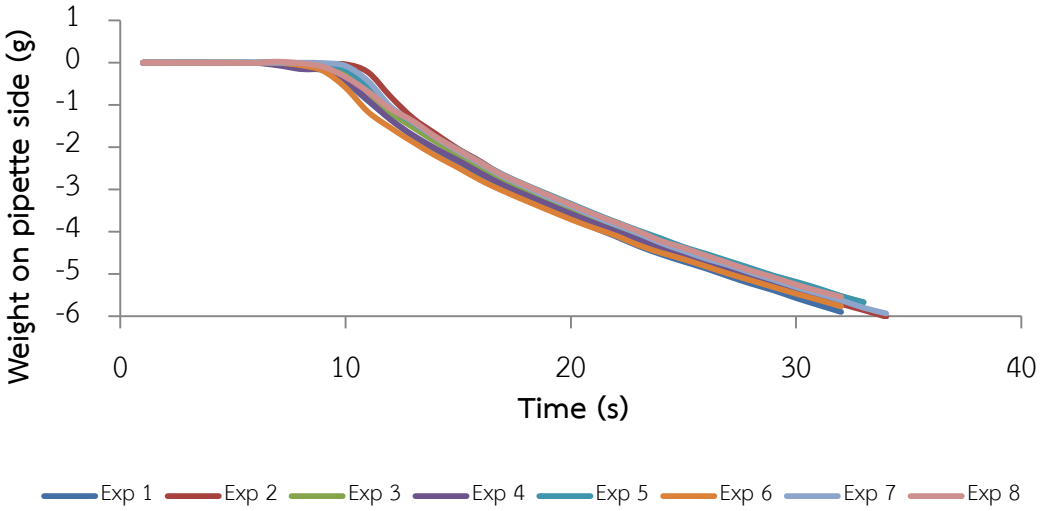

Figure 15 Weight on pipette side while liquid penetration was progressed by MCC with 2.5% HCO-40 solution; the measurement was repeated eight times

Weight decrease on pipette side was detected immediately after placing the tube on the screen in funnel (after small peak in Figure 14).

Generally, liquid weight on the pipette side was decreased as a function of time, indicating the liquid could penetrate into the packed beds. Relationship between weight decrease and time was not linear. The penetration rate (g/s) was decreased when great amount of liquid was filled in the CSD bed. The linear relationship for square of mass (m^2) of liquid uptake and time was found as shown in Figure 16. The slope and hence contact angle could be calculated according to modified Washburn equation (Equation 6).

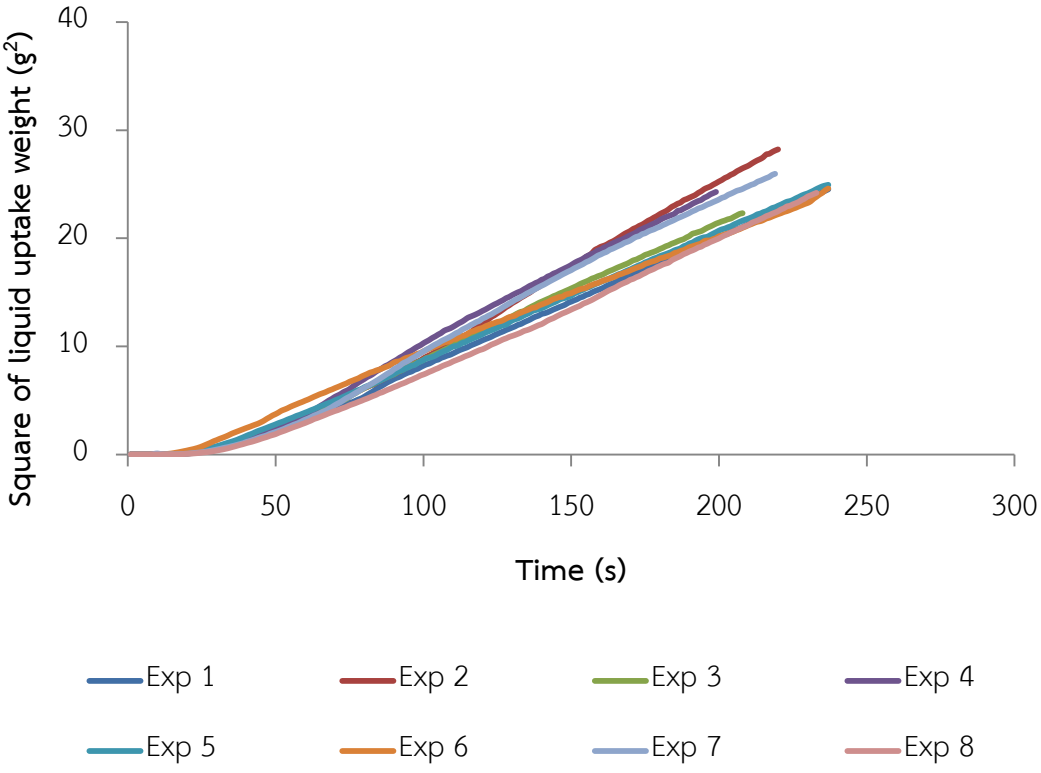

Figure 16 A profile of liquid uptake (m^2) against time for 2.5% HCO-40 with CSD

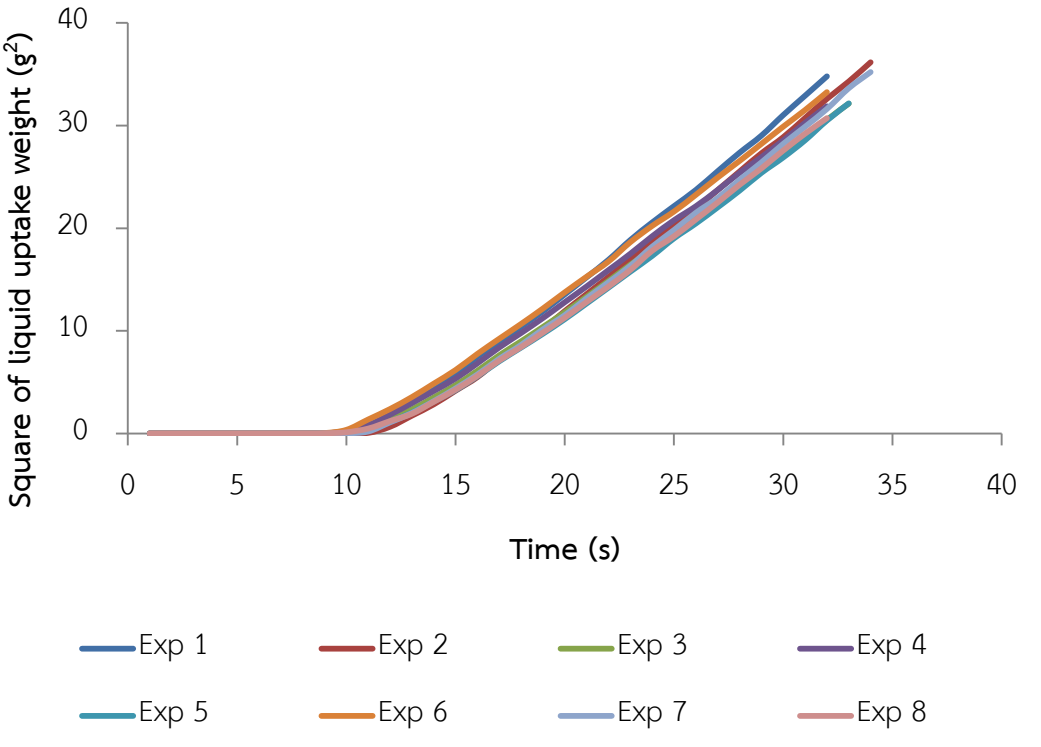

Figure 17 A profile of liquid uptake (m^2) against time for 2.5% HCO-40 with MCC

The liquid penetration ability and contact angle are shown in Table 9. Variation of the amount of liquid penetration and contact angle was high because CSD is a fluffy material which was difficult for packing into the tube resulting in inconsistent packed CSD bed and voids in the bed. Therefore, the liquid could not continuously penetrate through these voids and the penetration was delayed.

Example penetration profiles from MCC are shown in Figure 15 and Figure 17. They indicated that penetration rate from MCC was much faster than from CSD.

Table 9 Liquid uptake rate and contact angle of CSD and MCC

HCO-40 Concentration (%w/w)	Liquid uptake rate (g^2/s), mean (SD)		Contact angle (°), mean (SD)	
	CSD, n=8	MCC, n=8	CSD, n=8	MCC, n=8
0	0.085 (0.017)	2.422 (0.234)	75.4 (2.9)	0.0 (0.0)
0.1	0.077 (0.008)	1.893 (0.143)	67.2 (2.6)	0.0 (0.0)
0.5	0.104 (0.006)	1.669 (0.111)	57.7 (2.3)	0.0 (0.0)
1	0.145 (0.013)	1.429 (0.109)	39.8 (5.9)	0.0 (0.0)
1.5	0.109 (0.012)	1.597 (0.065)	54.0 (4.8)	0.0 (0.0)
2	0.134 (0.030)	1.583 (0.093)	40.5 (14.5)	0.0 (0.0)
2.5	0.133 (0.019)	1.606 (0.068)	41.4 (10.2)	0.0 (0.0)
3	0.154 (0.014)	1.344 (0.065)	28.8 (9.4)	0.0 (0.0)
5	0.090 (0.012)	1.210 (0.092)	56.5 (5.3)	0.0 (0.0)
7.5	0.085 (0.015)	0.876 (0.057)	56.7 (6.8)	0.0 (0.0)
10	0.060 (0.009)	0.720 (0.066)	65.8 (4.0)	3.1 (7.1)
12.5	0.036 (0.010)	0.519 (0.021)	75.7 (4.0)	36.1 (3.2)
Hexane	0.240 (0.080)	1.071 (0.142)	0 (as reference)	

Uptake rate of water into CSD was 0.085 g^2/s which was lower than that of the HCO-40 solution at concentrations ranging from 0.5 – 3% w/w, but higher than that

of HCO-40 solution at concentrations of 10 and 12.5% w/w. HCO-40 as a surfactant reduced surface tension of the water as shown in Table 5. The reduction of surface tension resulted in an increased liquid uptake. However, at the high concentrations of HCO-40 above 5% w/w, the uptake rate began to reduce probably because an increase in viscosity and density of the liquid as shown Table 5.

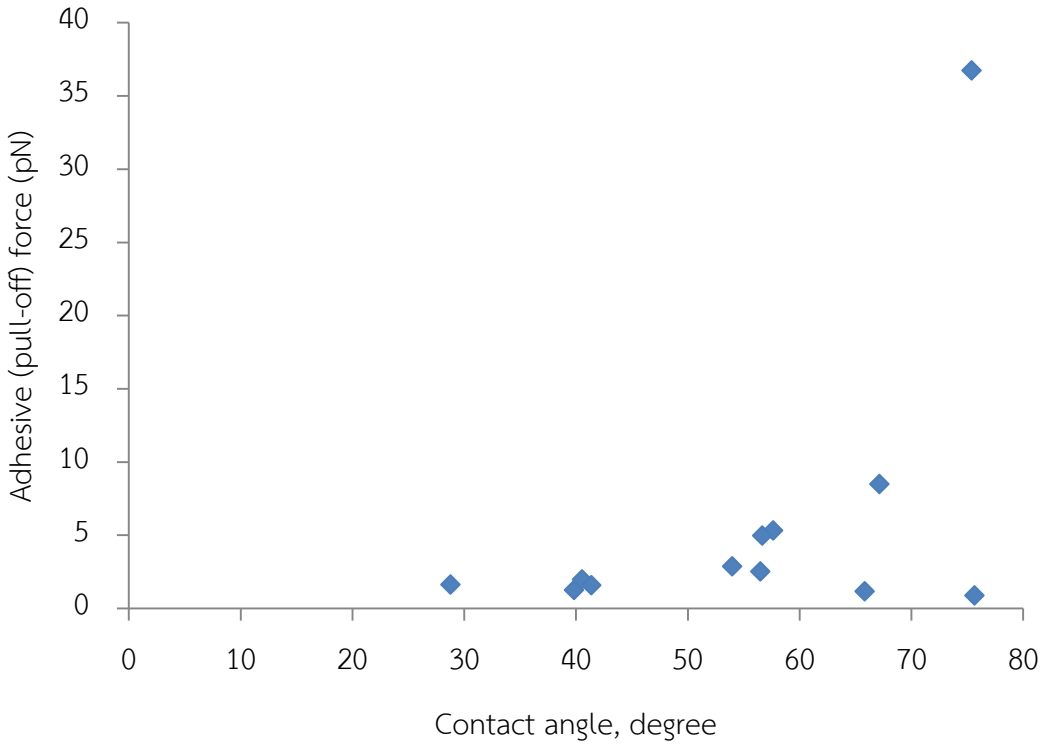

Figure 18 Adhesive force versus contact angle of the liquid on CSD surface

The calculated contact angles agreed with liquid uptake ability. The lower the contact angle or better wettability, the higher rate of penetration. Changes in contact angle of the binding liquid on the CSD surface resulted from the interaction between the liquid and CSD surface (Figure 18). The contact force based on adhesive force value measured by contact mode AFM indicated that the force was reduced by addition of HCO-40. The contact force approached to zero with 1% w/w HCO-40 and higher concentrations. A slight change in contact force at the concentration higher than 1% w/w HCO-40 could induce lower contact angle (up to

3% w/w HCO-40) and raise contact at higher concentrations. The adhesive force was reduced because HCO-40 molecules were adsorbed on to the surface of CSD.

Patist et al. [117] proposed that micellization was not static i.e. they were dynamically disintegrating and reforming. There are also surfactant monomers in the bulk solution. The disintegrated surfactant molecules and/ or surfactant monomers in the bulk could interact with CSD surface through hydrophobic interaction between hydrocarbon chain and hydrophobic siloxane group which led to exposure of hydrophilic groups i.e. polyoxyethylene group to outer surface of CSD. This assisted in penetration of water by interaction with polar group of surfactant. At the high concentration, because the micelles were stable, the free HCO-40 molecules were less available on the surface of CSD. Therefore, slow penetration rate was obtained.

The results of contact angle between HCO-40 solution and MCC surface were zero due to that the HCO-40 solution wetted the MCC bed, better than hexane which was used as a reference, and readily to penetrate into the MCC bed. The high penetration ability of water into MCC bed can be explained by hydrophilicity of MCC which contained hydroxyl groups. This allowed MCC could be wetted easily. In HCO-40 solution, hydration of MCC might be interfered with the hydrocarbon chain of the surfactant.

Liquid binding ability of CSD

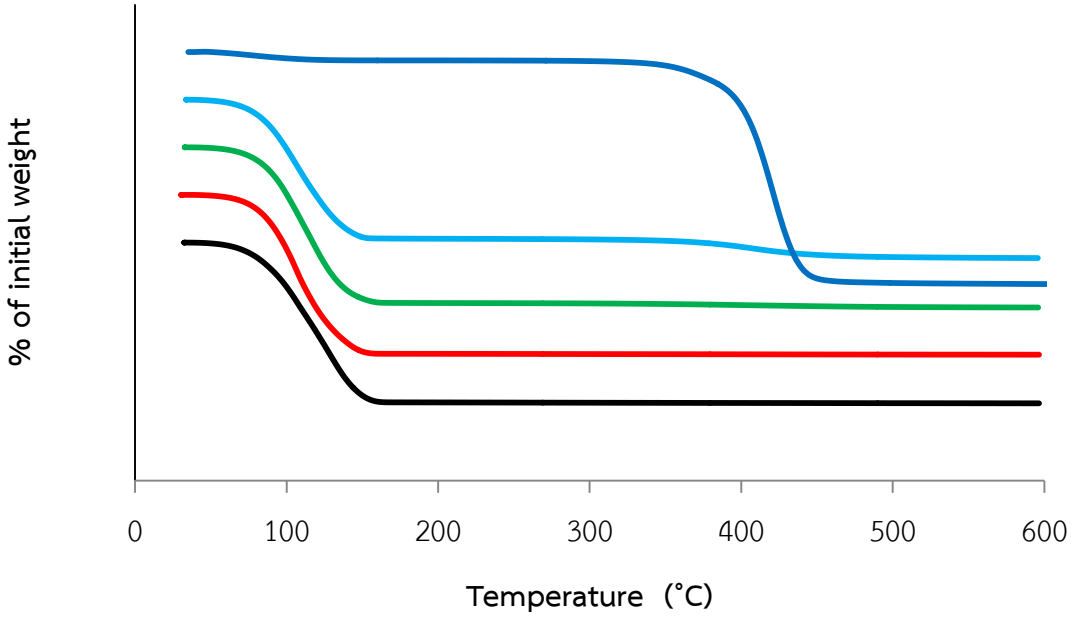

Figure 19 Normalized thermogram in the range of 50-600°C of untreated HCO-40 (blue) and the CSD wet mass made with water (black), HCO-40 solution at concentration 0.1% w/w (red), 2.5% w/w (green) and 12.5% w/w (light blue)

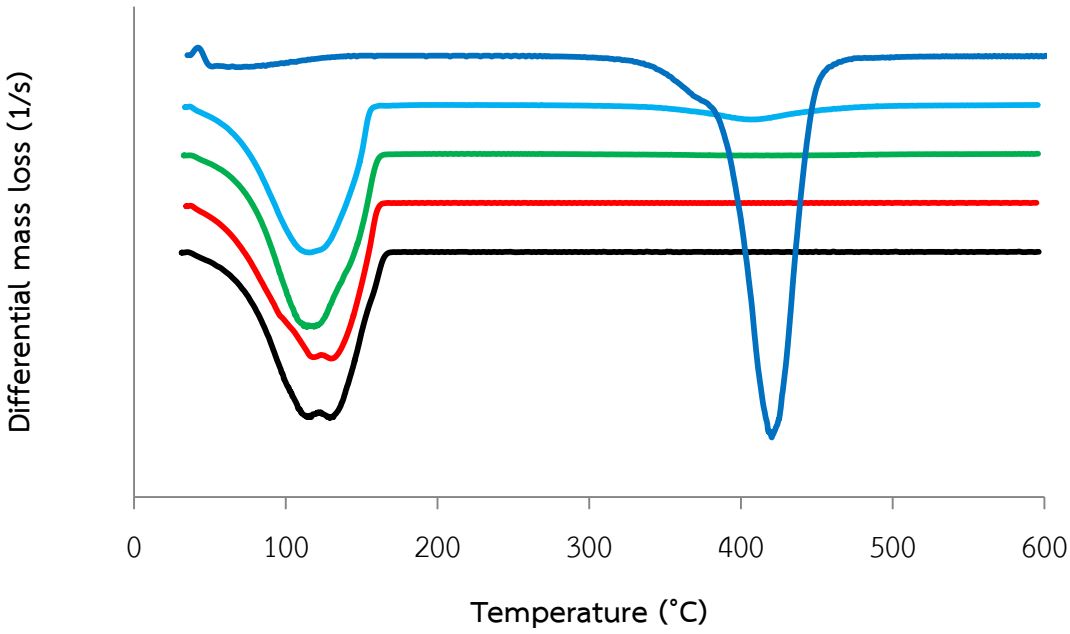

Figure 20 First derivative thermogram in the range of 50-600°C of untreated HCO-40 (blue) and the CSD wet mass made with water (black), HCO-40 solution at concentration 0.1% w/w (red), 2.5% w/w (green) and 12.5% w/w (light blue)

Table 10 Desorption temperature (T_{desorp}) of water and HCO-40 from wet mass

HCO-40 Concentration (% w/w)	CSD		MCC
	T_{desorp} Water (° C) Mean (SD), n=3	HCO-40 degradation temperature (° C) Mean (SD) , n=3	T_{desorp} Water (° C) Mean (SD) , n=3
water	131.3 (1.9)	NA	110.7 (7.4)
0.1	130.4 (1.9)*	399.0 (78.6)**	109.4 (1.4)
0.5	121.2 (5.0)	361.9 (2.2)	109.0 (2.5)
1	121.7 (2.5)	376.6 (16.7)	113.4 (2.9)
1.5	118.4 (1.3)	382.7 (6.3)	113.8 (4.2)
2	117.3 (3.4)	388.5 (3.5)	116.0 (4.4)
2.5	119.7 (5.1)	401.5 (4.8)	108.3 (2.5)
3	115.4 (3.7)	402.8 (4.2)	111.5 (9.8)
5	114.3 (2.6)	414.3 (7.6)	107.8 (1.5)
7.5	116.3 (4.3)	408.4 (0.8)	112.3 (2.9)
10	115.7 (4.7)	406.7 (1.9)	111.4 (1.5)
12.5	116.8 (1.7)	406.5 (0.4)	109.9 (2.2)

*n=4; **n=6; NA: Not applicable

Desorption temperature (T_{desorb}) was determined from 1st derivation of the normalized TGA thermogram i.e. the rate of weight loss. The temperature which showed the maximum rate of weight loss for wet masses was considered as the temperature that the molecule was desorbed from substrates, (T_{desorb}).

For CSD wet mass, the T_{desorb} of water molecule was shifted to lower temperature. It was 131.3° C when binding liquid was only water, while shifted to 116.8° C when binding liquid was 12.5% w/w HCO-40. This indicated change in interaction between water molecule and silicon dioxide. Water molecules could

hydrate hydrophilic CSD by interacting with silanol group via hydrogen bond. HCO-40 molecules having long hydrocarbon chain that were adhered on to CSD surface might disturb the interaction.

In addition, two minima were observed in the first derivative profiles of CSD wet mass using water and 0.1% w/w HCO-40. The behavior of water desorption was therefore different from other concentrations. The first minima occurring at lower temperature could be due to desorption of bulk water. It appeared at 114.6±3.9° C and 115.2±3° C for the wet mass made with water and 0.1% w/w HCO-40, respectively. The second minima occurring at a higher temperature resulted from desorption of bound water. The second minima were shown at 131.3±1.9° C for wet mass made with water. For wet mass made with 0.1% w/w HCO-40, only 4 from 6 experiments were found the second minima at 130.4±1.9° C. The single minima found at higher concentrations of the binding liquid might be caused by bulk or weakly bound water due to a decrease in interaction.

Bulk water and bound water was reported by Wang and Wunder [77] who found the bulk water was present in a greater quantity than the bound water in Aerosil® OX50 and Aerosil® 380. They also found that the isolated silanol group was less active to water therefore water formed hydrogen bond with vicinal silanol and geminal silanol. Using of TGA for defining the type of water was also reported from Piotr Staszczuk [12, 13].

The water desorption behavior as observed for CSD wet mass was not similar to the behavior of MCC wet masses (Appendix Figure II-3 and Figure II-4). Fielden et al. reported that water in the MCC wet mass was mainly free water. Therefore, the first derivative profile for MCC wet mass which showed only one minima was loss of the bulk water [26]. The mechanism or model of water retention for CSD and MCC wet mass could be different.

Degradation temperature of HCO-40 was about 300° C [118] which was close to the onset of weight loss in the thermogram under this experiment. A maximum rate of weight loss for HCO-40 was determined at 419.8° C. However, desorption temperatures of HCO-40 in CSD wet mass could not be identified. With the presence of water, the maximum rate of weight loss occurred at lower temperatures than the degradation temperature of HCO-40. Therefore, water in the binding liquid could induce degradation of HCO-40 to occur at the lower temperature; and CSD could not stabilize HCO-40.

1.3. Wet mass characterization

Rheology of wet mass

Amplitude sweep was performed in order to find the appropriate stress for use in frequency sweep in rheology study of the paste.

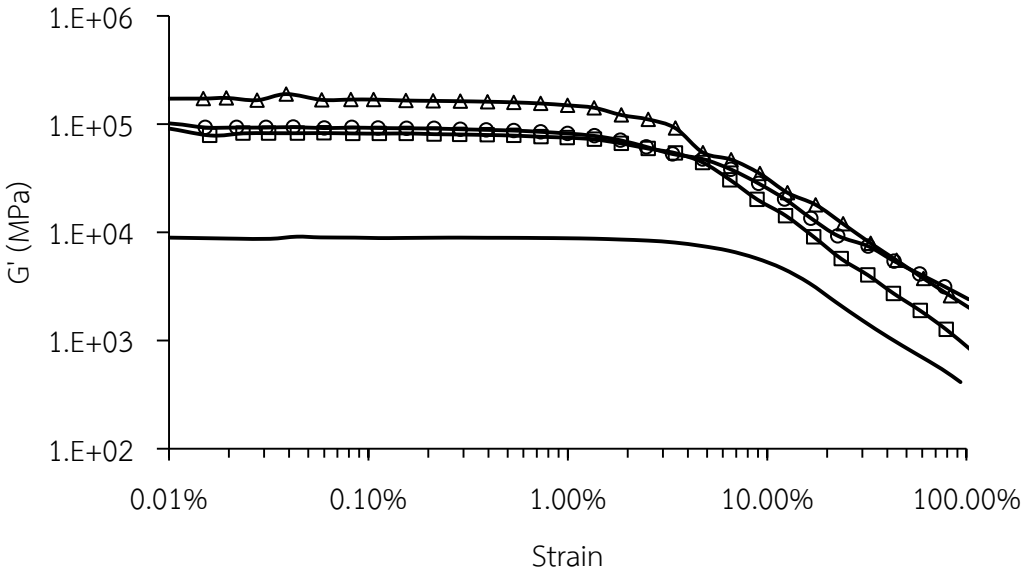

Figure 21 Amplitude sweep (strain sweep) test results of CSD paste using dispersing liquid: water (-), HCO-40 at 0.1% w/w (□), 2.5% w/w (Δ), 12.5% w/w (O)

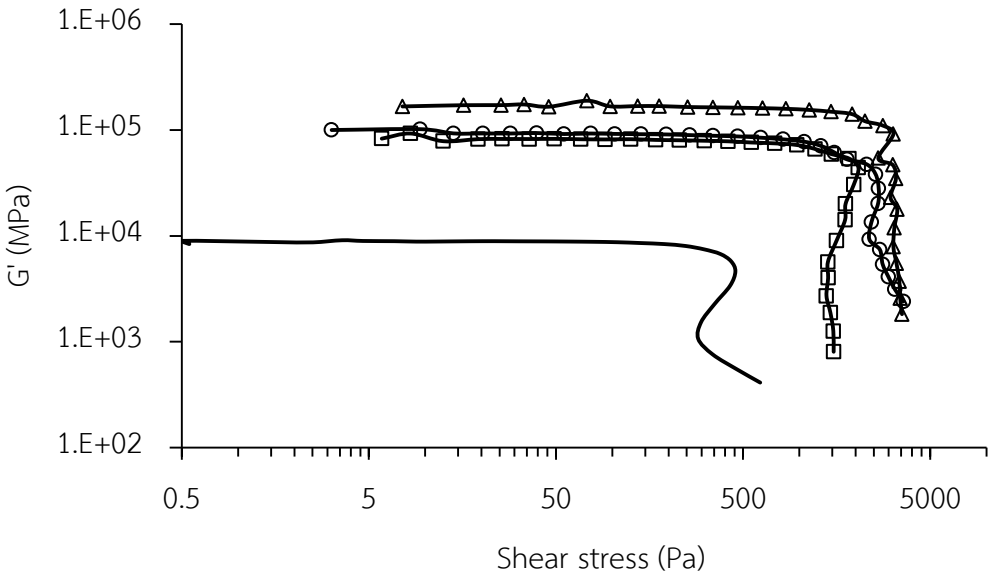

Figure 22 Amplitude sweep (stress sweep) test results of CSD paste using dispersing liquid: water (-), HCO-40 at 0.1% w/w (□), 2.5% w/w (Δ), 12.5% w/w (O)

From Figure 21 and Figure 22, amplitude sweep showed viscoelastic property from 0.01 – 100% of strain and 0.5 – 5800 Pa of stress. Generally, after Linear viscoelastic range (LVR), G' (storage or elastic modulus) was decreased while strain or stress was increased. This meant structure of paste was collapsed. The LVR of the paste made with water, as shown in Figure 22, was selected for determining stress value used in the frequency sweep test. The LVR range of the paste with water was about 0.5-350 Pa; and the LVR range of the paste made with HCO-40 solution was up to 5800 Pa. The optimum stress value for the frequency sweep test was therefore 200 Pa because this value was in the LVR ranges of all pastes.

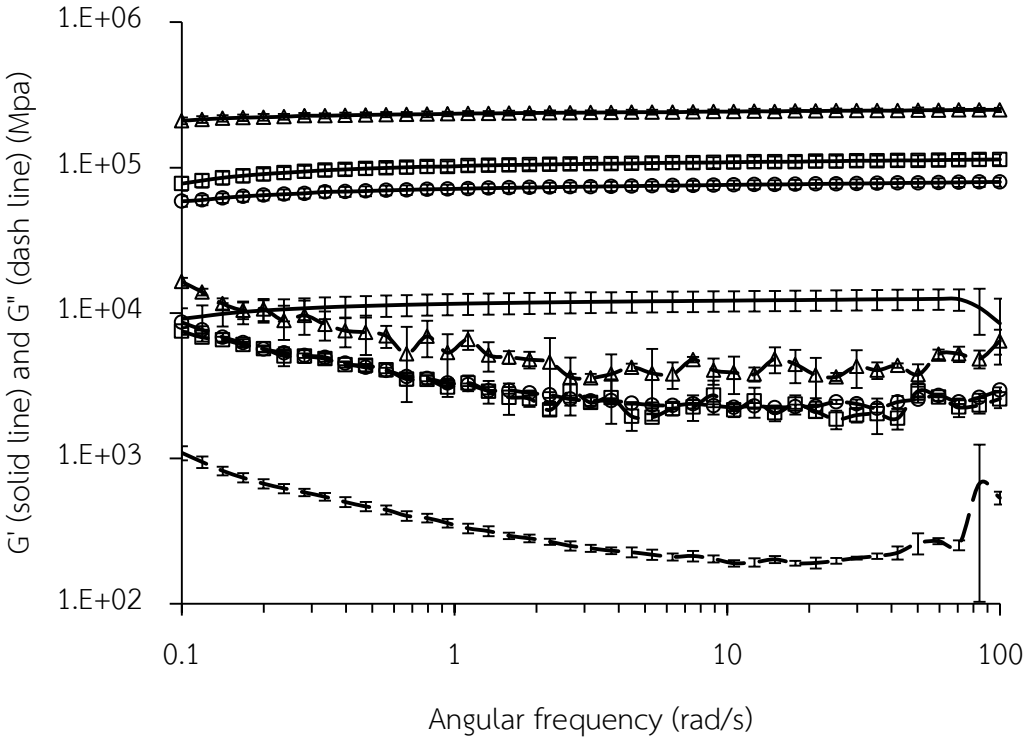

Figure 23 G' (solid line) and G" (dash line) from frequency sweep at 0.1-100 rad/s when the dispersing liquid was water (-), HCO-40 at 0.1% w/w (□), 2.5% w/w (Δ), 12.5% w/w (O)

The result of frequency sweep test showed that G' (elastic modulus or solid behavior) was higher than G" (viscous modulus or liquid behavior) over the frequency range studied (Figure 23). This indicated that solid behavior dominated consistency of the paste. No transition of G' across G" was observed. The G' values were almost constant through frequency range. In addition, frequency sweeps of G' was parallel to each other. The constant G' value signified frequency independent of the samples although, it showed an increase in G'. The increased G' with increasing frequency indicating frequency dependent was insignificant here.

The frequency independence has been found in the dispersion of hydrophobic fume silica (Aerosil® R805) in polar solvent, polyethylene glycol 300, indicating formation of floccules and stable colloid gel [119]. It was also found in the mixture

of hydrophilic fume silica and the less polar solvent, modified polyethylene glycol 300 having hydroxyl group substituted by methyl group [120].

In addition, Raghaven et al. reported that when hydrophilic fume silica (Aerosil® 200) was dispersed in polyethylene glycol 300, which is a polar solvent, the G' was dominated by G" [119]. This indicated behavior of non-floccules dispersion and presence of the interaction between hydrophilic fume silica and polyethylene glycol 300. Moreover, Raghavan et al. also proved that viscoelastic property of this system was due to hydrogen bond, not the Van de Waals force. Hydrogen bond between silanol group on Aerosil® 200 and hydroxyl group of solvent may make the solvation layer [120].

According to the work reported by Raghaven et al. [119, 120], in the present systems, water molecules should hydrate hydrophilic CSD and form hydrogen bonding between hydroxyl groups of water with silanol group of CSD, resulting in behavior of viscous (G"). With the surfactant, HCO-40 molecule should modify polarity of medium and reduce hydration effect. Behavior of the solid (G') should be more significant due to interaction between silanol-silanol groups.

However, in the water system studied, the result showed that G" was dominated by G' which was not consistent with the work reported by Raghaven [119, 120]. It may be because solid content of this experiment was 15% w/w of CSD. High CSD content made silanol group density in the system increased. Then viscoelastic from paste made with CSD and water showed G' dominated due to high solid content [121]. However, the paste made with only water showed the lowest G', indicating less solid behavior than the paste made with HCO-40 solutions.

In this experiment, G' was increased with the HCO-40 concentration until the concentration of HCO-40 reached 5% w/w. Then, the G' decreased after HCO-40 concentration over 5% w/w may be due to that floccules of CSD particles were disturbed by rich HCO-40 molecules. It could be that long hydrocarbon tail of HCO-

40 may reduce interaction between CSD particles. This strength of the paste was therefore reduced.

The possibility of surfactant aggregated on the CSD surface may also found in rheology studied. With the surfactant, HCO-40 molecules were possibly adsorbed on to CSD surface through interaction between hydrocarbon chain and siloxane group. This led to that the outer surface was more hydrophilic and readily to be hydrated with water molecules. Therefore, at the high HCO-40 concentration G' in both amplitude and frequency sweep experiment was reduced.

A little frequency dependent property which was shown in CSD pastes was also found in the MCC wet mass. Majidi et al., reported that using Avicel PH102 as extrusion-spheronization aid also showed that G' dominated over G" for the studied wet mass with little frequency dependent in frequency sweep experiment [18].

The G' value, which was the dominating properties, of one point of shear rate was used to represent viscoelastic properties for further discussion. The G' value at an angular frequency of 3.1 rad/s, which was in the middle of frequency sweep, was selected (Figure 24).

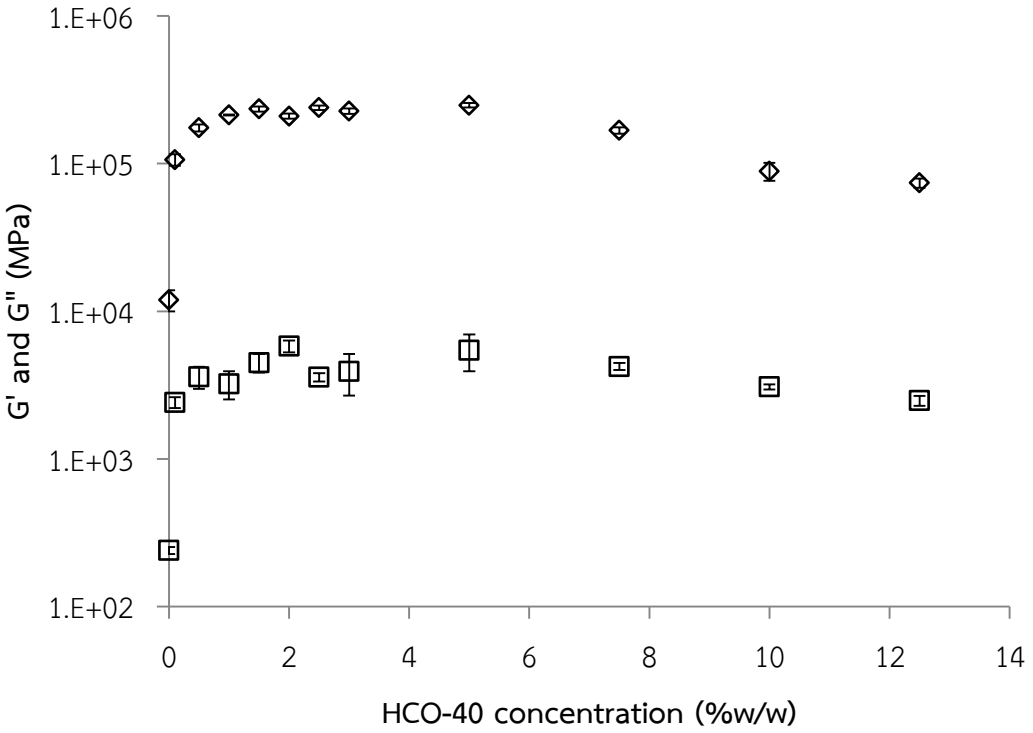

Figure 24 G' (◊) and G" (□) from CSD paste presented against various concentrations of HCO-40. Data obtained from 3.1 rad/s shear rate.

Viscoelastic properties at the frequency of 3.1 rad/s is shown in Figure 24. All paste showed G' dominated over loss modulus (G") by 100 times. G* (Complex modulus) which was calculated by vector addition of G' and G", revealed the similar magnitude as G'. G* which was the vector quantity containing magnitude and direction that was not commonly used in determining properties of wet masses.

G' for the paste which made with 0.1% w/w HCO-40 was suddenly increased, comparing with that of the paste made with DI water. G' value for the paste made with HCO-40 concentrations of 1 – 5% w/w was almost constant. MacRitchie reported that MCC wet mass could produce acceptable pellets when G' or G" value was not much varied with increased water content [20].

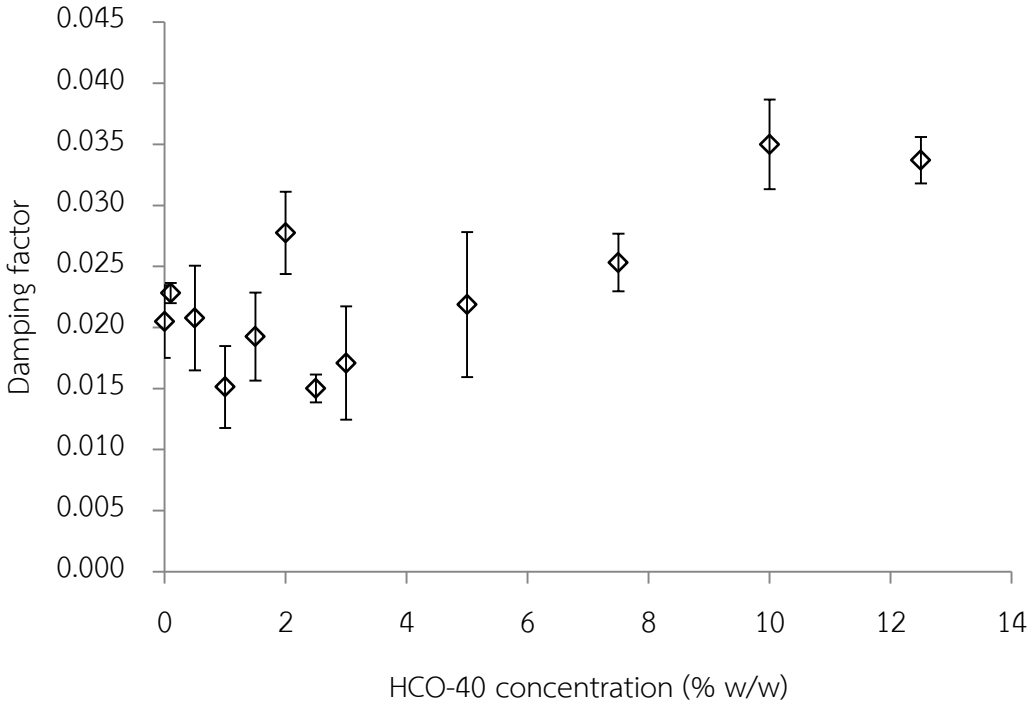

Figure 25 Damping factor from CSD paste presented with various concentration of HCO-40. Data obtained from 3.1 rad/s of shear rate.

Damping factor was the ratio of G" and G'. In Figure 25, low values of damping factor, less than 1, were found. This confirmed dominating elastic properties (G') of these pastes. The paste contained 2.5 and 3% HCO-40 solution showed low damping factor. The damping factor values were not much different for the pastes that contained 7.5% w/w HCO-40 solution or lower as shown in Figure 25. The HCO-40 concentrations of 10 and 12.5% w/w in the paste had relatively higher in damping factor.

Decreasing in G' and increasing in G" observed for 10% and 12.5% w/w HCO-40 containing paste was also found in the work reported by Ryo et al. In their work, when the amount of a polymer in dispersing medium was increased, there were more free non-adsorbed polymer chains resulting in weakly aggregated silica particles. Therefore, G' was decreased and G" was increased [121]. In this work, it

was possible that the relatively higher proportion of HCO-40 molecules and lower solid content in the paste led to weakly formed CSD aggregated.

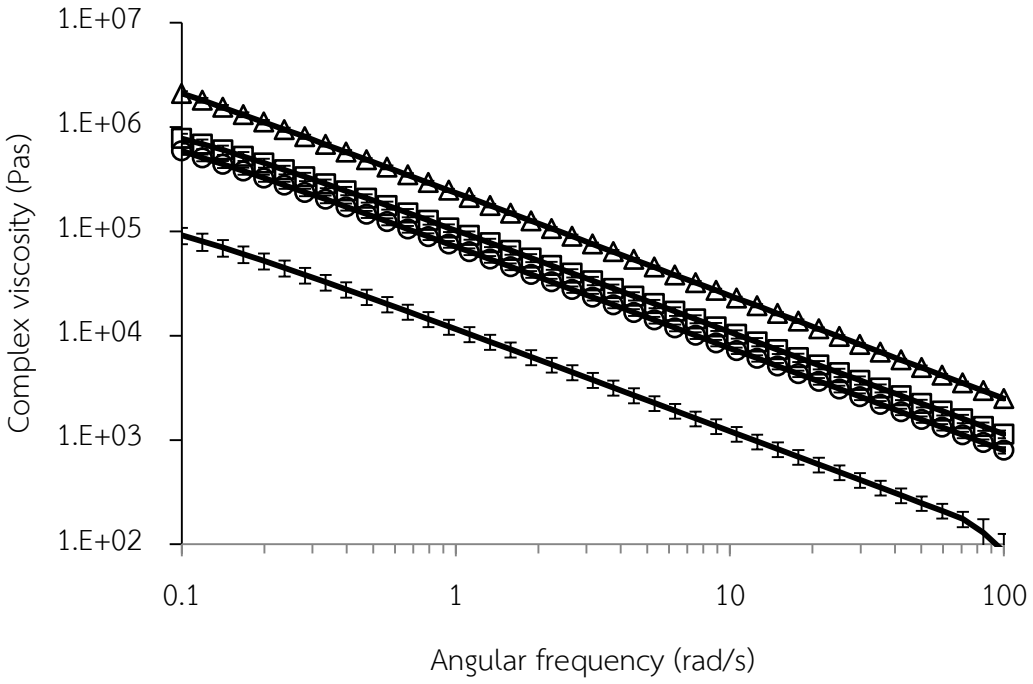

Figure 26 Complex viscosity of paste from frequency sweep at 0.1-100 rad/s which the dispersing liquid was water (-), HCO-40 at 0.1% w/w (□), 2.5% w/w (Δ), 12.5% w/w (O)

Figure 26 showed decreasing in complex viscosity with increasing angular frequency or shear rate. It meant that paste used in this experiment exhibited the shear thinning properties. The result was consistent with the rheology of MCC wet mass reported by MacRitchie et al. [20] and Majidi et al. [18]. Due to shear thinning properties, the wet mass of CSD was less viscous during extrusion with high rate through the die.

2. Pellet formulations studied

Extrusion

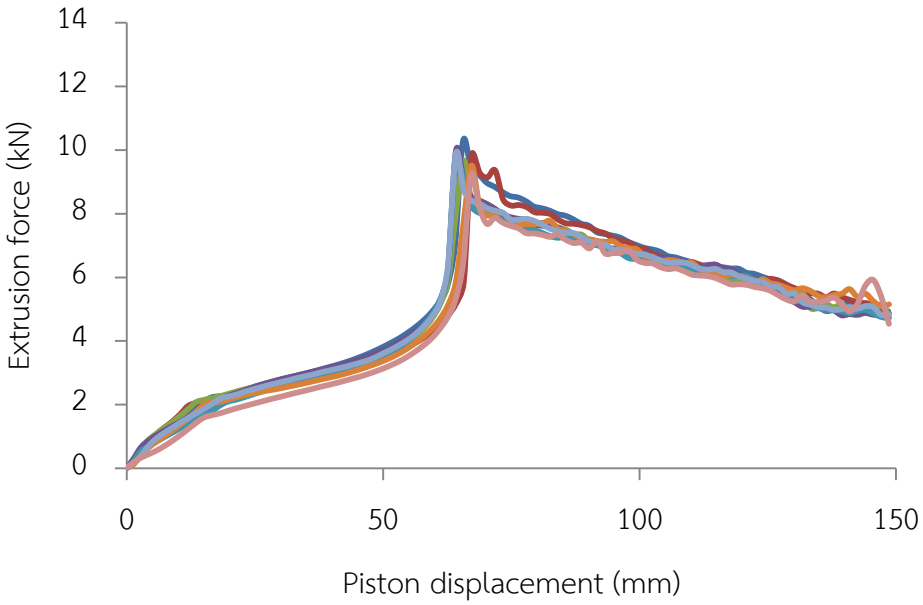

Figure 27 Force-displacement profiles (n=8) of the second batch containing 0.1% HCO-40 in the binding liquid

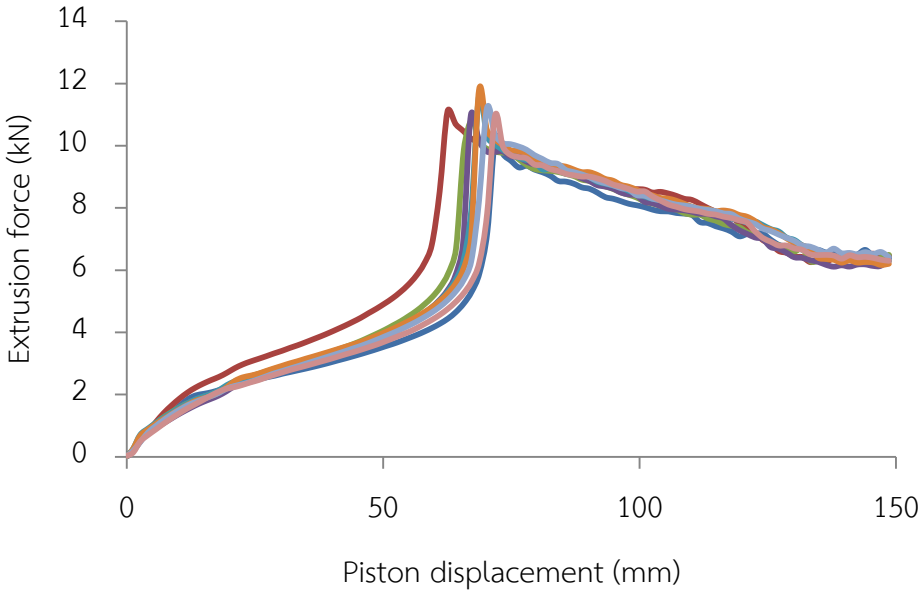

Figure 28 Force-displacement profiles (n=8) of the second batch containing 2.5% HCO-40 in the binding liquid

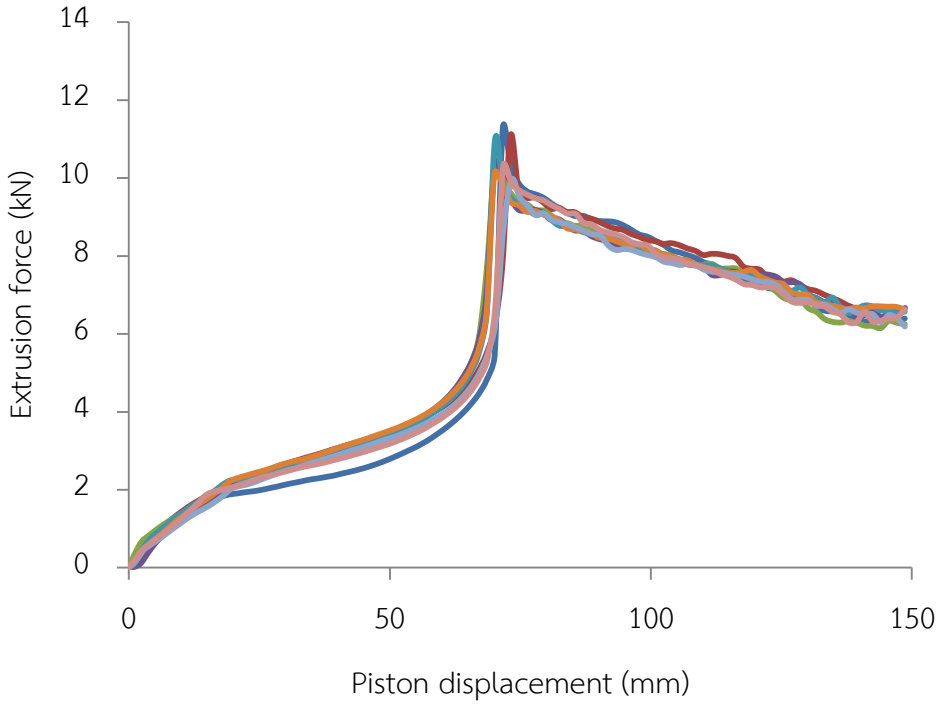

Figure 29 Force-displacement profiles (n=8) of the second batch containing 3% HCO-40 in the binding liquid

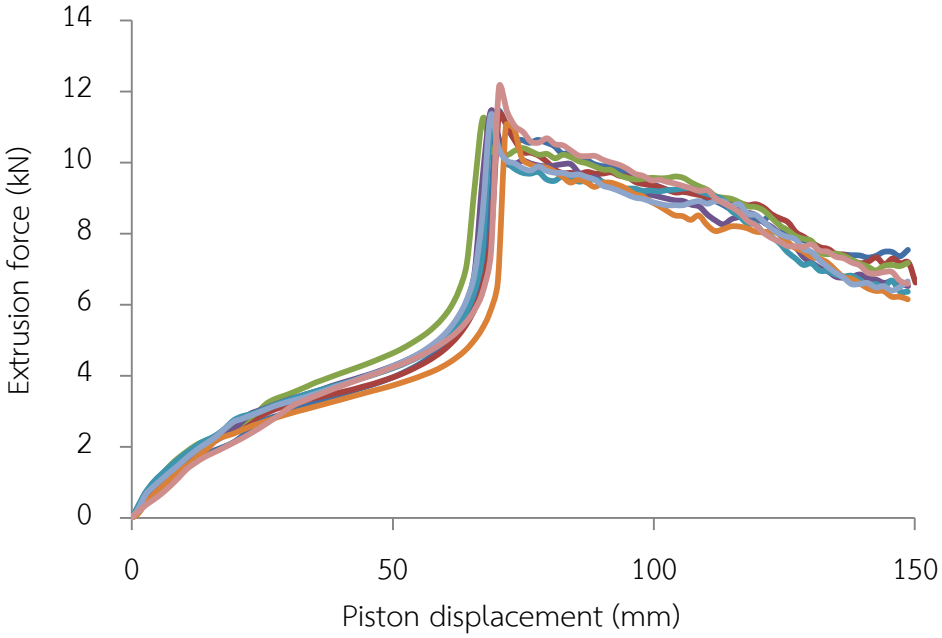

Figure 30 Force-displacement profiles (n=8) of the second batch containing 12.5% HCO-40 in the binding liquid

In extrusion process, extrusion force was measured while piston was moved downward in order to extrude the wet mass in the barrel. The force measurement was present as force-displacement profiles as shown in Figure 27 to Figure 30.

The decreased extrusion force could be due to reduction in friction between sliding surface. Initially, the wet mass was forced from wide cross section area of the barrel into small cross section area of the die. The force was high at this stage. After extrusion began, there was a film of CSD wet mass on the wall of barrel and die. This film might help to lubricate the subsequent extrusion.

The forced flow stages were not commonly found for all formulations. In this study, the piston displacement was fixed after detection of preloading force. From the profile, the last 10 mm of displacement showed constant force due to reaction of the die plate. Liquid migration did not occur in the extrusion, and uniform extrudates were produced. They have smooth surface and brittle.

The higher surfactant concentration gave higher extrusion force and more variation as shown in Figure 31. Linearity was observed when plotted against HCO-40 concentration in log scale as shown in Figure 32.

This agreed with the work reported by Podczeck [64]. Podczeck et al. reported that the higher surfactant content in the Avicel PH101 wet mass caused higher extrusion force. The extrusion force may increase by effect of viscosity from non-ionic surfactant in the binding liquid [64]. In this study, the extrusion force was also increased with increased viscosity of binding liquid.

However, the rheology properties of the CSD paste indicated that G' (solid behavior) was increased with up to 1% w/w HCO-40, and almost constant with 1 – 5% w/w HCO-40; then it was decreased with 7.5 – 12.5% HCO-40. The behavior of increasing high extrusion force of wet mass with increased concentrations of surfactant could not be directly related to rheological properties. The wet mass contained more solid content than the studied paste. Therefore, in the wet mass,

the interaction between silanol-silanol group of CSD could strengthen CSD aggregates and dominate the structure of wet mass for the whole range of binding liquid concentration studied.

It was also possible that the higher extrusion force measured for the wet mass with the higher HCO-40 concentrations was caused by less amount of water in the wet mass available for lubricating the die.

The performance of extrusion process and the extrudate with smooth surface obtained in this study may be due to long die i.e. length to radius ratio was 4 and small particle size of CSD.

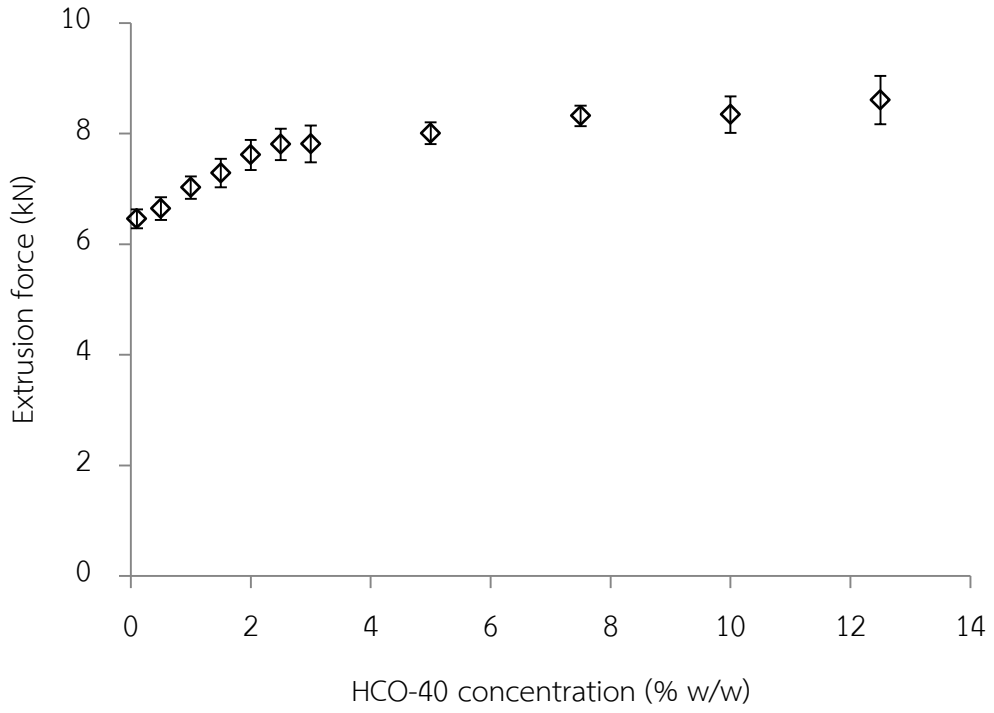

Figure 31 Average extrusion force of CSD wet mass with concentration of HCO-40 in linear scale.

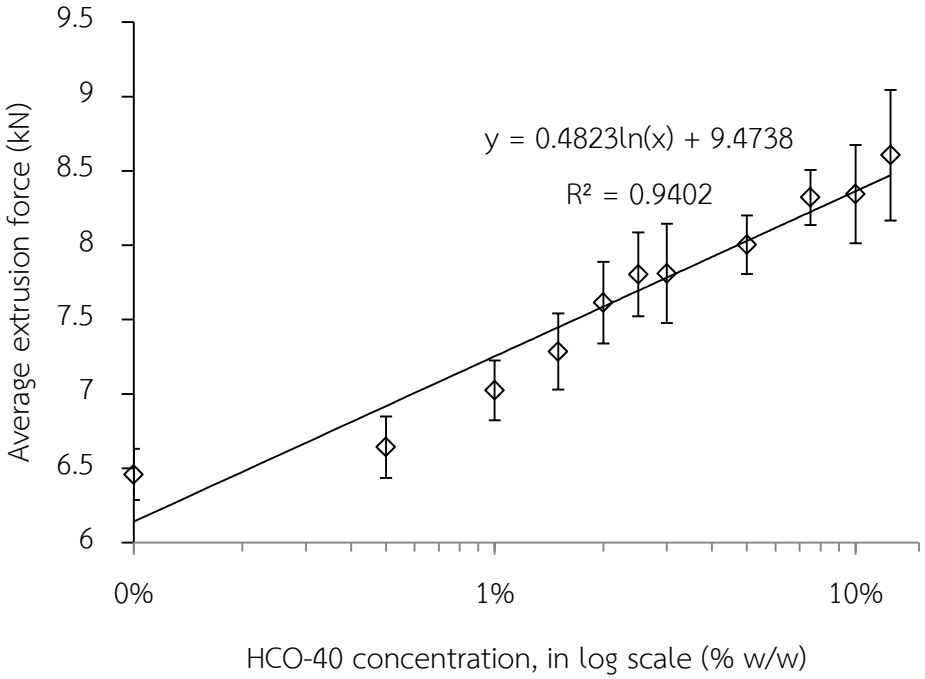

Figure 32 Average extrusion force of CSD wet mass with concentration of HCO-40 in log scale.

Pellet morphology

The appearance of pellets in modal size of the 3rd batch is shown in Figure 33. It showed that pellets produced with low concentration of HCO-40 had greater size; and pellets produced with high concentration of HCO-40 had rod shape.

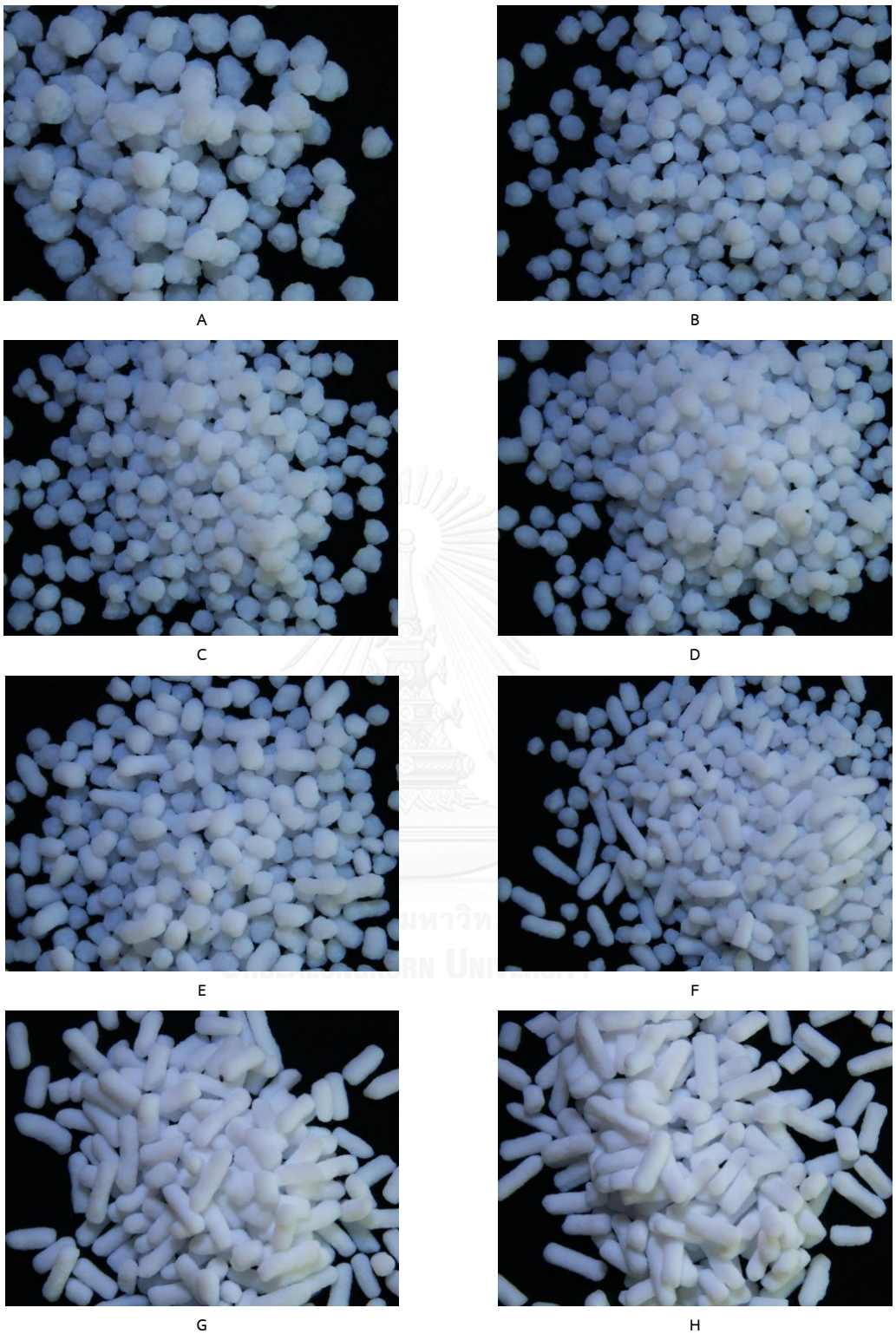

Figure 33 Pellets at magnification of 0.67x observed by stereo microscope; pellets made with varied HCO-40 concentrations: 1.5% w/w (A), 2% w/w (B), 2.5% w/w (C), 3% w/w (D), 5% w/w (E), 7.5% w/w (F), 10% w/w (G) and 12.5% w/w (H)

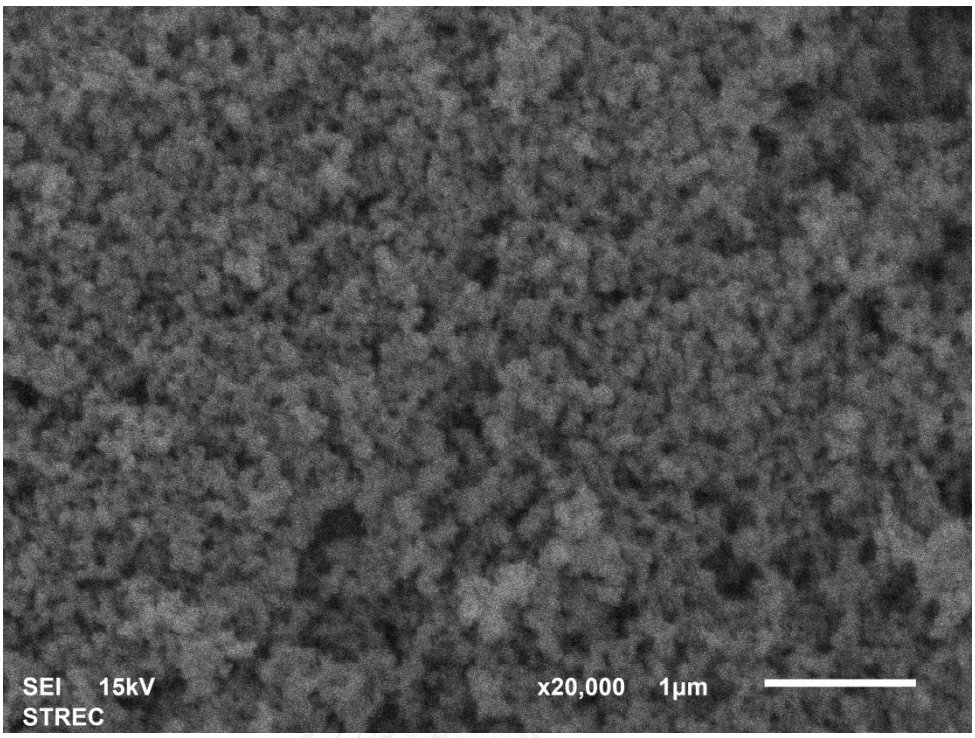

Figure 34 Untreated CSD at magnification of 20000x

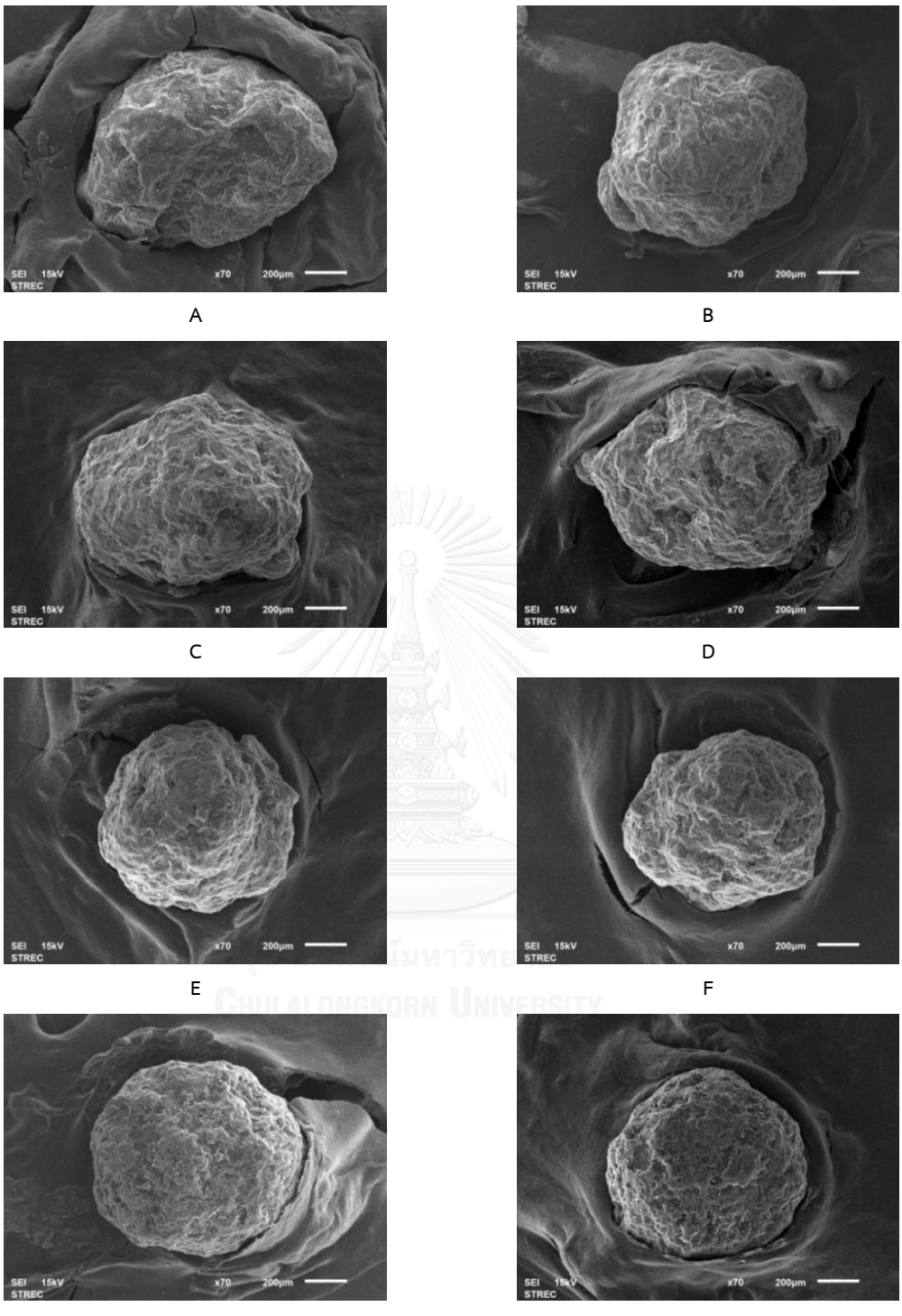

Figure 35 SEM image of pellets at magnification of 70x; pellet made with varied HCO-40 concentrations: 1.5% w/w (A), 2% w/w (B), 2.5% w/w (C), 3% w/w (D), 5% w/w (E), 7.5% w/w (F), 10% w/w (G) and 12.5% w/w (H)

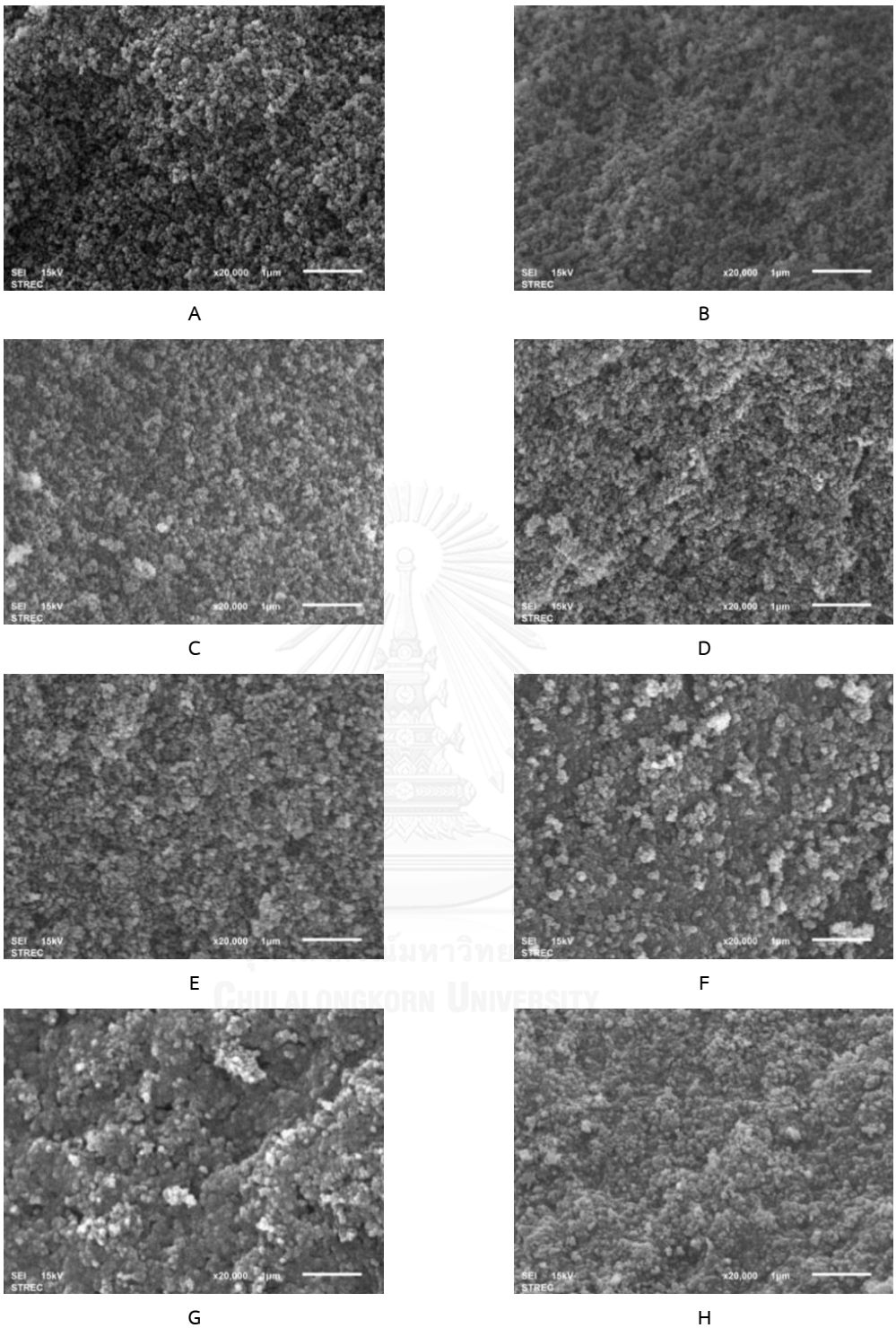

Figure 36 SEM image of cross-section of pellets at magnification of 20000x; pellet made with varied HCO-40 concentrations: 1.5% w/w (A), 2% w/w (B), 2.5% w/w (C), 3% w/w (D), 5% w/w (E), 7.5% w/w (F), 10% w/w (G) and 12.5% w/w (H)

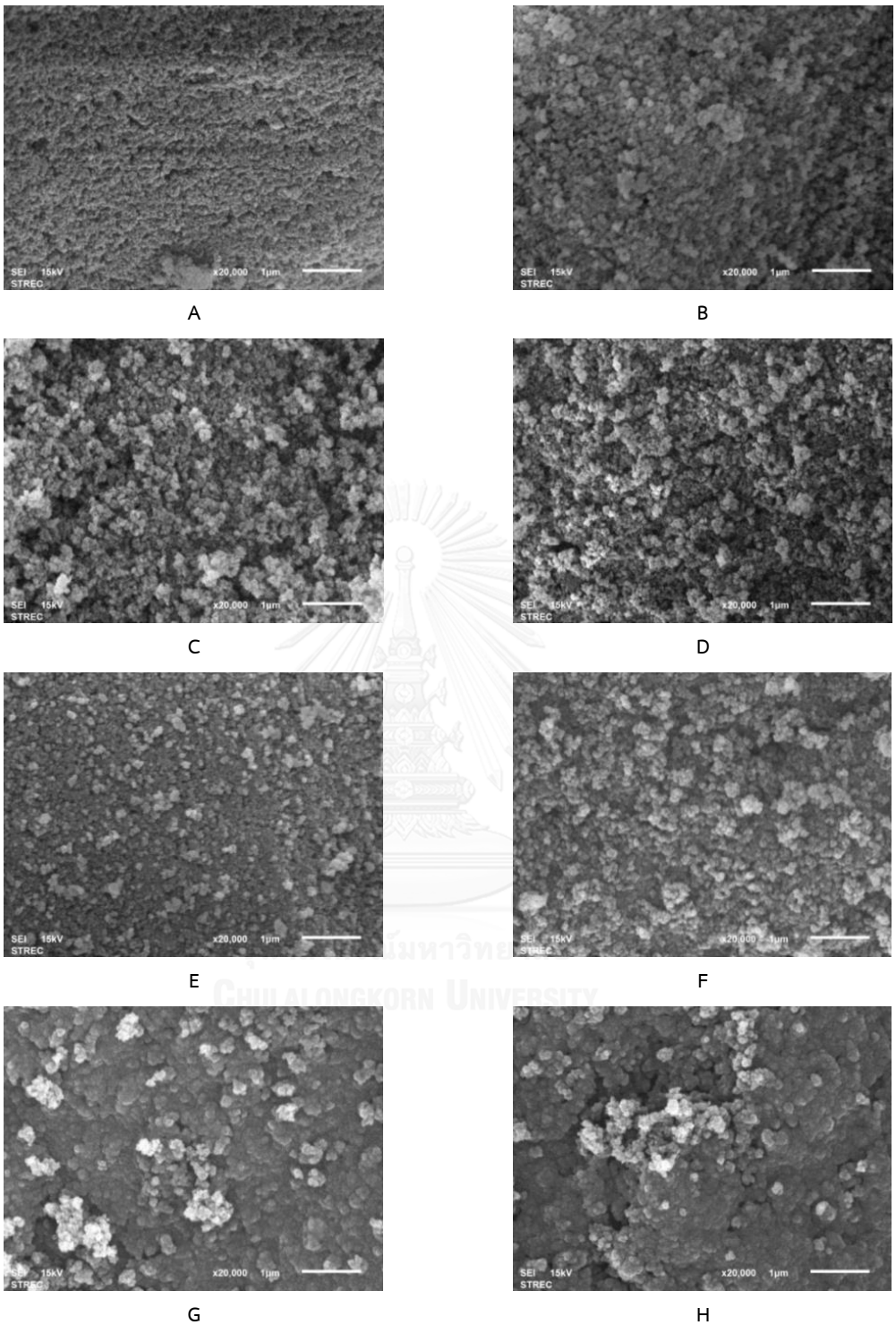

Figure 37 SEM image of surface of pellets at magnification of 20000x; pellet made with varied HCO-40 concentrations: 1.5% w/w (A), 2% w/w (B), 2.5% w/w (C), 3% w/w (D), 5% w/w (E), 7.5% w/w (F), 10% w/w (G) and 12.5% w/w (H)

Table 11 Pellet studied: Processes and physical properties

Formulation No.	HCO-40 Concentration (% w/w)	Geometric mean, mm Mean (SD)	Geometric standard deviation, Mean (SD)	Pellet yield, 0.71-1.4 mm (%) (SD)	Aspect ratio Mean (SD)	True density, g/mL	Tensile strength, MPa Mean (SD)
1	0.1	Pellets cannot be formed					
2	0.5	> 2 mm	NA	NA	NA	1.94, n=1	NA
3	1	> 2 mm	NA	NA	NA	1.99, n=1	NA
4	1.5	2.07 (0.04), n=2	1.62 (0.15), n=2	14.05 (1.90) , n=2	1.18 (0.13), n=1000	1.91, n=1	0.288 (0.151), n=60
5	2	1.26 (0.13), n=3	1.39 (0.03), n=3	74.91 (19.22), n=3	1.15 (0.10), n=1500	1.96, n=1	0.266 (0.130), n=90
6	2.5	1.05 (0.05), n=3	1.34 (0.02), n=3	94.13 (4.17), n=3	1.15 (0.10), n=1500	1.92, n=1	0.326 (0.157), n=90
7	3	0.91 (0.11), n=3	1.28 (0.02), n=3	90.36 (14.19), n=3	1.16 (0.14), n=1500	1.92, n=1	0.312 (0.122), n=90
8	5	0.78 (0.08), n=3	1.23 (0.03), n=3	69.35 (42.63), n=3	1.24 (0.30), n=1500	1.91, n=1	0.251 (0.114), n=90
9	7.5	0.71 (0.05), n=3	1.22 (0.01), n=3	59.92 (30.50), n=3	1.27 (0.40), n=1500	1.86, n=1	0.241 (0.106), n=90
10	10	0.69 (0.09), n=3	1.24 (0.02), n=3	49.00 (31.40), n=3	1.42 (0.55), n=1500	1.79, n=1	0.332 (0.196), n=90
11	12.5	0.69 (0.04), n=3	1.28 (0.00), n=3	56.39 (9.03), n=3	1.66 (0.66), n=1500	1.78, n=1	0.255 (0.201), n=90

Table 12 Modal size of pellets

Formulation No.	HCO-40 concentration (% w/w)	Batch No.	Modal size		2nd size		Yield two sieve (%)
			Size (mm)	Weight retained (%)	Size (mm)	Weight retained (%)	
4	1.5	1	-	-	-	-	-
		2	1.4-2.0	56.5	1.0-1.4	14.4	70.9
		3	1.4-2.0	68.9	1.0-1.4	12.0	80.9
5	2	1	1.0-1.4	50.7	1.4-2.0	44.4	95.1
		2	1.0-1.4	81.7	1.4-2.0	12.8	94.5
		3	1.0-1.4	76.6	1.4-2.0	10.5	87.2
6	2.5	1	1.0-1.4	89.2	0.71-1.0	6.8	96.0
		2	0.71-1.0	47.9	1.0-1.4	41.5	89.4
		3	1.0-1.4	80.9	0.71-1.0	16.1	97.0
7	3	1	1.0-1.4	85.4	0.71-1.0	13.0	98.4
		2	0.71-1.0	67.7	0.50-0.71	24.1	91.8
		3	1.0-1.4	77.1	0.71-1.0	21.6	98.7
8	5	1	0.71-1.0	84.0	1.0-1.4	9.6	93.7
		2	0.50-0.71	78.2	0.71-1.0	19.3	97.5
		3	1.0-1.4	58.5	0.71-1.0	35.7	94.3
9	7.5	1	0.71-1.0	68.3	0.50-0.71	28.3	96.5
		2	0.50-0.71	73.4	0.71-1.0	24.9	98.3
		3	0.71-1.0	60.4	1.0-1.4	23.8	84.1
10	10	1	0.50-0.71	61.9	0.71-1.0	32.9	94.8
		2	0.50-0.71	65.0	0.71-1.0	27.0	92.1
		3	1.0-1.4	44.6	0.71-1.0	40.6	85.1
11	12.5	1	0.71-1.0	45.8	0.50-0.71	43.5	89.3
		2	0.50-0.71	37.1	0.71-1.0	26.0	63.0
		3	1.0-1.4	39.6	0.71-1.0	24.7	64.3

Pellets morphology observed by SEM showed similar cross-section and surface (Figure 35-Figure 37). Pellet surface was rough (Figure 35). The cross-section show dense agglomeration of CSD in pellets (Figure 36), comparing with untreated CSD powder (Figure 34).

In this studied, the wet mass prepared with water was able to be extruded by long die-ram extruder but it failed to form pellet during spheronization. In general, it was found that the wet masses containing 2.0 – 3.0% w/w HCO-40, which were extruded with the force between 7.61 – 7.81 kN, could produce pellets with desired properties.

For the wet mass with 0.1% HCO-40, it could be extruded. However, uncontrollable agglomeration of the extrudates occurred and the mass adhered to the wall and plate during spheronization. Uniform large pellets (> 2mm) were obtained with the formulation containing 0.5 – 1.5% w/w HCO-40. Size of pharmaceutical pellets are usually in the range of 0.5 – 2.0 mm [21]. The pellets made from 2% w/w to 12.5% w/w HCO-40 were in this size range. The geometric mean of the pellet size was decreased with increased HCO-40 concentrations.

Size distribution according to the value of standard deviation was not much varied. Narrow size distribution was observed for the pellets made from 5% - 10% HCO-40 which had rod shape.

Yield of pellets in each batch calculated from pellets in size range 0.71 – 1.4 mm. Pellets made with 2.5% w/w HCO-40 gave the highest yield with reproducibility i.e. low variation between batches.

Spherical pellets should have the aspect ratio less than 1.2 [17, 35-37]. According to this criterion, the pellets made with 1.5 – 3% w/w HCO-40 were spherical. The aspect ratio was increased but geometric mean was decreased with extrusion forces, depending on the HCO-40 concentrations. It was possible that higher extrusion force produced denser extrudate which was difficult to deform to

round pellets. In addition, these wet mass contained relatively low water content which may be insufficient for deformation of pellets. At the high concentration, there appeared to be more rod shape pellets, as shown in Figure 33.

Overall results indicated that the most desired properties of pellets, in term of yield, size and shape, could be obtained from the formulation containing 2.5% w/w HCO-40. Podczeck et al, reported that content and type of surfactant may not influence the MCC pellet shape [66]. Addition of surfactant in the MCC formulation could produce pellets with shape factor value more than 0.6 indicating acceptable shape of pellets.

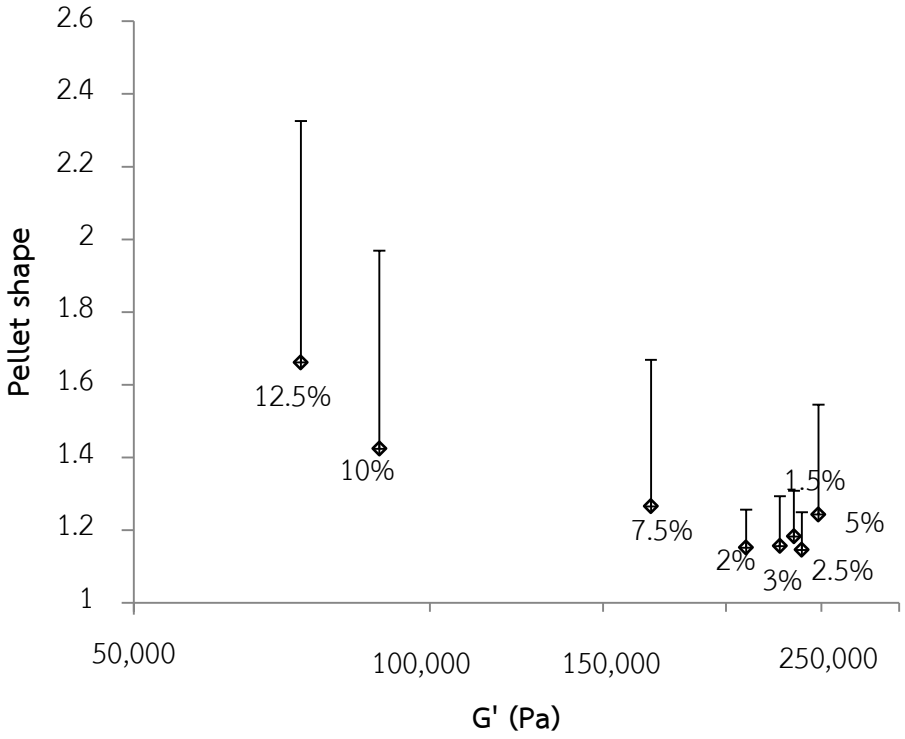

Figure 38 Aspect ratio of CSD pellets plotted against G'

The shape of pellets might be related to G' (solid behavior) of the formulation. The aspect ratio was reduced with an increase in G', as shown in Figure 38. The round pellets with the aspect ratio less than 1.2 obtained from the wet mass containing 1.5 – 3.0% w/w HCO-40 and having G' value of 209 – 239 kPa. In addition,

these values were considerably constant in the range of plateau found in Figure 24. The result agreed with reported work for MCC pellets which suggested that acceptable properties of MCC pellets were obtained with G' or G" value was not very much changed while water content was increased [20].

True density, true density of pellets made from 0.5 to 12.5% w/w was decreased from 1.94 to 1.78 g/mL, respectively. Density of CSD and HCO-40 was 2.2 [44] and 1.03 g/mL [118], respectively, Basically, wet mass was denser after compression during extrusion process. In this study, the true density was not affected by extrusion force which was increased with the HCO-40 concentration. The reduction of true density was dependent on HCO-40 content in the formulation, as it could be seen in the SEM image, Figure 36 and Figure 37, which high concentration of HCO-40 filled in the space between CSD particles.

Mechanical strength of pellets in this experiment showed high variation. The highest value of mechanical strength was of the pellets made with 10% w/w HCO-40 which showed 0.332 MPa of mechanical strength. All CSD pellets in this study possessed low mechanical strength. Mechanical strength of CSD pellets showed in lower value than 0.5 MPa which was sufficient for further process [17]. However, Podczeck proposed that addition of drugs and other fillers may improve the pellet strength [4]

Overall the results indicated that interaction between silanol-silanol groups of CSD in the wet mass was attributed to pellet formulation. However, this should be modified with the presence of HCO-40 at the optimum level which was adsorbed onto CSD surface.

Addition of HCO-40 in water can change the interaction between water and CSD surface, leading to aggregation between CSD particles. Characterization of input materials suggested that rheological properties of the wet mass were important

attributes for pellet formation. The effect of rheology here was also influence by solid content of the system studied.

3. Chemical characteristics of CSD and surfactant in pellets

3.1. Infrared spectroscopy

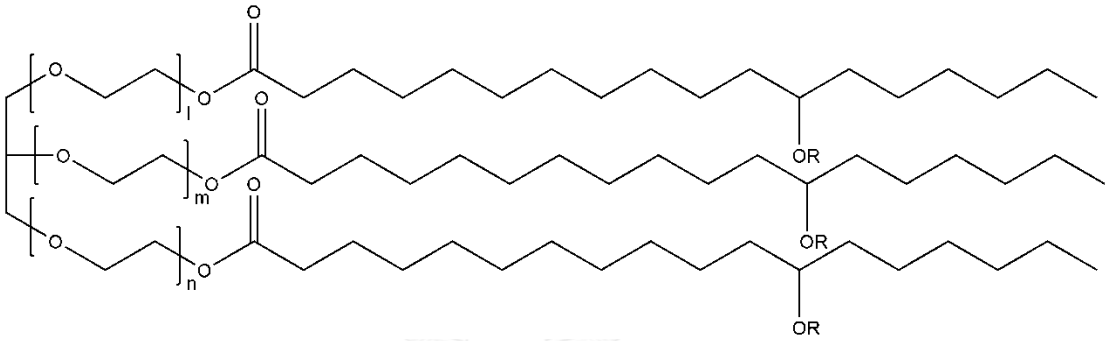

Figure 39 Chemical structure of Kolliphor® RH40 (HCO-40) where l+m+n = 40 – 45, R = H of polyethylene glycol residue, modified from Reintjes, 2011 [122]

On the surface of CSD, there are silanol groups i.e. isolated silanol, geminal silanol and vicinal or bridge silanol as shown in Figure 1, are hydrophilic parts. The siloxane group which is also present on the surface is a hydrophobic area of CSD. The chemical structure of HCO-40 is shown in Figure 39. It is a hydrophilic surfactant which HLB value is 14 – 16 [5].

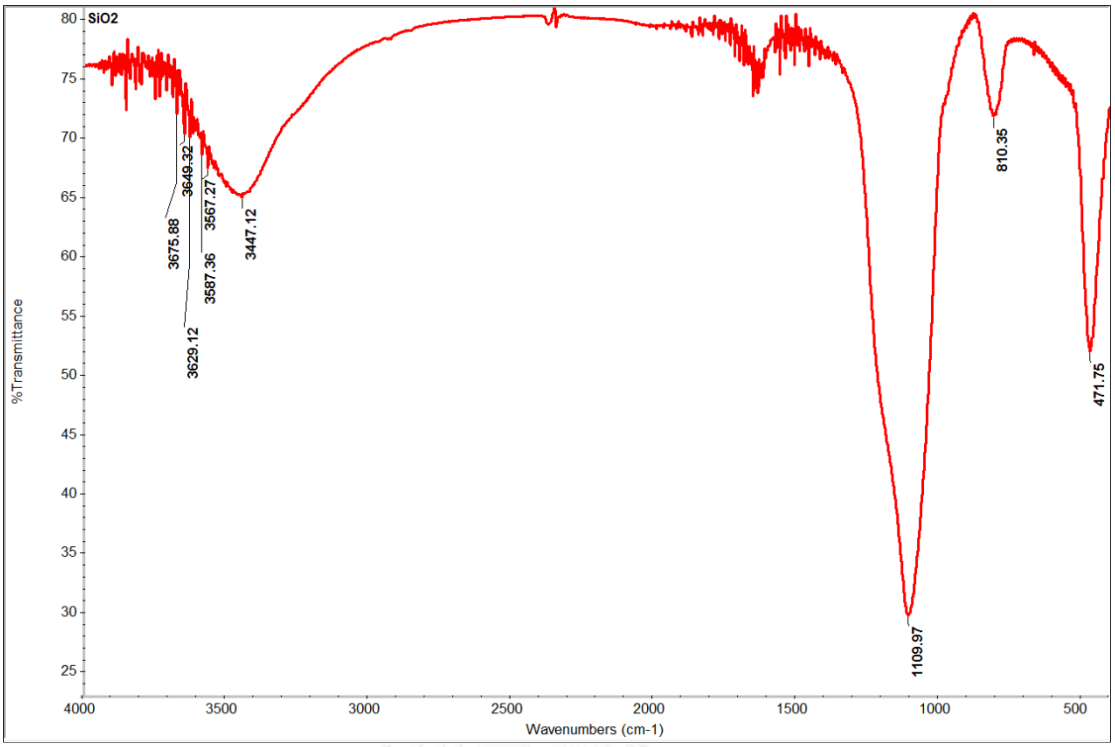

Figure 40 FT-IR spectrum of untreated CSD

The FT-IR spectrum of CSD showed a broad peak at 3447.1, 1110.0, 807.6 and 470.2 cm^{-1} as shown in Figure 40. The FT-IR spectra of pellet samples also showed broad peaks at the same positions. The board peak at around 3400-3500 cm^{-1} is the peak of OH stretching, indicating the presence of water and hydrogen bonded silanol group according to Wang and Wunder [77].

In addition, Wang and Morrow found that there may be little peaks of hydrogen bonded silanol group at 3550 and 3650 cm^{-1} and the shoulder of the peak at 3720 cm^{-1} [123]. However, these characters were not found in the present study.

The peaks at 807.6 and 1110.0 cm^{-1} found in the FT-IR spectrum of CSD are character Si-O-Si stretching which has been reported around 800 and 1100 cm^{-1}, respectively [124, 125]. The peak at 470.2 cm^{-1} may be Si-O-Si bending which has been reported at 450 cm^{-1} [125]. Although KBr used in this experiment was dried before used, the noise from adsorbed water and carbon dioxide was shown around 1650 and 3700 cm^{-1}.

Table 13 Show peak position for FT-IR spectrometer from pellets (n = 3)

Formulation No.	HCO-40 concentration (% w/w)	Peak position		
		Si-O-Si stretching (Mean (SD))	$-CH_3$ stretching (Mean (SD))	-OH stretching (Mean (SD))
1	0.1	1106.9 (0.2)	-	3446.9 (0.3)
2	0.5	1107.2 (0.3)	-	3447.4 (0.4)
3	1	1107.5 (0.2)	-	3447.2 (0.1)
4	1.5	1107.5 (0.1)	-	3447.1 (0.2)
5	2	1107.2 (0.2)	-	3447.0 (0.4)
6	2.5	1107.1 (0.1)	-	3447.1 (0.1)
7	3	1106.6 (0.3)	-	3447.3 (0.2)
8	5	1106.6 (0.1)	2926.3**	3447.4 (0.0)
9	7.5	1103.6 (0.2)	2927.1 (0.3)	3447.0 (0.2)
10	10	1103.6 (0.1)	2926.9 (0.1)	3447.3 (0.2)
11	12.5	1103.3 (0.2)	2927.1 (0.0)	3447.4 (0.3)
Untreated CSD		1110.0 (0.8)	-	3447.1 (0.1)
CSD (processed with water)		1107.3 (0.3)	-	3447.3 (0.1)
HCO-40		-	2924.6 (0.3)	3447.3 (0.2)

* CSD powder mixed with water and dried in oven at 50°C for 2 h.

** n = 2

The characteristic peaks of isolated single silanol and geminal silanol groups which should be located around 3747 cm^{-1} were not found in the FT-IR spectra of CSD and pellets. These peaks were reported by Tripp and Hair for Aerosil® 380 after storage under vacuum condition at high temperature [98].

In all samples, the characteristic peak for OH stretching was not shifted i.e. 3446.9 – 3447.4 cm^{-1}, comparing the FT-IR spectrum of untreated CSD and that of the pellet samples. This indicated that interaction of adsorbed water and silanol group was not affected by addition of HCO-40. The characteristic peaks of Si-O-Si bending and stretching around 470 and 800 cm^{-1} were also not influenced.

The FT-IR spectra showed that the peak shift was found for Si-O-Si stretching. However, Si-O-Si stretching at 1110 cm^{-1} was shifted from 1110.0 cm^{-1} for CSD to 1103.3 cm^{-1} for pellets made with 12.5% w/w HCO-40.

Perry et al. suggested that the shifting of Si-O-Si stretching was found with thermal treatment. The peak was shifted to higher wavenumbers due to changing in bond length and/ or bond angle by higher temperature [126].

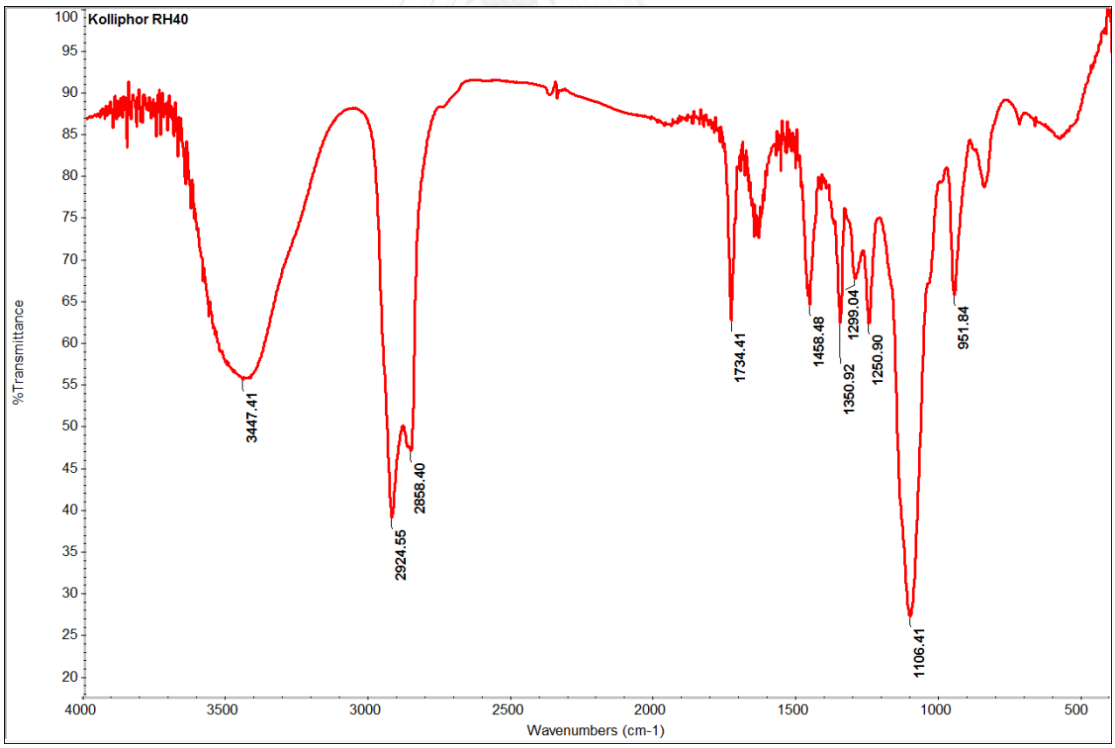

Figure 41 FT-IR spectrum of HCO-40

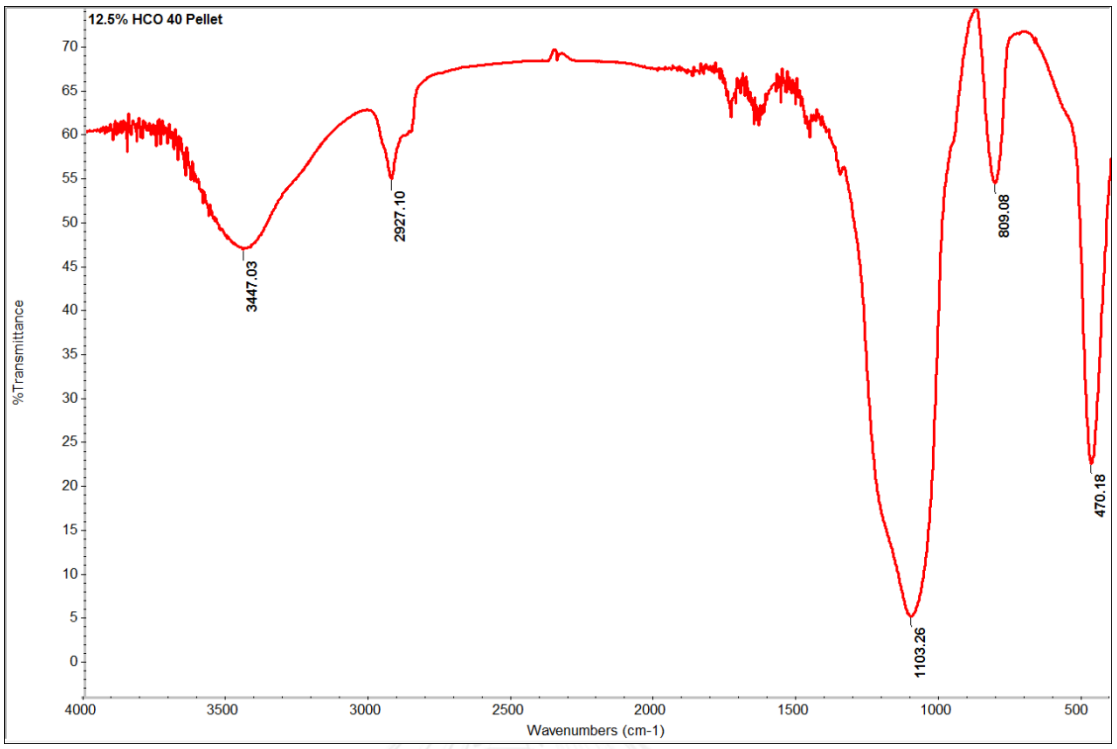

Figure 42 FT-IR spectrum of pellets made with 12.5% w/w HCO-40 solution

The FT-IR spectrum of HCO-40 showed a sharp peak at 1106.8 and 2924.6 cm^{-1} as shown in Figure 41. The peaks at 1106.8 may be due to the C-O stretching [127] from polyoxyl part of HCO-40 and the peak at 2924.6 cm^{-1} may be due to C-H stretching of CH_3 in the alkyl chain which was reported at 2952 cm^{-1} by Erkelens and Liefkens [128].

The peak of C-H stretching was found only in the FT-IR spectra of pellets made with HCO-40 concentration at 5% w/w and higher. It was shifted from 2924.6 cm^{-1} for HCO-40 to 2927.1 cm^{-1} for the pellets made with 12.5% w/w HCO-40 (Figure 42). This indicated that the hydrophobic interaction between HCO-40 and CSD occurred in pellets through adsorption of hydrophobic chain of HCO-40 on CSD surface. The evidence of interaction between surfactant molecules was found in the AFM result where the presence of HCO-40 molecules could reduce adhesion force on the CSD surface. The adsorption of long hydrocarbon chain on the surface of silica was shown by shifting in the band of CH_3 stretching, which was about 5 cm^{-1} higher

wavenumbers than that of the pure compound, was also reported by Erkelens and Liefkens. [128].

3.2. Solid state nuclear magnetic resonance spectroscopy

Solid state ^{1}H MAS NMR

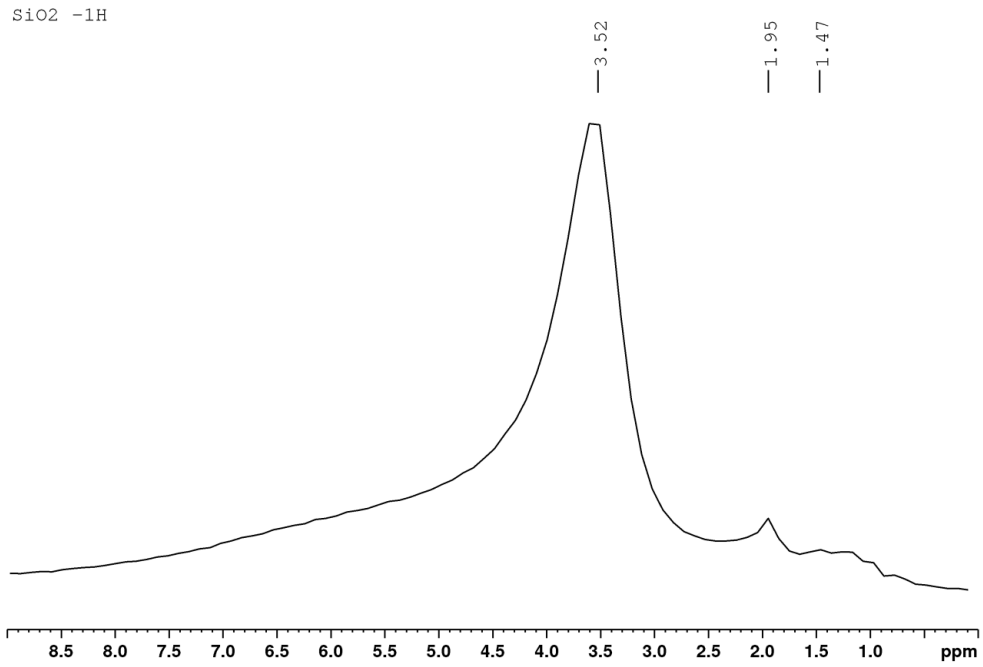

Figure 43 ^{1}H MAS NMR spectrum of untreated CSD

^{1}H MAS NMR of untreated CSD showed a peak at 3.52 ppm and a little peak at 1.95 ppm (Figure 43). These peaks could be hydrogen bonded silanol and isolated silanol group, respectively.

Caillerie et al. reported that the chemical shift around 3 – 7 ppm indicated hydrogen bonding between silanol groups on pyrogenic silica and water. The peak was shifted to upper value when the silica was exposed to relatively high humidity [129]. In addition, it was possible that the chemical shift was hydrogen linking silanol groups as reported by Deleplanque et al. who found this chemical shift at 3.1 ppm for ^{1}H MAS NMR spectra of Aerosil® 380 [130].

Table 14 Peak position for ^{1}H MAS NMR of CSD pellets

Formulation No.	HCO-40 concentration (% w/w)	Peak position (ppm)			
		H-bonding	H of isolated silanol	$-CH_2-$	$-CH_3$
1	0.1	4.03	-	1.64	1.28
2	0.5	3.57	-	1.07	0.71
3	1	3.91	-	1.62	1.33
4	1.5	4.20	-	1.66	1.29
5	2	4.04	-	1.63	1.30
6	2.5	4.13	-	1.64	1.29
7	3	3.52	-	1.16	0.70
8	5	4.05	-	1.68	1.28
9	7.5	4.07	-	1.69	1.27
10	10	4.03	-	1.72	1.32
11	12.5	3.57	-	1.18	0.77
Untreated CSD		3.52	1.95	-	-
CSD (process with water)		3.89	-	-	-

The little peak observed at 1.95 ppm was supported by the ^{1}H MAS NMR spectra of Aerosil® 380 which showed the peak of isolated silanol group at 1.85 ppm [130].

The ^{1}H MAS NMR spectra CSD processed with water showed only peak at 3.89 ppm of hydrogen bonding between silanol group and water or silanol groups. The disappearing of the peak at 1.95 ppm of isolated silanol group was because it was accessible by water during the process.

Similarly, the broad peaks at 3.52 – 4.13 ppm were also found for the ^{1}H MAS NMR spectra of all pellet samples (appendix Figure VI-1-Figure VI-2) with absence of

the peak at 1.95 ppm. This could be due to the addition of water in the formulation of pellets which introduced the conversion of isolated silanol group to hydrogen bonded silanol groups.

When there was the surfactant, there appeared to be chemical shifts at 0.77 – 1.33 ppm and at 1.07 – 1.72 ppm in the ^{1}H MAS NMR spectra of pellets. These peaks corresponded to the amount of surfactant in the pellets. The characteristic peaks may be explained by -CH_3 and -CH_2- on the hydrocarbon chain of HCO-40. Rub et al. found that the chemical shift of -CH_3 in ^{1}H NMR spectra of TX-100 surfactant located at 0.549 and 1.124 ppm; and that of -CH_2- showed a peak at 1.495 ppm [131, 132]. Saveyn et al., also found that the chemical shift of -CH_3 group and –CH_2- in ^{1}H NMR spectra of Tween 20 showed peak at 1 and 1.2 ppm, respectively [133].

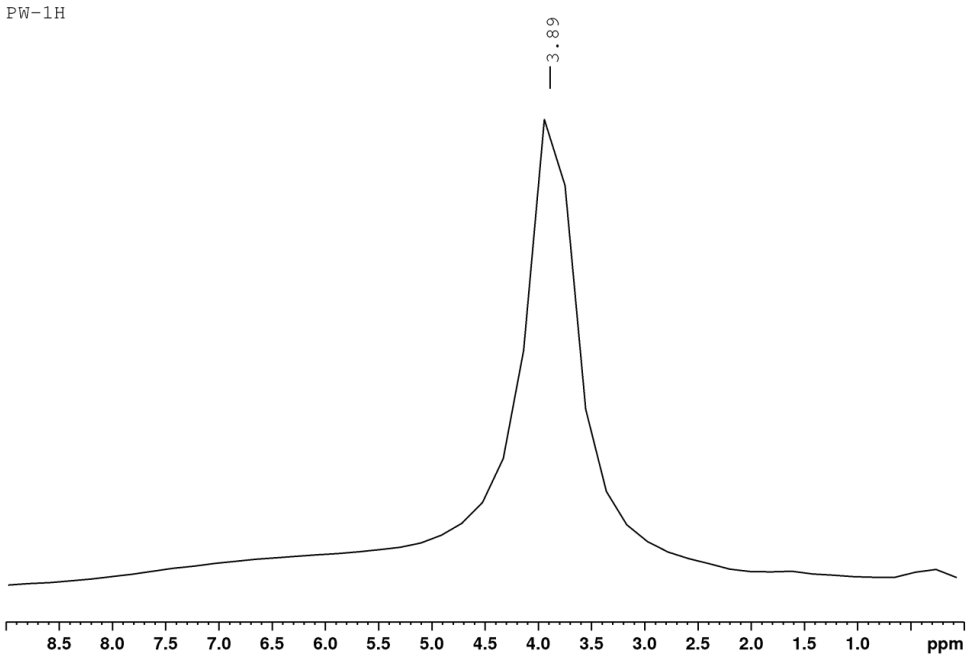

Figure 44 ^{1}H MAS NMR spectrum of CSD processed with water

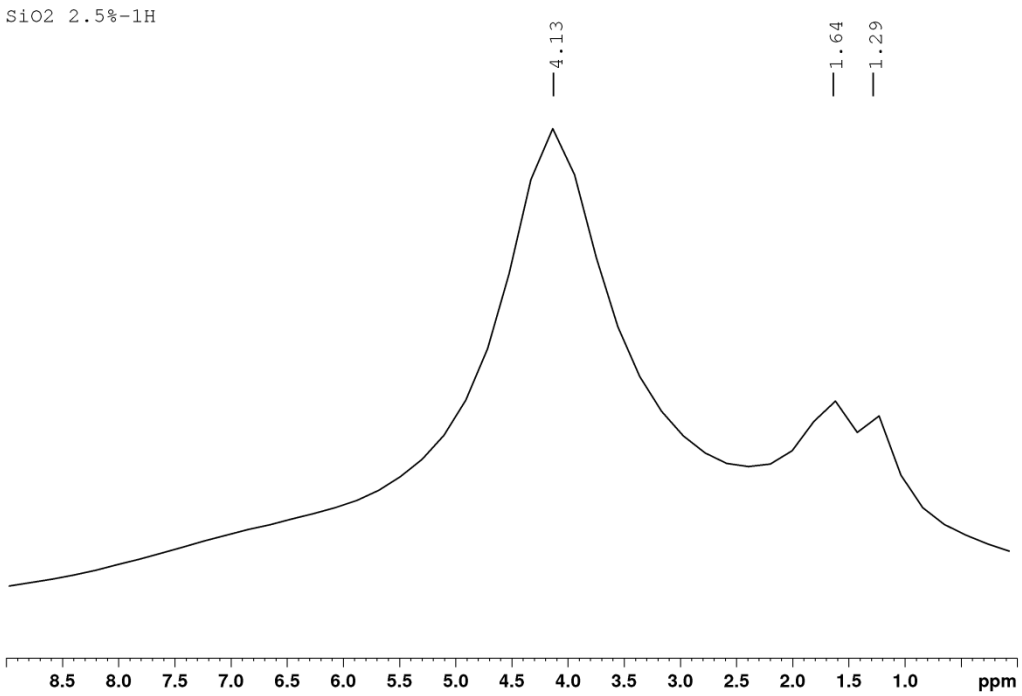

Figure 45 ^{1}H MAS NMR spectrum of CSD pellets made with 2.5% w/w HCO-40

Solid state CP MAS ^{29}Si NMR

Table 15 Peak position for ^{29}Si CP MAS NMR of CSD pellets

Formulation No.	HCO-40 concentration (% w/w)	Peak position (ppm)		
		Q2	Q3	Q4
1	0.1	-94.06	-102.54	-
2	0.5	-95.35	-105.17	-111.06
3	1	-94.30	-103.01	-110.92
4	1.5	-93.71	-102.59	-113.07
5	2	-92.54	-102.27	-109.38
6	2.5	-95.06	-102.98	-115.22
7	3	-96.78	-104.86	-111.36
8	5	-93.71	-103.28	-112.76
9	7.5	-94.40	-102.95	-112.99
10	10	-94.59	-102.98	-111.53
11	12.5	-96.01	-103.76	-113.42
Untreated CSD		-91.90	-98.45	-112.18
CSD (process with water)		-92.70	-102.38	-112.11

It has been reported by Tuel el at. that ^{29}Si CP MAS NMR could separate silanol groups into 3 species. The geminal silanol specie containing 2 silanol groups connected to one silicon atom showed a chemical shift at -90 ppm (Q2). Isolated silanol groups and vicinal silanol groups which are hydrogen bonded silanols were present at -100 ppm (Q3). Silicon dioxide of which the silanol group was lost showed chemical shift at -110 ppm (Q4) [134]. While in the experiment by Humbert, it was found that isolated silanol groups and vicinal silanol groups showed the chemical shift at -96 ppm [135].

In this study, it was found that ^{29}Si CP MAS NMR spectra of untreated CSD showed chemical shift at –91.90, -98.45 and -112.18 ppm (Figure 46). These chemical shifts were due to the presence of geminal silanols, isolated silanols or vicinal silanols and surface siloxanes, respectively.

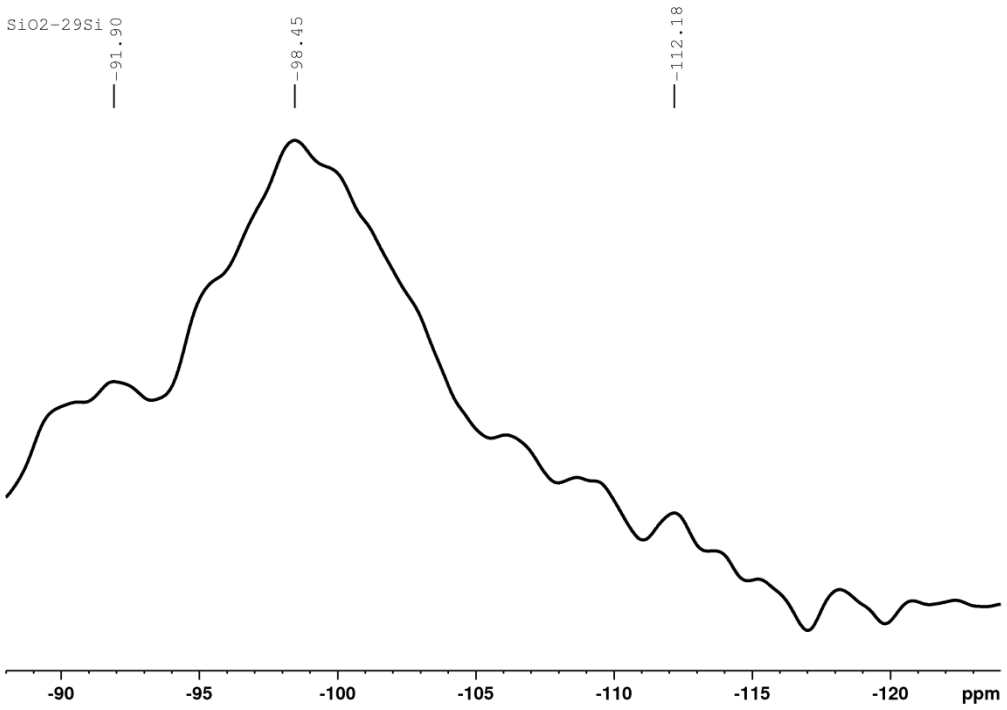

Figure 46 ^{29}Si CP MAS NMR spectrum of untreated CSD

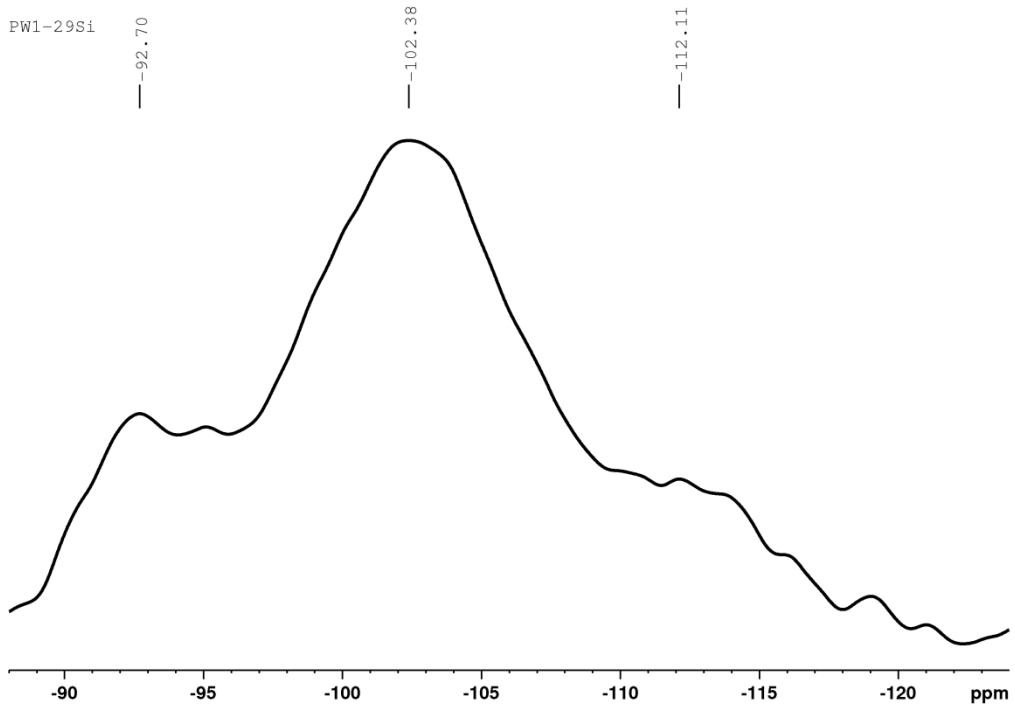

Figure 47 ^{29}Si CP MAS NMR spectrum of CSD processed with water

The ^{29}Si CP MAS NMR spectra shows a slight change in the chemical shift of CSD processed with water to -92.70 and -102.38 ppm for geminal silanol groups and isolated silanol groups and/or hydrogen bonded silanol groups, respectively. Therefore these species might be sensitive to presence of water.

When there was HCO-40 in the pellets, there were inconsistent chemical shifts for geminal silanol groups, isolated silanol groups or vicinal silanols, and siloxanes as shown in Table 15. The chemical shift around -110 ppm was clearly seen as a shoulder of the broad peak in the pellets made HCO-40 which was shown in the spectra (Figure 48, appendix Figure VI-3-Figure VI-4). These might be occurrence of siloxanes.

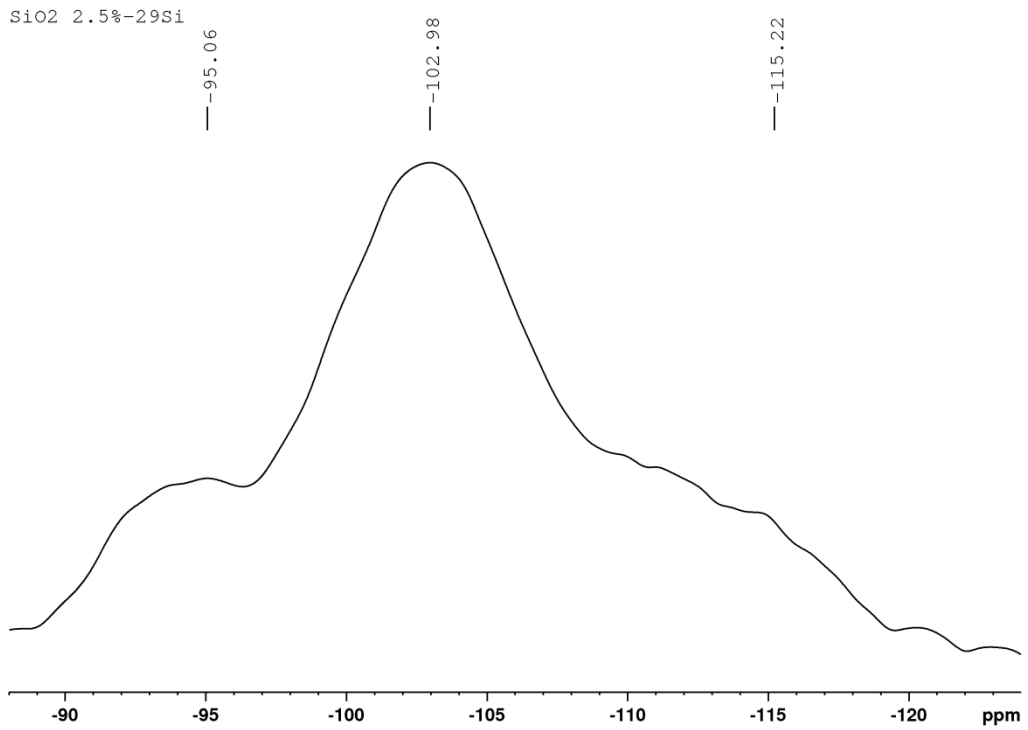

Figure 48 ^{29}Si CP MAS NMR spectrum of CSD pellets made with 2.5% w/w HCO-40

The results from AFM, FT-IR and solid state NMR spectroscopy showed that there was the interaction between CSD and HCO-40.

AFM technique suggested that HCO-40 reduced the contact angle between water and CSD by change in adhesion force. However, AFM result could not indicate adsorption of HCO-40 molecules on surface of CSD. Liquid penetration study using Enslin apparatus indicated that HCO-40 molecules could be aggregated on the CSD surface and help in liquid penetration particularly at the low HCO-40 concentrations. Upon drying, the FT-IR spectroscopy results informed that CSD and HCO-40 in the pellets may interact via weak interaction, like Van de Waals force. This interaction was from hydrocarbon chain of HCO-40 and hydrophobic area of CSD. This was also consistent with both ^{1}H MAS NMR and ^{29}Si CP MAS NMR experiment. However, this weak interaction found in the CSD pellets may not be related to ability of pellet formation.

The formation of pellets could be involved with hydrogen bonding between silanol-silanol groups which allowed CSD particles to form clusters. The clusters required an appropriate elastic property for pellet formation as suggested by rheological study.

In addition, interaction between water and silanol group as indicated by TGA results may play an important role in the extrusion-spheronization of CSD. The interaction between water and CSD surface should be optimal so that the interaction between CSD and CSD particles could dominate the system.

The interaction between water and silanol groups may be modified by addition of HCO-40. HCO-40 molecules could reduce hydration effect and limit the interaction between silanol group from CSD and water via hydrogen bonding. Then the properties of wet mass and extrudate could be adjusted by adjusting content of the HCO-40.

CHAPTER V
CONCLUSIONS

In this study, the effect of a surfactant, polyoxyl 40 hydrogenated castor oil (HCO-40), on the formation of silicon dioxide (CSD) pellets was investigated. The conclusions could be drawn as the following:

The CSD pellets could be formed with CSD to binding liquid ratio at 1: 2. The ability to form pellets was dependent on binding liquid concentrations. Too low concentrations caused uncontrollable agglomeration and too high concentrations resulted in rod shape pellets. The appropriate concentration of binding liquid that formed pellets with rounded shape and narrow size distribution was 2.5 – 3% w/w. The role of binding liquid concentrations was found to be due to change in interaction between water and CSD surface which could be influenced by addition of HCO-40.

In addition, the ability to form pellets was dependent on proportion of solid content to water. The higher solid content was likely to form strong clusters of CSD particles through interaction between silanols which were hard to deform to be spherical particles. The rheological properties may suggest the optimum proportion of solid content to water that could form pellets with the desired property.

Overall results suggested that CSD pellet formation could be achieved by adjusting the amount of CSD, water and HCO-40. It is noted that CSD grade used in this study was fumed hydrophilic silicon dioxide on which its surface contains silanol species and siloxanes.

Further study should be carried out with other surfactants with varied HLB values and with additional fillers.

REFERENCES

[1] SchrÖDer, M. and P. Kleinebudde, Development of disintegrating pellets obtained from extrusion/spheronization. Pharmacy and Pharmacology Communications, 1995, **1**(9): p. 415-418.

[2] Thommes, M. and P. Kleinebudde, Use of **K**-carrageenan as alternative pelletisation aid to microcrystalline cellulose in extrusion/spheronisation. II. Influence of drug and filler type. European Journal of Pharmaceutics and Biopharmaceutics, 2006, **63**(1): p. 68-75.

[3] Basit, A.W., J.M. Newton, and L.F. Lacey, Formulation of ranitidine pellets by extrusion-spheronization with little or no microcrystalline cellulose. Pharmaceutical Development and Technology, 1999, **4**(4): p. 499-505.

[4] Podczeck, F., A novel aid for the preparation of pellets by extrusion/spheronization. Pharmaceutical Technology Europe, 2008, **20**(12).

[5] Rowe, R.C., P.J. Sheskey, M.E. Quinn, and A.P. Association, Handbook of Pharmaceutical Excipients, 6th Edition, Frome, Somerset, : Pharmaceutical Press,2009.

[6] Jonat, S., S. Hasenzahl, M. Drechsler, P. Albers, K.G. Wagner, and P.C. Schmidt, Investigation of compacted hydrophilic and hydrophobic colloidal silicon dioxides as glidants for pharmaceutical excipients. Powder Technology, 2004, **141**(1–2): p. 31-43.

[7] You, J., F.-d. Cui, Y.-s. Wang, Y.-w. Yu, X. Li, and Q.-p. Li, The study of the emulsification efficiency of Aerosil and HPMCAS type and their ratio to stabilize emulsions of zedoary turmeric oil. Colloids and Surfaces A: Physicochemical and Engineering Aspects, 2006, **280**(1–3): p. 76-80.

[8] Oh, D.H., et al., Comparison of solid self-microemulsifying drug delivery system (solid SMEDDS) prepared with hydrophilic and hydrophobic solid carrier. International Journal of Pharmaceutics, 2011, **420**(2): p. 412-418.

[9] Agarwal, V., A. Siddiqui, H. Ali, and S. Nazzal, Dissolution and powder flow characterization of solid self-emulsified drug delivery system (SEDDS). International Journal of Pharmaceutics, 2009, **366**(1–2): p. 44-52.

[10] Dutreilh-Colas, M., M. Yan, P. Labrot, N. Delorme, A. Gibaud, and J.-F. Bardeau, AFM evidence of perpendicular orientation of cylindrical craters on hybrid silica thin film templated by triblock copolymer. Surface Science, 2008, **602**(4): p. 829-833.

[11] Alejandro, G.M. 2004 Viscoelasticity, Fat Crystal Networks, CRC Press. p. 143-159.

[12] Staszczuk, P., Novel studies of phase and structural transitions in bulk and vicinal water. Colloids and Surfaces A, 1995, **94**(2–3): p. 213-224.

[13] Staszczuk, P., Studies of the adsorbed water layers on solid surfaces by means of the thermal analysis special technique. Thermochimica Acta, 1998, **308**(1–2): p. 147-157.

[14] Lee, J.-H. and J.C. Meredith, Non-DLVO silica interaction forces in NMP–water mixtures. II. An asymmetric system. Langmuir, 2011, **27**(16): p. 10000-10006.

[15] Tomer, G. and J.M. Newton, A centrifuge technique for the evaluation of the extent of water movement in wet powder masses. International Journal of Pharmaceutics, 1999, **188**(1): p. 31-38.

[16] Tomer, G., H. Patel, F. Podczeck, and J.M. Newton, Measuring the water retention capacities (MRC) of different microcrystalline cellulose grades. European Journal of Pharmaceutical Sciences, 2001, **12**(3): p. 321-325.

[17] Thommes, M. and P. Kleinebudde, The behavior of different carrageenans in pelletization by extrusion/spheronization. Pharmaceutical Development and Technology, 2008, **13**(1): p. 27-35.

[18] Majidi, S., G.H. Motlagh, B. Bahramian, B. Kaffashi, S.A. Nojoumi, and I. Haririan, Rheological evaluation of wet masses for the preparation of pharmaceutical pellets by capillary and rotational rheometers. Pharmaceutical Development and Technology, 2013, **18**(1): p. 112-120.

[19] Luukkonen, P., J.M. Newton, F. Podczeck, and J. Yliruusi, Use of a capillary rheometer to evaluate the rheological properties of microcrystalline cellulose

and silicified microcrystalline cellulose wet masses. International Journal of Pharmaceutics, 2001, **216**(1-2): p. 147-157.

[20] MacRitchie, K.A., J.M. Newton, and R.C. Rowe, The evaluation of the rheological properties of lactose/microcrystalline cellulose and water mixtures by controlled stress rheometry and the relationship to the production of spherical pellets by extrusion/spheronization. European Journal of Pharmaceutical Sciences, 2002, **17**(1-2): p. 43-50.

[21] Ghebre-Selassie, I., Pharmaceutical Pelletization Technology: Taylor & Francis,1989.

[22] Rough, S.L., J. Bridgwater, and D.I. Wilson, Effects of liquid phase migration on extrusion of microcrystalline cellulose pastes. International Journal of Pharmaceutics, 2000, **204**(1–2): p. 117-126.

[23] Mascia, S., M.J. Patel, S.L. Rough, P.J. Martin, and D.I. Wilson, Liquid phase migration in the extrusion and squeezing of microcrystalline cellulose pastes. European Journal of Pharmaceutical Sciences, 2006, **29**(1): p. 22-34.

[24] Tomer, G. and J.M. Newton, Water movement evaluation during extrusion of wet powder masses by collecting extrudate fractions. International Journal of Pharmaceutics, 1999, **182**(1): p. 71-7.

[25] Ek, R. and J.M. Newton, Microcrystalline cellulose as a sponge as an alternative concept to the crystallite-gel model for extrusion and spheronization. Pharmaceutical Research, 1998, **15**(4): p. 509-512.

[26] Fielden, K.E., J.M. Newton, P. O'Brien, and R.C. Rowe, Thermal studies on the interaction of water and microcrystalline cellulose. Journal of Pharmacy and Pharmacology, 1988, **40**(10): p. 674-8.

[27] Kleinebudde, P., The crystallite-gel-model for microcrystalline cellulose in wet-granulation, extrusion, and spheronization. Pharmaceutical Research, 1997, **14**(6): p. 804-809.

[28] Millili, G.P. and J.B. Schwartz, The strength of microcrystalline cellulose pellets: The effect of granulating with water/ethanol mixtures. Drug Development and Industrial Pharmacy, 1990, **16**(8): p. 1411-1426.

[29] Lindner, H. and P. Kleinebudde, Use of powdered cellulose for the production of pellets by extrusion/spheronization. The Journal of Pharmacy and Pharmacology, 1994, **46**(1): p. 2-7.

[30] Fechner, P., S. Wartewig, M. Füting, A. Heilmann, R.H. Neubert, and P. Kleinebudde, Properties of microcrystalline cellulose and powder cellulose after extrusion/spheronization as studied by fourier transform Raman spectroscopy and environmental scanning electron microscopy. AAPS PharmSci, 2003, **5**(4): p. 77-89.

[31] Alvarez, L., A. Concheiro, J.L. Gómez-Amoza, C. Souto, and R. Mart1 nez-Pacheco, Powdered cellulose as excipient for extrusion spheronization pellets of a cohesive hydrophobic drug. European Journal of Pharmaceutics and Biopharmaceutics, 2003, **55**(3): p. 291-295.

[32] Chatlapalli, R. and B.D. Rohera, Physical characterization of HPMC and HEC and investigation of their use as pelletization aids. International Journal of Pharmaceutics, 1998, **161**(2): p. 179-193.

[33] Chatlapalli, R. and B.D. Rohera, Rheological characterization of diltiazem HCl/cellulose wet masses using a mixer torque rheometer. International Journal of Pharmaceutics, 1998, **175**(1): p. 47-59.

[34] Jess, K. and H. Steckel, The extrusion and spheronization of chitosan. Pharmaceutical Technology Europe, 2007.

[35] Bornhöft, M., M. Thommes, and P. Kleinebudde, Preliminary assessment of carrageenan as excipient for extrusion/spheronisation. European Journal of Pharmaceutics and Biopharmaceutics, 2005, **59**(1): p. 127-131.

[36] Thommes, M. and P. Kleinebudde, Properties of pellets manufactured by wet extrusion/spheronization process using kappa-carrageenan: effect of process parameters. AAPS PharmSciTech, 2007, **8**(4): p. E95.

[37] Thommes, M. and P. Kleinebudde, Use of **K**-carrageenan as alternative pelletisation aid to microcrystalline cellulose in extrusion/spheronisation. I. Influence of type and fraction of filler. European Journal of Pharmaceutics and Biopharmaceutics, 2006, **63**(1): p. 59-67.

[38] Tho, I., S. Arne Sande, and P. Kleinebudde, Cross-linking of amidated low-methoxylated pectin with calcium during extrusion/spheronisation: Effect on particle size and shape. Chemical Engineering Science, 2005, **60**(14): p. 3899-3907.

[39] Tho, T., P. Kleinebudde, and S.A. Sande, Extrusion/spheronization of pectin-based formulations. I. Screening of important factors. AAPS PharmSciTech, 2001, **2**(4): p. 26.

[40] Verheyen, P., K.J. Steffens, and P. Kleinebudde, Use of crospovidone as pelletization aid as alternative to microcrystalline cellulose: Effects on pellet properties. Drug Development and Industrial Pharmacy, 2009, **35**(11): p. 1325-1332.

[41] Chatchawalsaisin, J., F. Podczeck, and J.M. Newton, The preparation by extrusion/spheronization and the properties of pellets containing drugs, microcrystalline cellulose and glyceryl monostearate. European Journal of Pharmaceutical Sciences, 2005, **24**(1): p. 35-48.

[42] Nowak, R. and U. Schachtel, Aerosil® fume silica and Sipernat® in sealant, in *Technical Bulletin Fine Particles 63*, D. AG, Editor. 2015, Evonik Degussa GmbH.

[43] Jesionowski, T., M. Pokora, K. Sobaszkiewicz, and J. Pernak, Preparation and characterization of functionalized precipitated silica SYLOID® 244 using ionic liquids as modifiers. Surface and Interface Analysis, 2004, **36**(11): p. 1491-1496.

[44] Basic characteristics of AEROSIL® fumed silica, in *Technical Bulletin Fine Particles 11*, D. AG, Editor., Evonik Degussa GmbH.

[45] Mathias, J. and G. Wannemacher, Basic characteristics and applications of aerosil: 30. The chemistry and physics of the aerosil Surface. Journal of Colloid and Interface Science, 1988, **125**(1): p. 61-68.

[46] AEROPERL® Granulated fumed oxides, in *Technical Information 1341*, D. AG, Editor., Evonik Degussa GmbH.

[47] Zhuravlev, L.T., The surface chemistry of amorphous silica. Zhuravlev model. Colloids and Surfaces A: Physicochemical and Engineering Aspects, 2000, **173**(1–3): p. 1-38.

[48] Mallick, S., S. Kumar Pradhan, M. Chandran, M. Acharya, T. Digdarsini, and R. Mohapatra, Study of particle rearrangement, compression behavior and dissolution properties after melt dispersion of ibuprofen, Avicel and Aerosil. Results in Pharma Sciences, 2011, **1**(1): p. 1-10.

[49] Jonat, S., S. Hasenzahl, A. Gray, and P.C. Schmidt, Influence of compacted hydrophobic and hydrophilic colloidal silicon dioxide on tableting properties of pharmaceutical excipients. Drug Development and Industrial Pharmacy, 2005, **31**(7): p. 687-96.

[50] Ohta, K.M., M. Fuji, T. Takei, and M. Chikazawa, Effect of geometric structure and surface wettability of glidant on tablet hardness. International Journal of Pharmaceutics, 2003, **262**(1–2): p. 75-82.

[51] Meyer, K. and I. Zimmermann, Effect of glidants in binary powder mixtures. Powder Technology, 2004, **139**(1): p. 40-54.

[52] Perge, L., M. Robitzer, C. Guillemot, J.-M. Devoisselle, F. Quignard, and P. Legrand, New solid lipid microparticles for controlled ibuprofen release: Formulation and characterization study. International Journal of Pharmaceutics, 2012, **422**(1–2): p. 59-67.

[53] Kittipongpatana, O.S. and N. Kittipongpatana, Preparation and physicomechanical properties of co-precipitated rice starch-colloidal silicon dioxide. Powder Technology, 2012, **217**(0): p. 377-382.

[54] Vongsurakrai, V. and S. Varavinit, Effect of nano silicon dioxide on tablet properties of rice starch Advanced Materials Research, 2010, **93-94**: p. 679-682.

[55] Podczeck, G.F., Pellet formulation comprising colloidal silicon dioxide U.S.P.A. Publication, Editor. 2009. p. 1 - 6.

[56] Desai, D., et al., Surfactant-mediated dissolution of Metformin hydrochloride tablets: Wetting effects versus Ion pairs diffusivity. Journal of Pharmaceutical Sciences, 2014, **103**(3): p. 920-926.

[57] Mah, P.T., L. Peltonen, D. Novakovic, T. Rades, C.J. Strachan, and T. Laaksonen, The effect of surfactants on the dissolution behavior of

amorphous formulations. European Journal of Pharmaceutics and Biopharmaceutics, 2016, **103**: p. 13-22.

[58] Allaboun, H., K.A. Alkhamis, and N.D. Al Jbour, Effect of surfactant on dissolution of spherical particles in micellar systems. European Journal of Pharmaceutics and Biopharmaceutics, 2007, **65**(2): p. 188-197.

[59] Alkhamis, K.A., H. Allaboun, and W.a.Y. Al‐Momani, Study of the solubilization of gliclazide by aqueous micellar solutions. Journal of Pharmaceutical Sciences, 2003, **92**(4): p. 839-846.

[60] Balakrishnan, A., B.D. Rege, G.L. Amidon, and J.E. Polli, Surfactant-mediated dissolution: Contributions of solubility enhancement and relatively low micelle diffusivity. Journal of Pharmaceutical Sciences, 2004, **93**(8): p. 2064-2075.

[61] Kolašinac, N., K. Kachrimanis, I. Homšek, B. Grujić, Z. Đurić, and S. Ibrić, Solubility enhancement of desloratadine by solid dispersion in poloxamers. International Journal of Pharmaceutics, 2012, **436**(1–2): p. 161-170.

[62] Ali, W., A.C. Williams, and C.F. Rawlinson, Stochiometrically governed molecular interactions in drug: Poloxamer solid dispersions. International Journal of Pharmaceutics, 2010, **391**(1–2): p. 162-168.

[63] Song, C.K., I.-S. Yoon, and D.-D. Kim, Poloxamer-based solid dispersions for oral delivery of docetaxel: Differential effects of F68 and P85 on oral docetaxel bioavailability. International Journal of Pharmaceutics, 2016, **507**(1–2): p. 102-108.

[64] Podczeck, F., A. Maghetti, and J.M. Newton, The influence of non-ionic surfactants on the rheological properties of drug/microcrystalline cellulose/water mixtures and their use in the preparation and drug release performance of pellets prepared by extrusion/spheronization. European Journal of Pharmaceutical Sciences, 2009, **37**(3–4): p. 334-340.

[65] Levis, S.R. and P.B. Deasy, Pharmaceutical applications of size reduced grades of surfactant co-processed microcrystalline cellulose. International Journal of Pharmaceutics, 2001, **230**(1–2): p. 25-33.

[66] Podczeck, F., P. Alessi, and J.M. Newton, The preparation of pellets containing non-ionic surfactants by extrusion/spheronization. International Journal of Pharmaceutics, 2008, **361**(1–2): p. 33-40.

[67] Newton, J.M., M.R. Pinto, and F. Podczeck, The preparation of pellets containing a surfactant or a mixture of mono- and di-gylcerides by extrusion/spheronization. European Journal of Pharmaceutical Sciences, 2007, **30**(3–4): p. 333-342.

[68] Matsaridou, I., P. Barmpalexis, A. Salis, and I. Nikolakakis, The influence of surfactant HLB and oil/surfactant ratio on the formation and properties of self-emulsifying pellets and microemulsion reconstitution. AAPS PharmSciTech, 2012, **13**(4): p. 1319-1330.

[69] Nikolakakis, I., A. Panagopoulou, A. Salis, and S. Malamataris, Relationships between the properties of self-emulsifying pellets and of the emulsions used as massing liquids for their preparation. AAPS PharmSciTech, 2014: p. 1-11.

[70] Newton, M., J. Petersson, F. Podczeck, A. Clarke, and S. Booth, The influence of formulation variables on the properties of pellets containing a self-emulsifying mixture. Journal of Pharmaceutical Sciences, 2001, **90**(8): p. 987-995.

[71] Newton, J.M., M. Bazzigialuppi, F. Podczeck, S. Booth, and A. Clarke, The rheological properties of self-emulsifying systems, water and microcrystalline cellulose. European Journal of Pharmaceutical Sciences, 2005, **26**(2): p. 176-183.

[72] Harrison, P.J., J.M. Newton, and R.C. Rowe, The application of capillary rheometry to the extrusion of wet powder masses. International Journal of Pharmaceutics, 1987, **35**(3): p. 235-242.

[73] Tomer, G., F. Podczeck, and J.M. Newton, The influence of model drugs on the preparation of pellets by extrusion/spheronization: II spheronization parameters. International Journal of Pharmaceutics, 2002, **231**(1): p. 107-119.

[74] Tomer, G., F. Podczeck, and J.M. Newton, The influence of type and quantity of model drug on the extrusion/spheronization of mixtures with

microcrystalline cellulose: I. Extrusion parameters. International Journal of Pharmaceutics, 2001, **217**(1-2): p. 237-248.

[75] Rough, S.L. and D.I. Wilson, Extrudate fracture and spheronisation of microcrystalline cellulose pastes. Journal of Materials Science, 2005, **40**(16): p. 4199-4219.

[76] Di Pretoro, G., L. Zema, A. Gazzaniga, S.L. Rough, and D.I. Wilson, Extrusion spheronisation of highly loaded 5-ASA multiparticulate dosage forms. International Journal of Pharmaceutics, 2010, **402**(1-2): p. 153-164.

[77] Wang, R. and S.L. Wunder, Effects of silanol density, distribution, and hydration state of fumed silica on the formation of self-assembled monolayers of n-octadecyltrichlorosilane. Langmuir, 2000, **16**(11): p. 5008-5016.

[78] Maretto, M., R. Vignola, C.D. Williams, R. Bagatin, A. Latini, and M. Petrangeli Papini, Adsorption of hydrocarbons from industrial wastewater onto a silica mesoporous material: Structural and thermal study. Microporous and Mesoporous Materials, 2015, **203**(0): p. 139-150.

[79] Zhang, Y., et al., Effect of a mixed anionic-nonionic surfactant adsorption on bentonite structure and on distribution of pentachlorophenol. Applied Clay Science, 2012, **69**(0): p. 93-98.

[80] Zhang, P., J. Forsgren, and M. Strømme, Stabilisation of amorphous ibuprofen in Upsalite, a mesoporous magnesium carbonate, as an approach to increasing the aqueous solubility of poorly soluble drugs. International Journal of Pharmaceutics, 2014, **472**(1–2): p. 185-191.

[81] Kratzer, A.M., Hydration, dough formation and structure development in durum wheat pasta processing, Doctoral dissertation, Swiss Federal Institute of Technology Zurich, 2007

[82] Caprez, A., E. Arrigoni, R. Amadò, and H. Neukom, Influence of different types of thermal treatment on the chemical composition and physical properties of wheat bran. Journal of Cereal Science, 1986, **4**(3): p. 233-239.

[83] Wu, J.-S., H.-O. Ho, and M.-T. Sheu, A statistical design to evaluate the influence of manufacturing factors and material properties on the mechanical

performances of microcrystalline cellulose. Powder Technology, 2001, **118**(3): p. 219-228.

[84] Shah, V., B. Bharatiya, A.D. Shukla, T. Mukherjee, and D.O. Shah, Adsorption of nonionic Brij and Tween surfactants at PTFE-water and air-water interfaces: Investigations on wetting, dispersion stability, foaming and drug solubilization. Colloids and Surfaces A: Physicochemical and Engineering Aspects, 2016, **508**: p. 159-166.

[85] Jaine, J.E. and M.R. Mucalo, Measurements of the wettability of catalyst support materials using the Washburn capillary rise technique. Powder Technology, 2015, **276**: p. 123-128.

[86] Soh, J.L.P., C.V. Liew, and P.W.S. Heng, Torque rheological parameters to predict pellet quality in extrusion–spheronization. International Journal of Pharmaceutics, 2006, **315**(1–2): p. 99-109.

[87] Alvarez, L., A. Concheiro, J.L. Gomez-Amoza, C. Souto, and R. Martinez-Pacheco, Effect of microcrystalline cellulose grade and process variables on pellets prepared by extrusion-spheronization. Drug Development and Industrial Pharmacy, 2002, **28**(4): p. 451-6.

[88] McNamee, C.E., et al., Surface and friction forces between grafted polysaccharide layers in the absence and presence of surfactant. Journal of Colloid and Interface Science, 2011, **364**(2): p. 351-358.

[89] Lüderitz, L.A.C. and R. v. Klitzing, Interaction forces between silica surfaces in cationic surfactant solutions: An atomic force microscopy study. Journal of Colloid and Interface Science, 2013, **402**(0): p. 19-26.

[90] Raghavan, D., X. Gu, T. Nguyen, M. VanLandingham, and A. Karim, Mapping polymer heterogeneity using atomic force microscopy phase imaging and nanoscale indentation. Macromolecules, 2000, **33**(7): p. 2573-2583.

[91] Silbert, G., N. Kampf, and J. Klein, Normal and shear forces between charged solid surfaces immersed in cationic surfactant solution: The role of the alkyl chain length. Langmuir, 2014, **30**(18): p. 5097-5104.

[92] Song, X., P. Li, Y. Wang, C. Dong, and R.K. Thomas, Solvent effect on the aggregate of fluorinated gemini surfactant at silica surface. Journal of Colloid and Interface Science, 2006, **304**(1): p. 37-44.

[93] Thomann, Y., H.-J. Cantow, G. Bar, and M.-H. Whangbo, Investigation of morphologies and nanostructures of polymer blends by tapping mode phase imaging. Applied Physics A, **66**(1): p. 1233-1236.

[94] Tamayo, J. and R. García, Deformation, contact time, and phase contrast in tapping mode scanning force microscopy. Langmuir, 1996, **12**(18): p. 4430-4435.

[95] Bar, G., R. Brandsch, and M.-H. Whangbo, Effect of viscoelastic properties of polymers on the phase shift in tapping mode atomic force microscopy. Langmuir, 1998, **14**(26): p. 7343-7347.

[96] Van Roosmalen, A.J. and J.C. Mol, An infrared study of the silica gel surface. 1. Dry silica gel. The Journal of Physical Chemistry, 1978, **82**(25): p. 2748-2751.

[97] Van Roosmalen, A.J. and J.C. Mol, An infrared study of the silica gel surface. 2. Hydration and dehydration. The Journal of Physical Chemistry, 1979, **83**(19): p. 2485-2488.

[98] Tripp, C.P. and M.L. Hair, An infrared study of the reaction of octadecyltrichlorosilane with silica. Langmuir, 1992, **8**(4): p. 1120-1126.

[99] Murray, D.K., Differentiating and characterizing geminal silanols in silicas by 29Si NMR spectroscopy. Journal of Colloid and Interface Science, 2010, **352**(1): p. 163-170.

[100] Sizun, C., J. Raya, A. Intasiri, A. Boos, and K. Elbayed, Investigation of the surfactants in CTAB-templated mesoporous silica by 1H HRMAS NMR. Microporous and Mesoporous Materials, 2003, **66**(1): p. 27-36.

[101] Kohlbrecher, J., SASfit: A program for fitting simple structural models to small angle scattering data, User guide for the SASfit software package, Villigen, Switzerland: Paul Scherrer Institute,2014.

[102] Rugmai, S., Small/Wide Angle X-ray Scattering (SAXS/WAXS) Station Manual, Thailand: Synchrotron light research institute,2014.

[103] Sarkar, B., V. Venugopal, M. Tsianou, and P. Alexandridis, Adsorption of Pluronic block copolymers on silica nanoparticles. Colloids and Surfaces A: Physicochemical and Engineering Aspects, 2013, **422**(0): p. 155-164.

[104] Bharti, B., J. Meissner, U. Gasser, and G.H. Findenegg, Surfactant adsorption and aggregate structure at silica nanoparticles: Effects of particle size and surface modification. Soft Matter, 2012, **8**(24): p. 6573-6581.

[105] Balmer, J.A., O.O. Mykhaylyk, A. Schmid, S.P. Armes, J.P.A. Fairclough, and A.J. Ryan, Characterization of polymer-silica nanocomposite particles with core–shell morphologies using Monte Carlo simulations and small angle X-ray scattering. Langmuir, 2011, **27**(13): p. 8075-8089.

[106] Brambilla, R., G.P. Pires, N.P. da Silveira, J.H.Z. dos Santos, M.S.L. Miranda, and R.L. Frost, Spherical and lamellar octadecylsilane hybrid silicas. Journal of Non-Crystalline Solids, 2008, **354**(45–46): p. 5033-5040.

[107] Brookfield DV-II+ Programmable Viscometer Operating Instructions, Brookfield Engineering Laboratories, Inc., Middleboro, USA.

[108] Ferrari, F., M. Bertoni, M.C. Bonferoni, S. Rossi, C. Caramella, and M.J. Waring, Comparative evaluation of hydrocolloid dressings by means of water uptake and swelling force measurements: II. International Journal of Pharmaceutics, 1995, **117**(1): p. 49-55.

[109] Jackson, B. Hexane, B&J Brand. Available from: https://labchemicals-honeywell.com/hexane-b-j-brandr-211.2015 [cited 2016, Aug, 13].

[110] Surface tension values of some common test liquids for surface energy analysis. DataPhysics Instruments GmbH.

[111] Sis, H. and M. Birinci, Wetting and rheological characteristics of hydrophobic organic pigments in water in the presence of non-ionic surfactants. Colloids and Surfaces A: Physicochemical and Engineering Aspects, 2014, **455**: p. 58-66.

[112] Galet, L., S. Patry, and J. Dodds, Determination of the wettability of powders by the Washburn capillary rise method with bed preparation by a centrifugal packing technique. Journal of Colloid and Interface Science, 2010, **346**(2): p. 470-475.

[113] Staszczuk, P., Studies of silica gel surface wetting phenomena by means of controlled-rate thermal analysis. Colloids and Surfaces A: Physicochemical and Engineering Aspects, 1995, **105**(2–3): p. 291-303.

[114] Madathingal, R.R. and S.L. Wunder, Thermal degradation of poly(methyl methacrylate) on SiO2 nanoparticles as a function of SiO2 size and silanol density. Thermochimica Acta, 2011, **526**(1–2): p. 83-89.

[115] Staszczuk, P., Special applications of thermal analysis in the investigation of liquid/solid systems. Thermochimica Acta, 1997, **299**(1–2): p. 133-140.

[116] Shipway, P.H. and I.M. Hutchings, Fracture of brittle spheres under compression and impact loading. I. Elastic stress distributions. Philosophical Magazine A, 1993, **67**(6): p. 1389-1404.

[117] Patist, A., S.G. Oh, R. Leung, and D.O. Shah, Kinetics of micellization: its significance to technological processes. Colloids and Surfaces A: Physicochemical and Engineering Aspects, 2001, **176**(1): p. 3-16.

[118] Sigma-Aldrich, Savety data sheet, in *Kolliphor® RH 40*. 2014, Sigma-Aldrich Pte Ltd: The Capricorn, Singapore Science Park Road II, Singapore.

[119] Raghavan, S.R., J. Hou, G.L. Baker, and S.A. Khan, Colloidal interactions between particles with tethered nonpolar chains dispersed in polar media: Direct correlation between dynamic rheology and interaction parameters. Langmuir, 2000, **16**(3): p. 1066-1077.

[120] Raghavan, S.R., H.J. Walls, and S.A. Khan, Rheology of silica dispersions in organic liquids: New evidence for solvation forces dictated by hydrogen bonding. Langmuir, 2000, **16**(21): p. 7920-7930.

[121] Ryo, Y., Y. Nakai, and M. Kawaguchi, Viscoelastic measurements of silica suspensions in aqueous cellulose derivative solutions. Langmuir, 1992, **8**(10): p. 2413-2416.

[122] Reintjes, T., Solubility Enhancement with BASH Pharma polymers: Solubilizer Compendium, Lampertheim, Germany: BASF,2011.

[123] Wang, Y. and B.A. Morrow, Infrared study of the chemisorption of pentamethylantimony on silica. Langmuir, 1996, **12**(17): p. 4153-4157.

[124] Kulkarni, S.A., S.B. Ogale, and K.P. Vijayamohanan, Tuning the hydrophobic properties of silica particles by surface silanization using mixed self-assembled monolayers. Journal of Colloid and Interface Science, 2008, **318**(2): p. 372-379.

[125] Kniffler, N., B. Schröder, and J. Geiger, Vibrational spectroscopy of hydrogenated evaporated amorphous silicon films. Journal of Non-Crystalline Solids, 1983, **58**(2): p. 153-163.

[126] Perry, C.C., X. Li, and D.N. Waters, Structural studies of gel phases—IV. An infrared reflectance and Fourier transform Raman study of silica and silica/titania gel glasses. Spectrochimica Acta Part A: Molecular Spectroscopy, 1991, **47**(9): p. 1487-1494.

[127] Brinck, J., B. Jönsson, and F. Tiberg, Kinetics of nonionic surfactant adsorption and desorption at the silica–water interface: Binary systems. Langmuir, 1998, **14**(20): p. 5863-5876.

[128] Erkelens, J. and T.J. Liefkens, Infrared spectra of some long-chain esters adsorbed on Aerosil. Journal of Catalysis, 1975, **39**(2): p. 173-180.

[129] d'espinose de la Caillerie, J.-B., M.R. Aimeur, Y.E. Kortobi, and A.P. Legrand, Water adsorption on pyrogenic silica followed by1H MAS NMR. Journal of Colloid and Interface Science, 1997, **194**(2): p. 434-439.

[130] Deleplanque, J., R. Hubaut, P. Bodart, M. Fournier, and A. Rives, 1H and 31P solid-state NMR of trimethylphosphine adsorbed on heteropolytungstate supported on silica. Applied Surface Science, 2009, **255**(9): p. 4897-4901.

[131] Rub, M.A., F. Khan, N. Azum, A.M. Asiri, and H.M. Marwani, Micellization phenomena of amphiphilic drug and TX-100 mixtures: Fluorescence, UV-visible and 1H NMR study. Journal of the Taiwan Institute of Chemical Engineers, 2016, **60**: p. 32-43.

[132] Rub, M.A., F. Khan, M.S. Sheikh, N. Azum, and A.M. Asiri, Tensiometric, fluorescence and 1H NMR study of mixed micellization of non-steroidal anti-inflammatory drug sodium salt of ibuprofen in the presence of non-ionic surfactant in aqueous/urea solutions. The Journal of Chemical Thermodynamics, 2016, **96**: p. 196-207.

[133] Saveyn, P., et al., Solubilization of flurbiprofen within non-ionic Tween 20 surfactant micelles: a 19F and 1H NMR study. Physical Chemistry Chemical Physics, 2009, **11**(26): p. 5462-5468.

[134] Tuel, A., H. Hommel, A.P. Legrand, and E.S. Kovats, A silicon-29 NMR study of the silanol population at the surface of derivatized silica. Langmuir, 1990, **6**(4): p. 770-775.

[135] Humbert, B., Estimation of hydroxyl density at the surface of pyrogenic silicas by complementary NMR and raman experiments. Journal of Non-Crystalline Solids, 1995, **191**(1–2): p. 29-37.

APPENDIX

Appendix I: Radius of gyration

Table I-1 Radius of gyration (R_g) from SAXS

HCO-40 concentration (% w/w)	R_g from Guinier fit (nm), n=1			
	Sample			
	Solution	Suspension	Wet mass	Pellet
DI water	NA	15.4*	NA	NA
0.1	12.6*	15.4*	16.9*	13.7*
0.5	5.9	15.6*	14.4*	13.8*
1	5.0	15.6*	14.2*	14.0*
1.5	5.3	15.7*	14.2*	13.9*
2	5.9	15.6*	13.8*	14.1*
2.5	6.4	15.6*	14.1*	14.2*
3	4.8	15.6*	14.1*	14.3*
5	4.6	15.6*	14.5*	14.3*
7.5	3.9	15.6*	14.5*	14.6*
10	4.0	15.5*	16.1*	14.8*
12.5	5.0	15.5*	15.2*	15.8*

* Data invalid due to R_g multiplied by maximum q-value was more than 1, fitted with 5 minimum q value; NA, no data.

Appendix II: Liquid binding ability of CSD

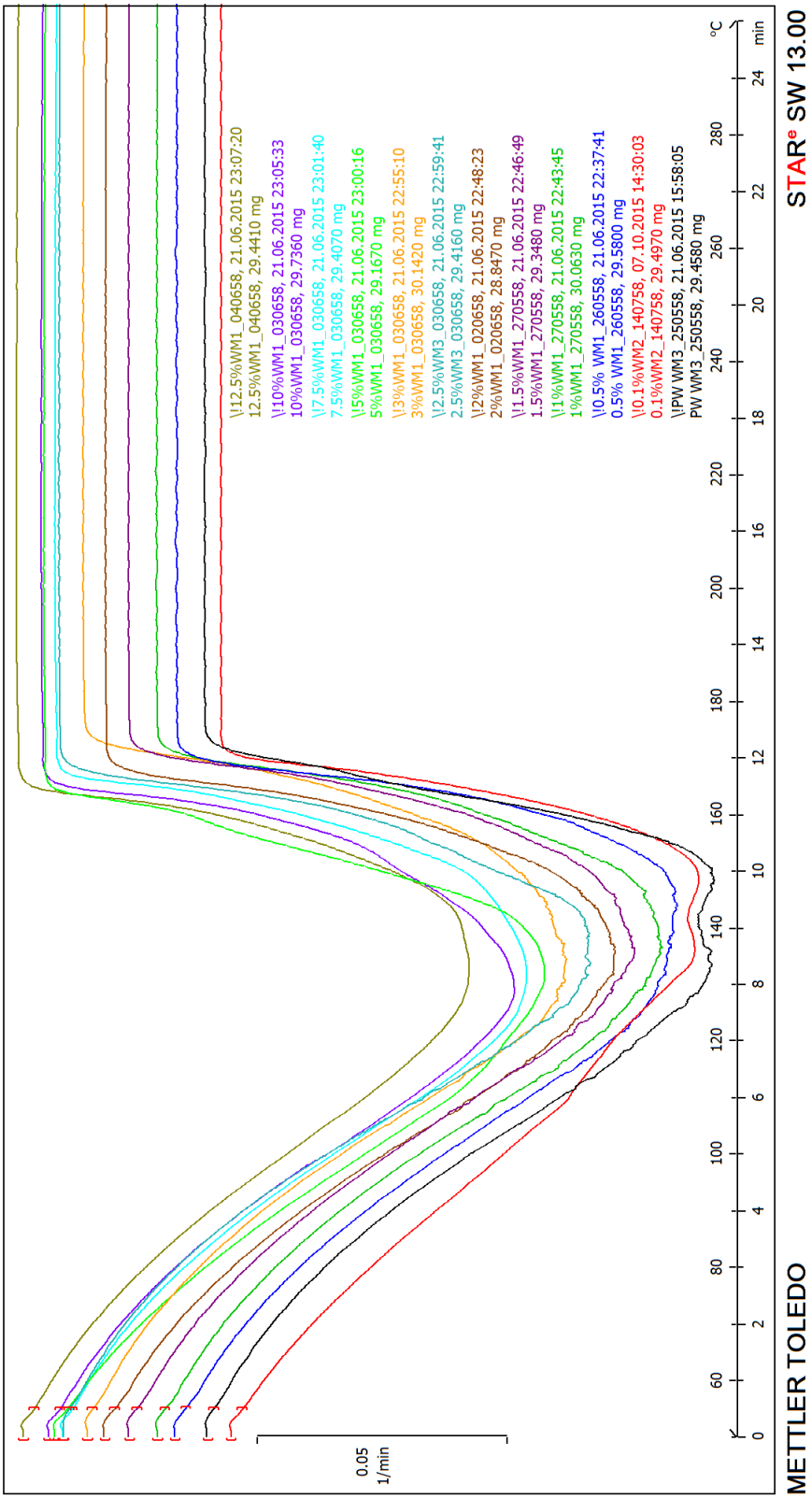

Figure II-1 First derivative thermogram in the range of 50 – 250°C of the CSD wet mass

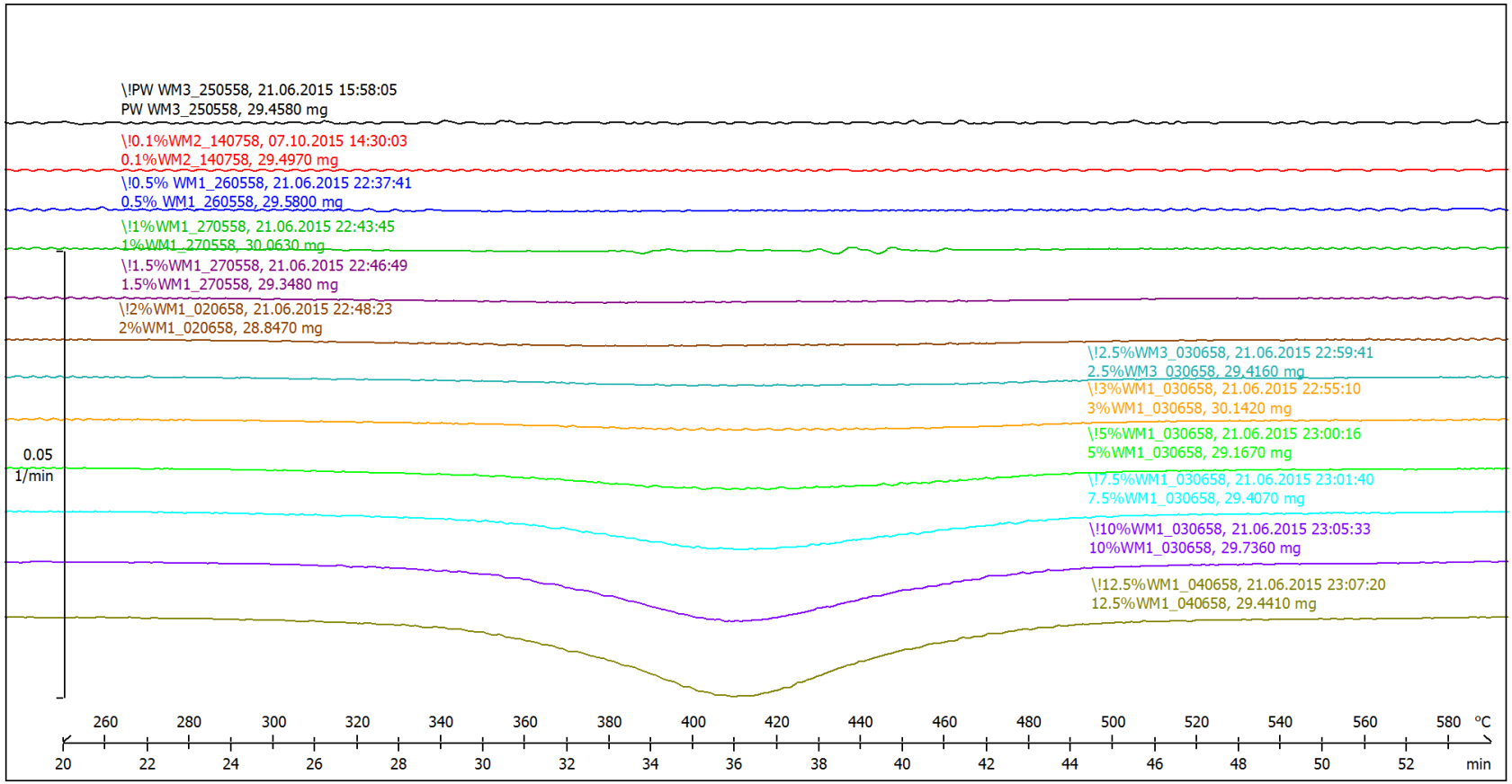

Figure II-2 First derivative thermogram in the range of 250 – 600°C of the CSD wet mass

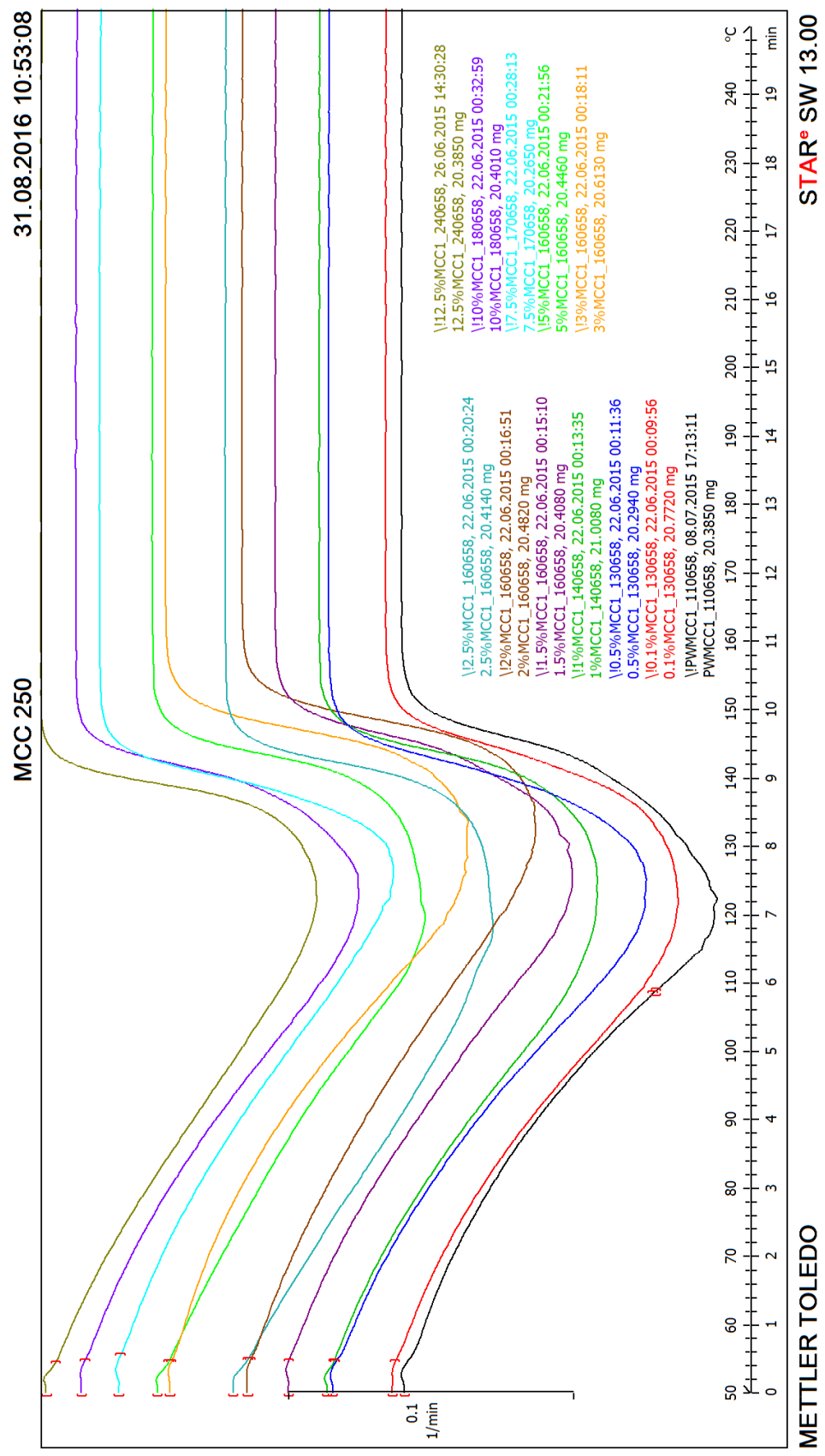

Figure II-3 First derivative thermogram in the range of 50-250°C of the MCC wet mass

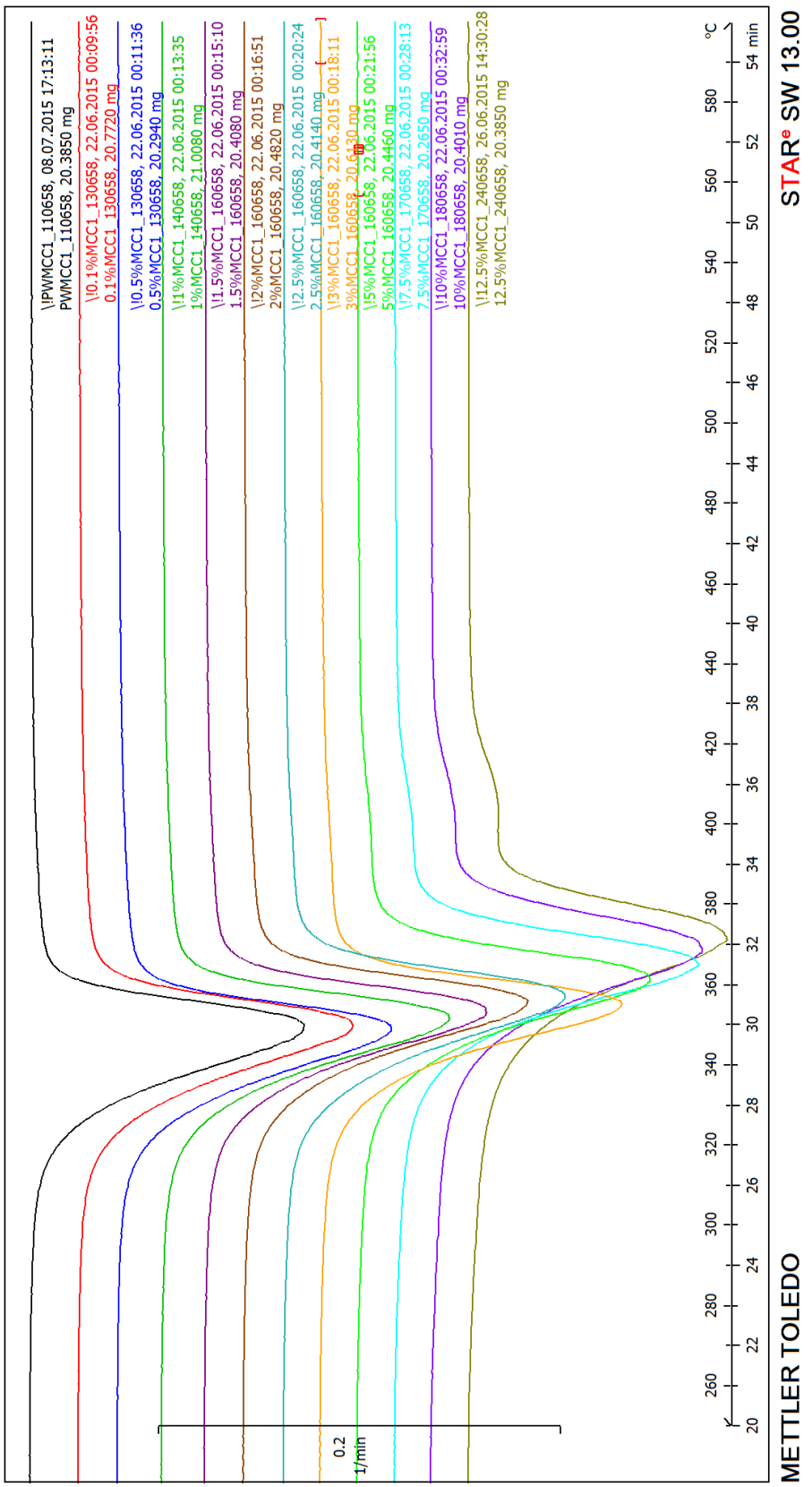

Figure II-4 First derivative thermogram in the range of 250-600°C of the MCC wet mass

Table II-1 Degradation temperature of MCC in wet mass

HCO-40 Concentration (% w/w)	MCC degradation (°C)
DI water	348.5 (0.9)
0.1	347.7 (0.4)
0.5	347.7 (1.5)
1	349.4 (1.0)
1.5	350.6 (0.3)
2	352.4 (1.1)
2.5	353.4 (1.1)
3	354.0 (0.9)
5	358.9 (0.6)
7.5	363.0 (0.5)
10	366.5 (0.5)
12.5	370.2 (0.7)

Appendix III: Rheological data

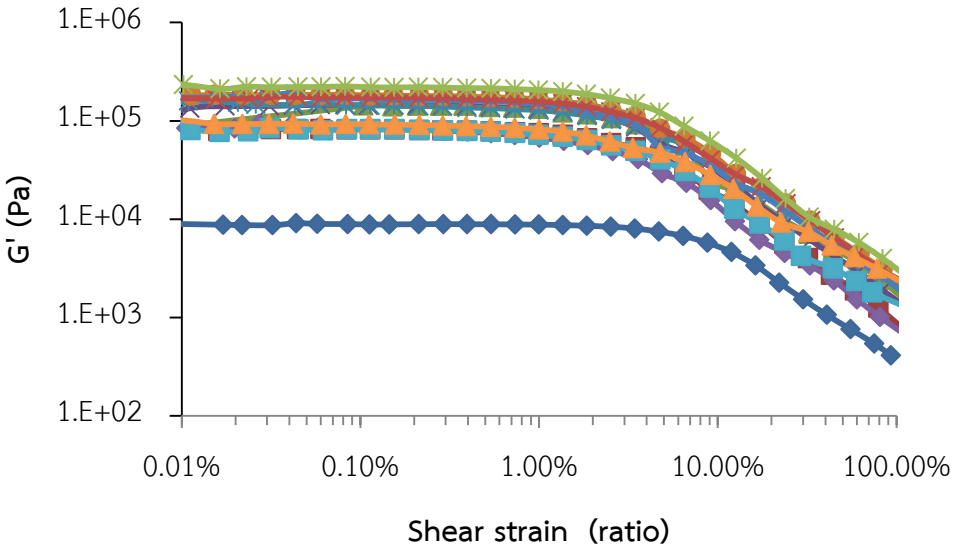

Figure III-1 Amplitude sweep (strain sweep) test results of CSD paste using dispersing liquid: water (◆), HCO-40 at 0.1% (■), 0.5% (▲), 1% (✕), 1.5% (✳), 2% (●), 2.5% (+), 3% (✕), 5% (✳), 7.5% (◆), 10% (■), 12.5% w/w (▲)

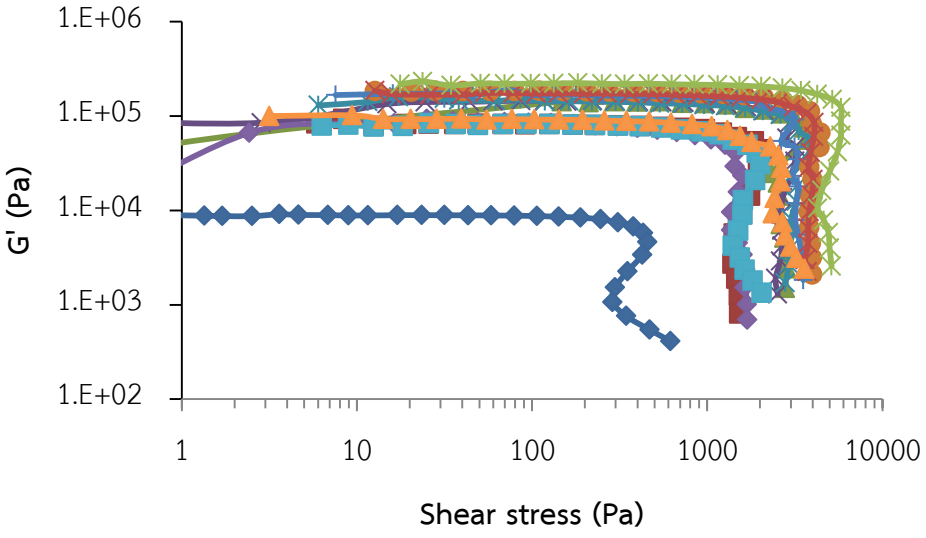

Figure III-2 Amplitude sweep (stress sweep) test results of CSD paste using dispersing liquid: water (◆), HCO-40 at 0.1% (■), 0.5% (▲), 1% (✕), 1.5% (✳), 2% (●), 2.5% (+), 3% (✕), 5% (✳), 7.5% (◆), 10% (■), 12.5% w/w (▲)

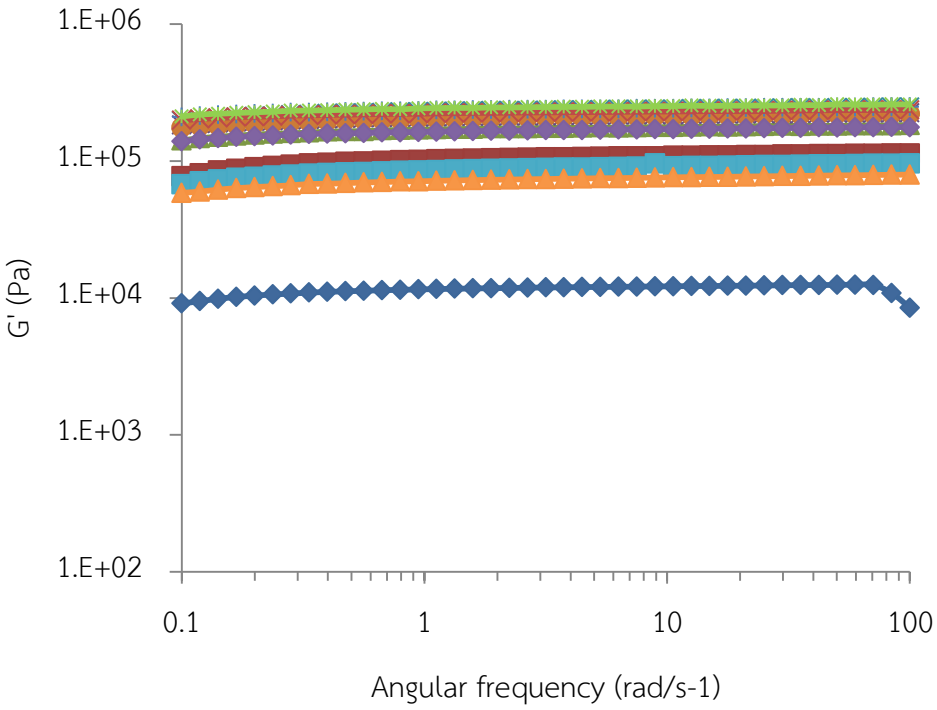

Figure III-3 G' from frequency sweep at 0.1-100 rad/s when the dispersing liquid: water (◆), HCO-40 at 0.1% (■), 0.5% (▲), 1% (✕), 1.5% (✳), 2% (●), 2.5% (+), 3% (✕), 5% (✳), 7.5% (◆), 10% (■), 12.5% w/w (▲)

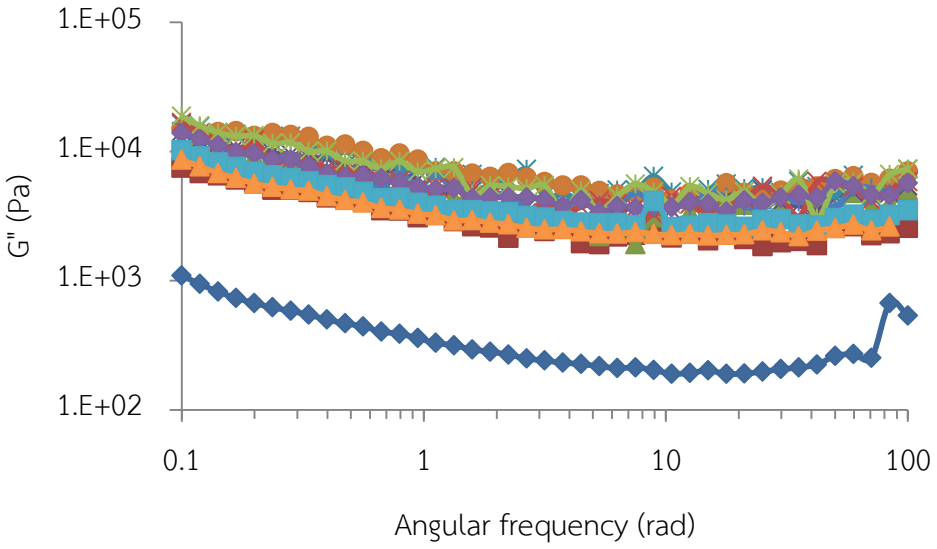

Figure III-4 G" from frequency sweep at 0.1-100 rad/s when the dispersing liquid: water (◆), HCO-40 at 0.1% (■), 0.5% (▲), 1% (✕), 1.5% (✳), 2% (●), 2.5% (+), 3% (✕), 5% (✳), 7.5% (◆), 10% (■), 12.5% w/w (▲)

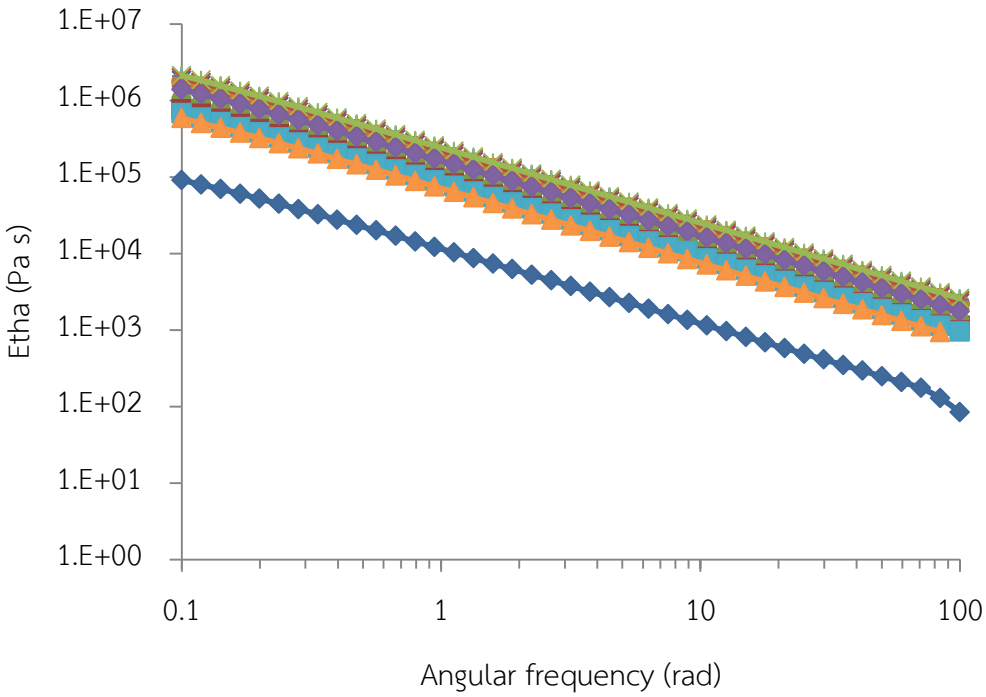

Figure III-5 Complex viscosity from frequency sweep at 0.1-100 rad/s when the dispersing liquid: water (◆), HCO-40 at 0.1% (■), 0.5% (▲), 1% (✕), 1.5% (✳), 2% (●), 2.5% (+), 3% (✕), 5% (✳), 7.5% (◆), 10% (■), 12.5% w/w (▲)

Appendix IV: Pellet morphology

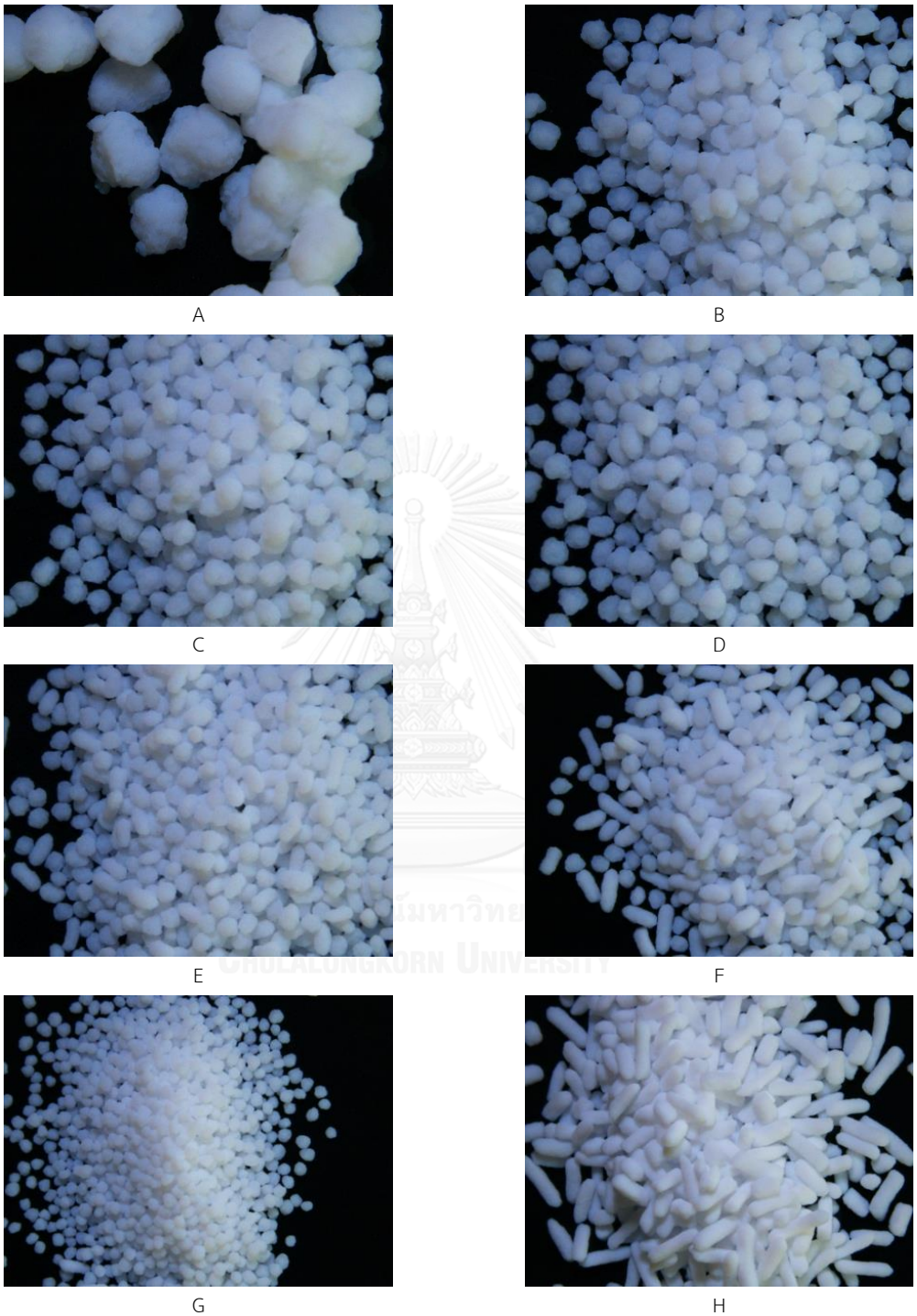

Figure IV-1 Pellets from 1st batch at magnification of 0.67x observed by stereo microscope; pellets made with varied HCO-40 concentrations: 1.5% w/w (A), 2% w/w (B), 2.5% w/w (C), 3% w/w (D), 5% w/w (E), 7.5% w/w (F), 10% w/w (G) and 12.5% w/w (H)

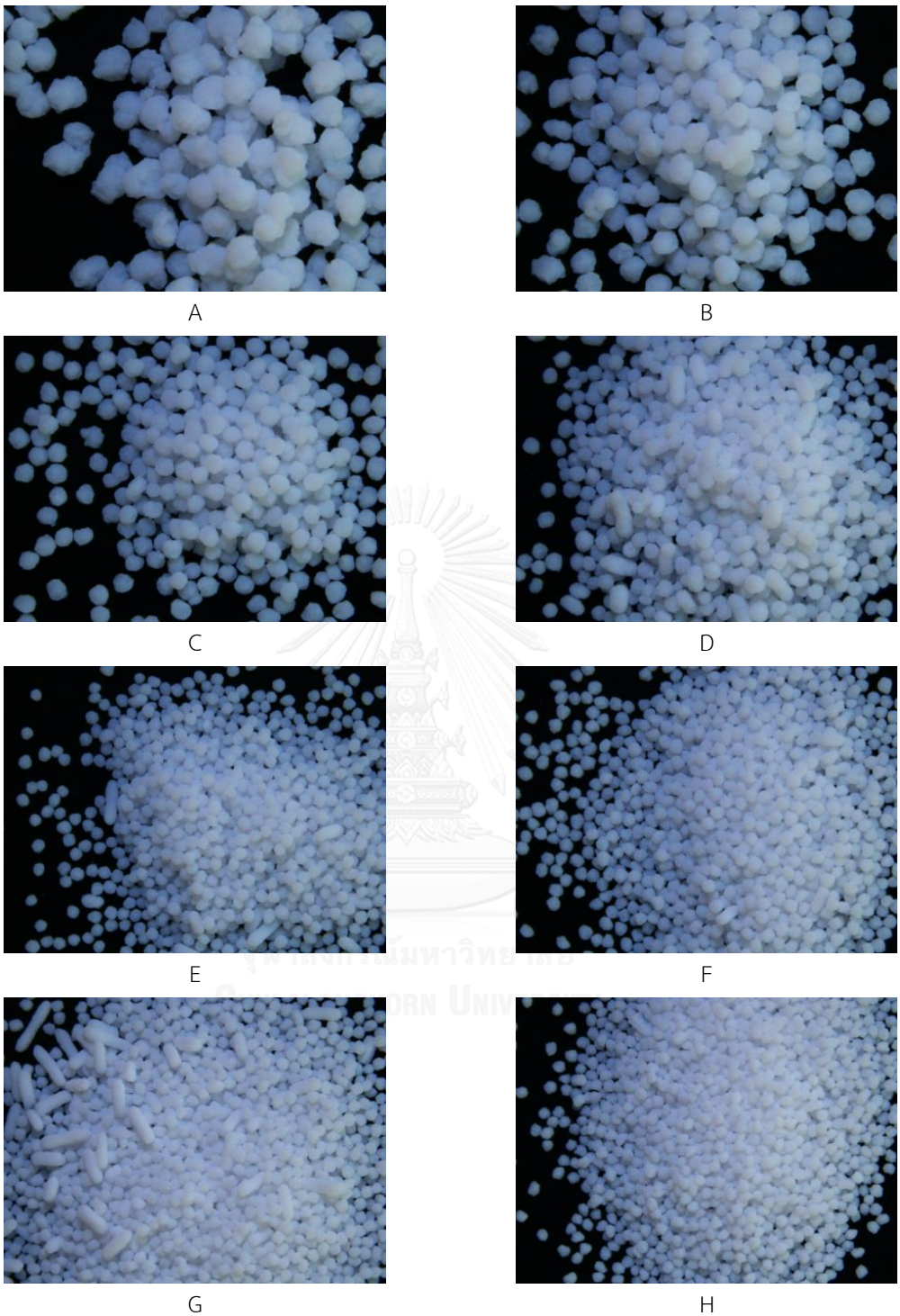

Figure IV-2 Pellets from 2nd batch at magnification of 0.67x observed by stereo microscope; pellets made with varied HCO-40 concentrations: 1.5% w/w (A), 2% w/w (B), 2.5% w/w (C), 3% w/w (D), 5% w/w (E), 7.5% w/w (F), 10% w/w (G) and 12.5% w/w (H)

Appendix V: Fourier-transform infrared spectra

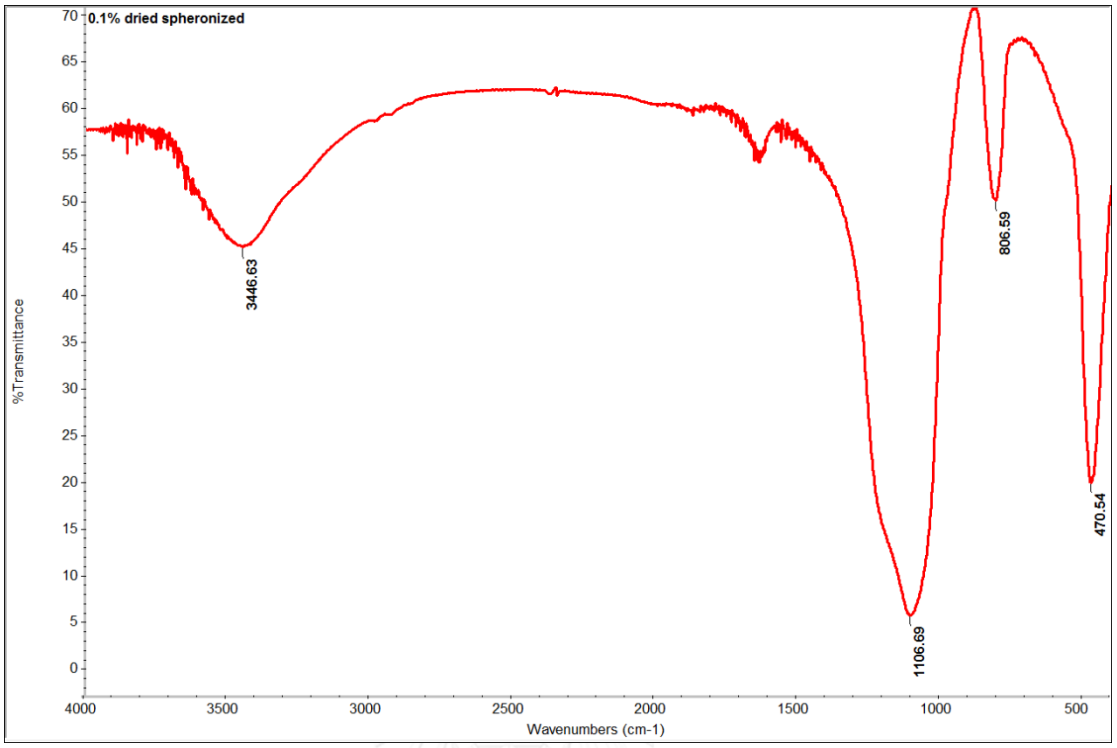

Figure V-1 FT-IR spectrum of dried spheronized CSD made with 0.1% w/w HCO-40 solution

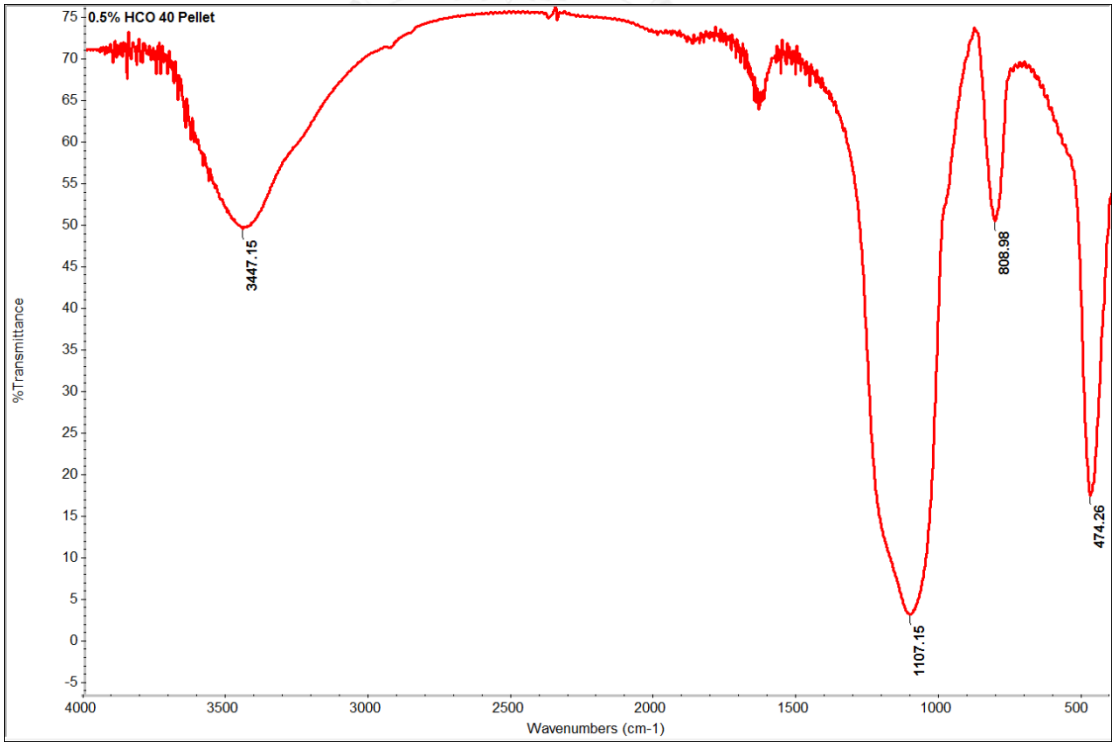

Figure V-2 FT-IR spectrum of pellets made with 0.5% w/w HCO-40 solution

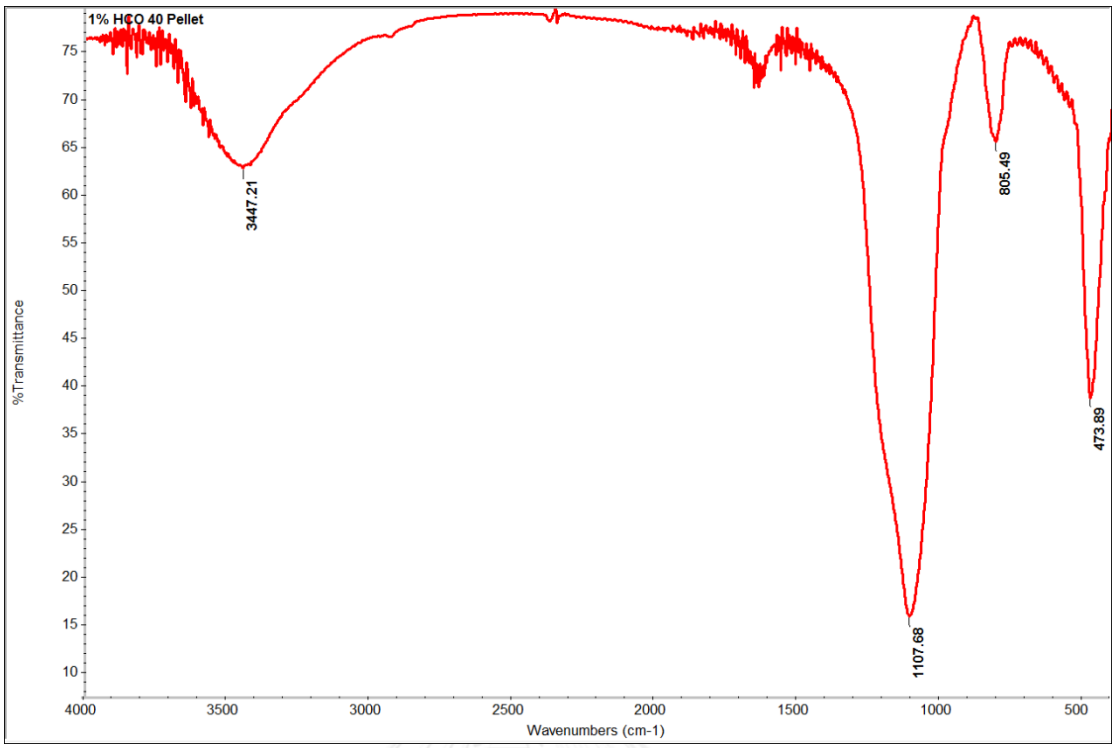

Figure V-3 FT-IR spectrum of pellets made with 1% w/w HCO-40 solution

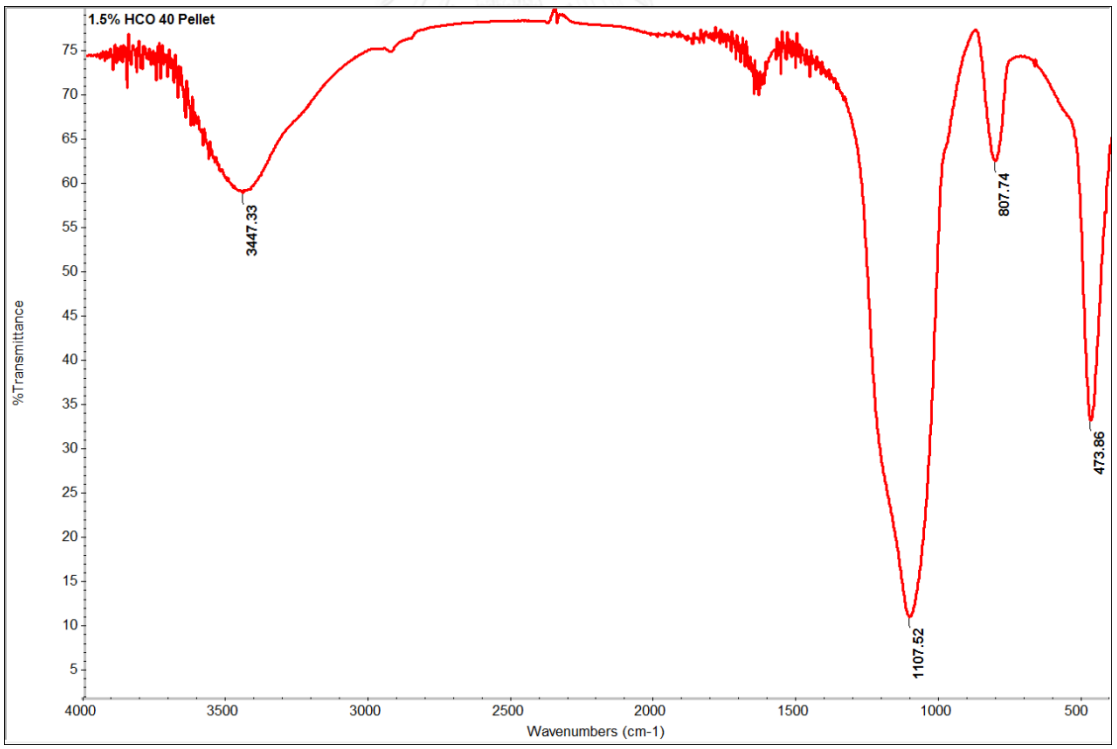

Figure V-4 FT-IR spectrum of pellets made with 1.5% w/w HCO-40 solution

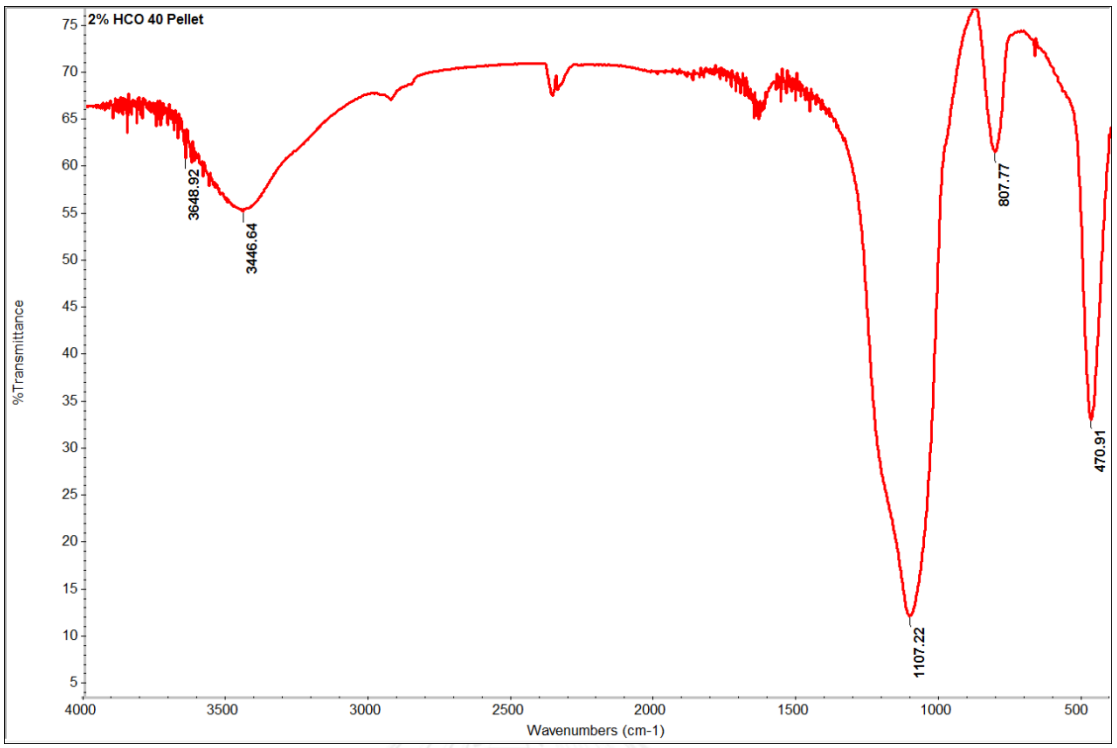

Figure V-5 FT-IR spectrum of pellets made with 2% w/w HCO-40 solution

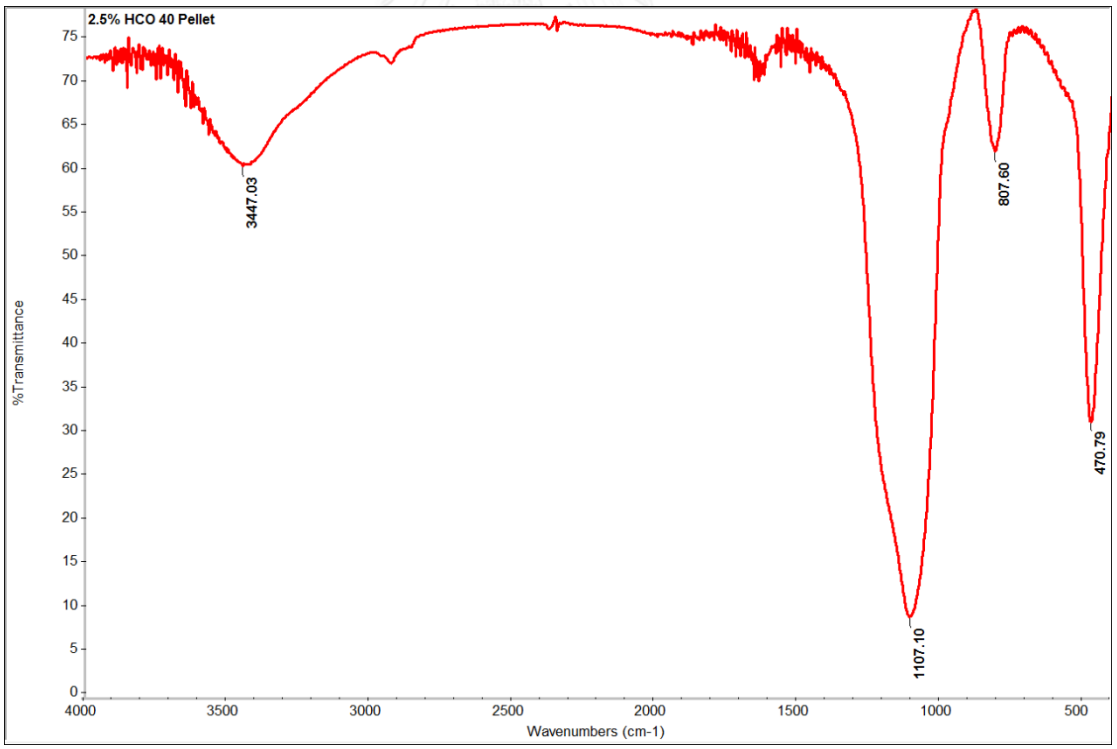

Figure V-6 FT-IR spectrum of pellets made with 2.5% w/w HCO-40 solution

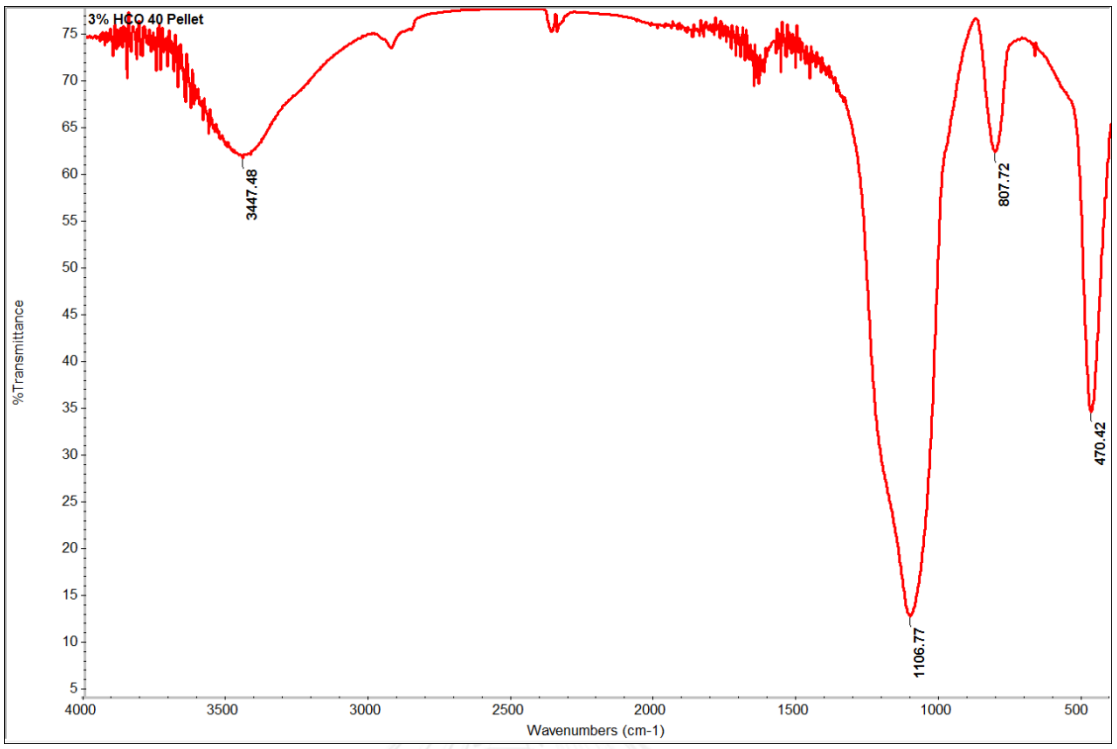

Figure V-7 FT-IR spectrum of pellets made with 3% w/w HCO-40 solution

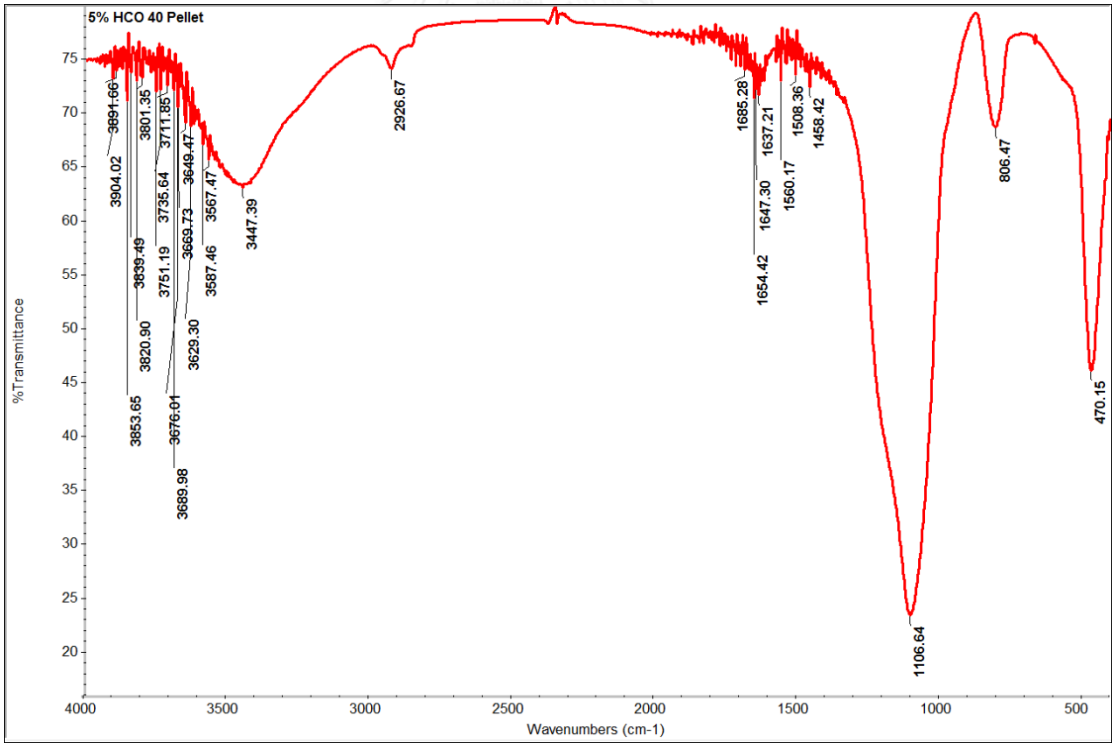

Figure V-8 FT-IR spectrum of pellets made with 5% w/w HCO-40 solution

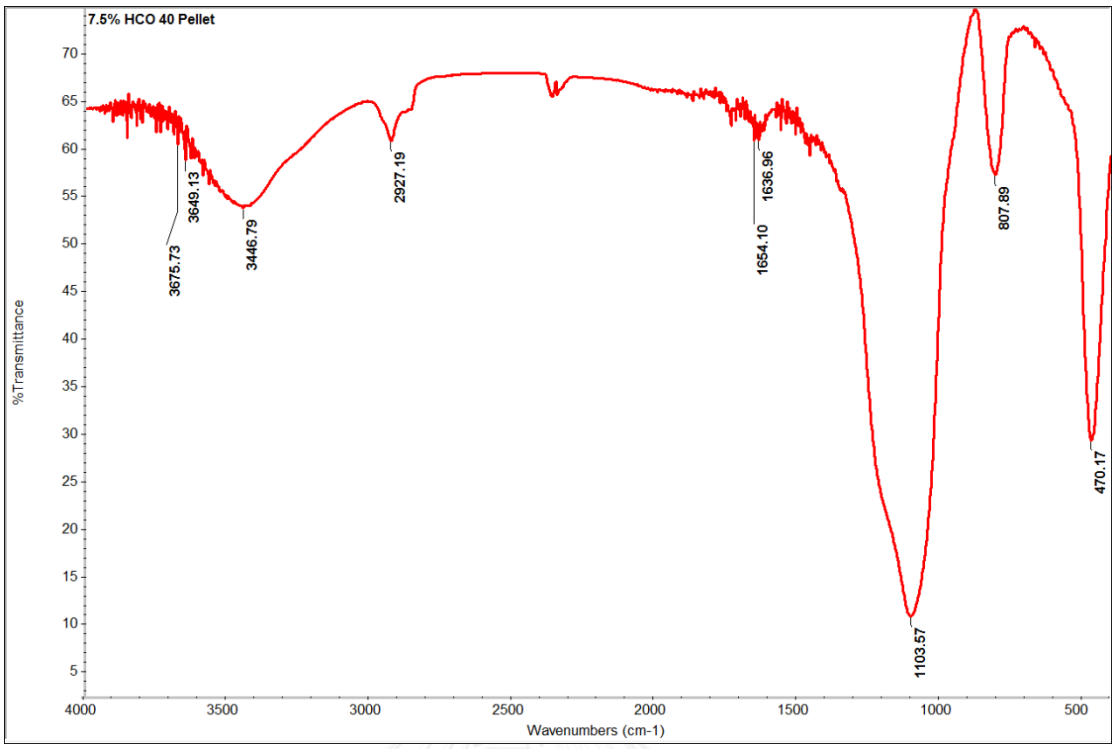

Figure V-9 FT-IR spectrum of pellets made with 7.5% w/w HCO-40 solution

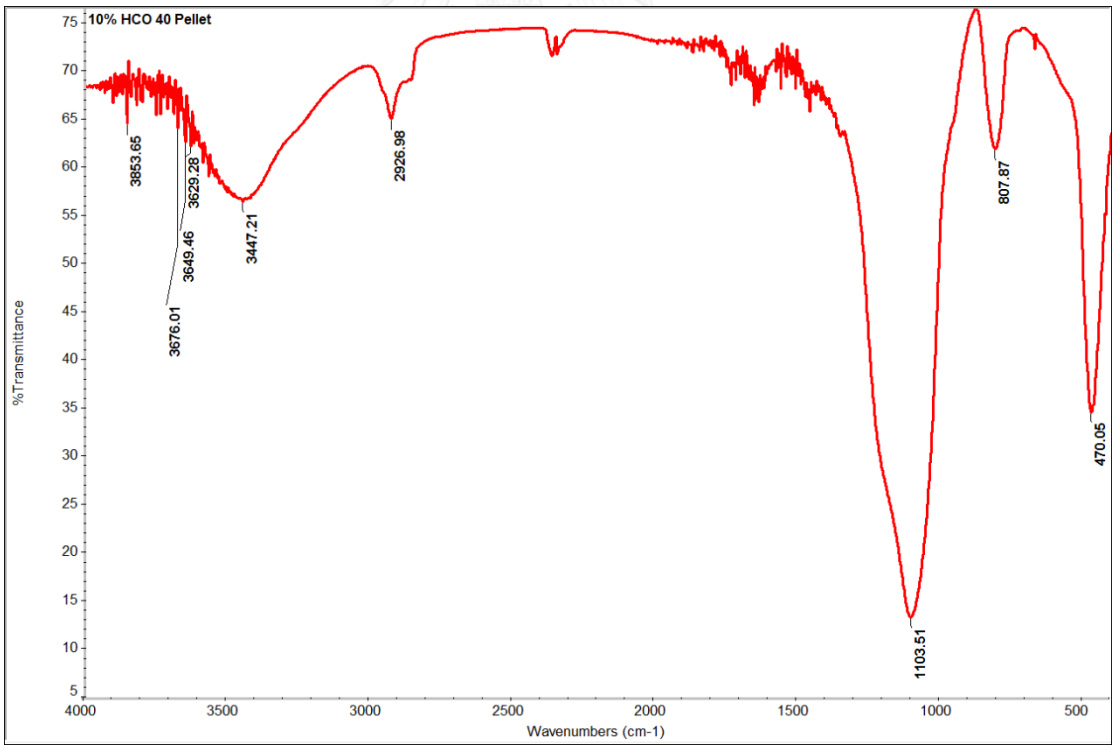

Figure V-10 FT-IR spectrum of pellets made with 10% w/w HCO-40 solution

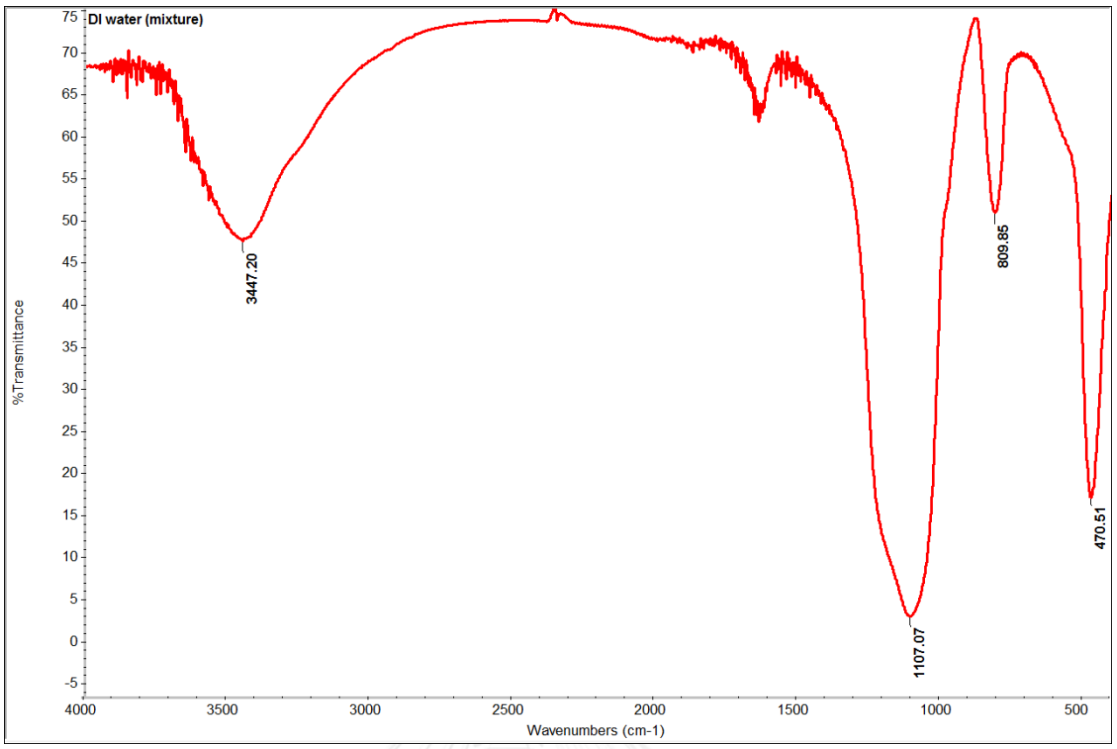

Figure V-11 FT-IR spectrum of CSD processed with water

Appendix VI: Solid-state Nuclear magnetic resonance spectra

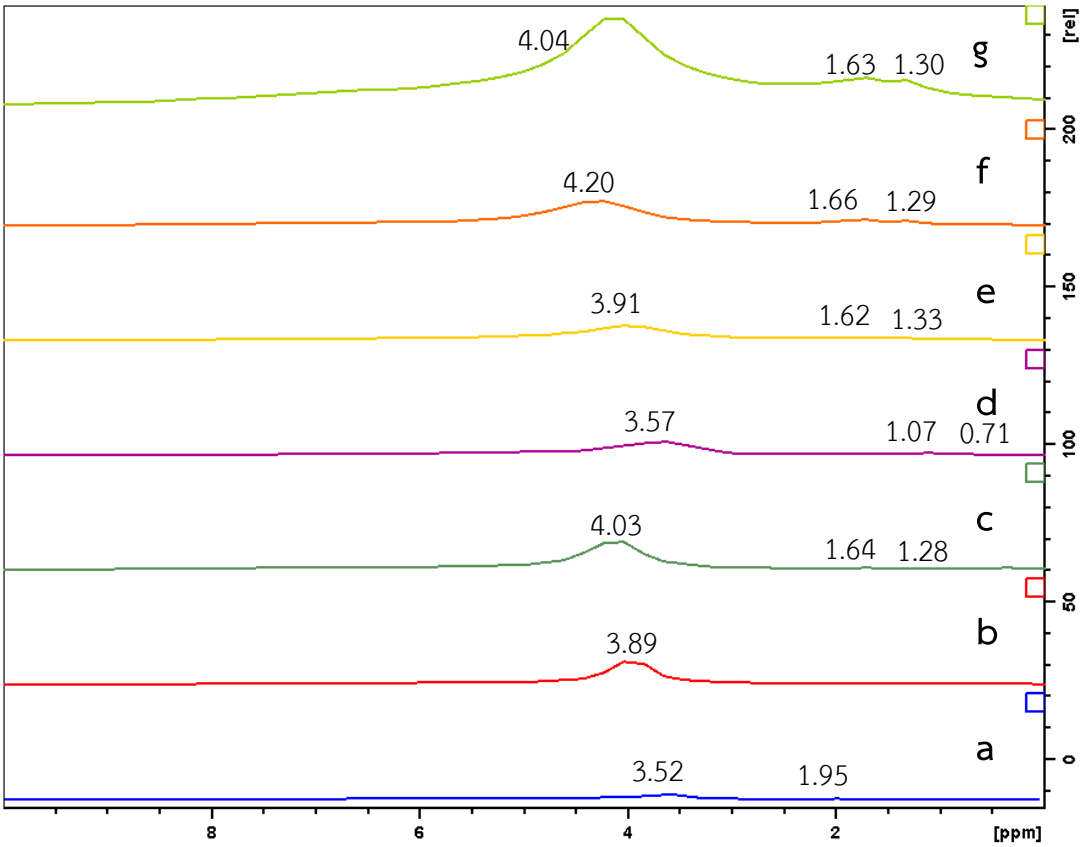

Figure VI-1 ^{1}H MAS NMR spectra of untreated CSD (a), CSD processed with water (b), dried spheronized CSD made with 0.1% w/w HCO-40 (c), CSD pellets made with HCO-40 solution at concentration 0.5% w/w (d), 1% w/w (e), 1.5% w/w (f), 2% w/w (g)

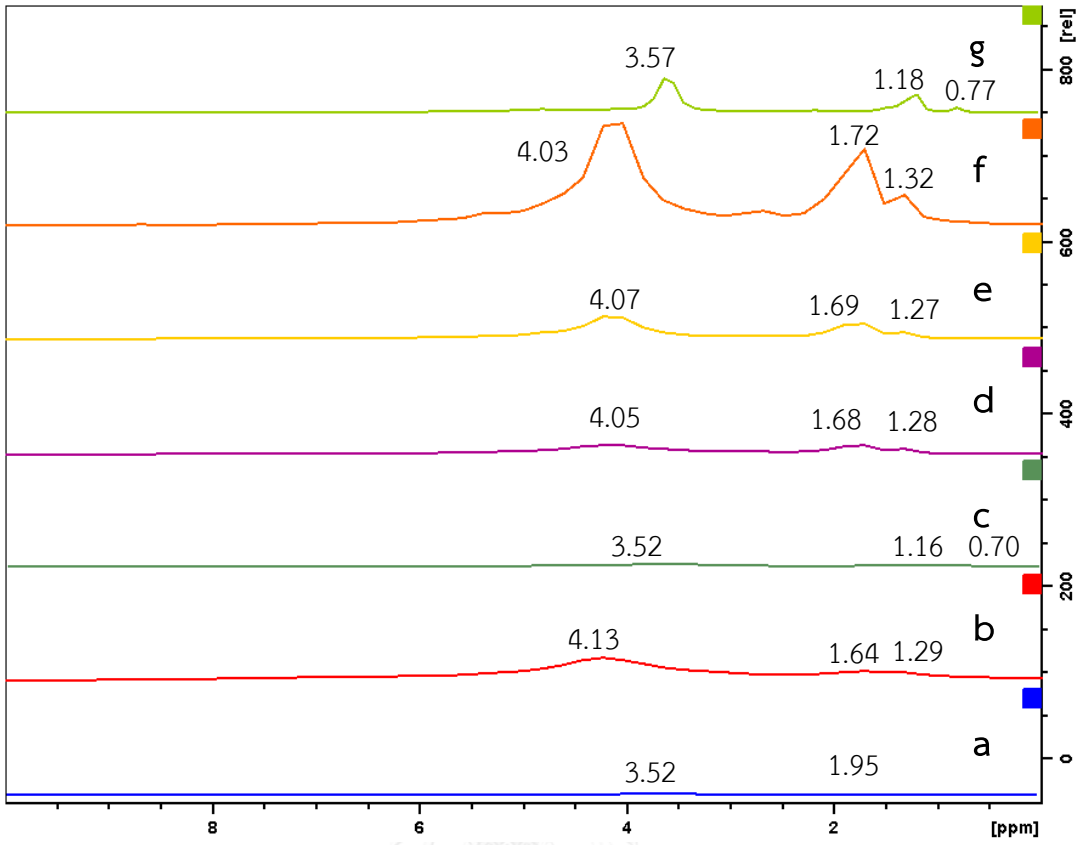

Figure VI-2 ^{1}H MAS NMR spectra of untreated CSD (a), CSD pellets made with HCO-40 solution at concentration 2.5% w/w (b), 3% w/w (c), 5% w/w (d), 7.5% w/w (e), 10% w/w (f), 12.5% w/w (g)

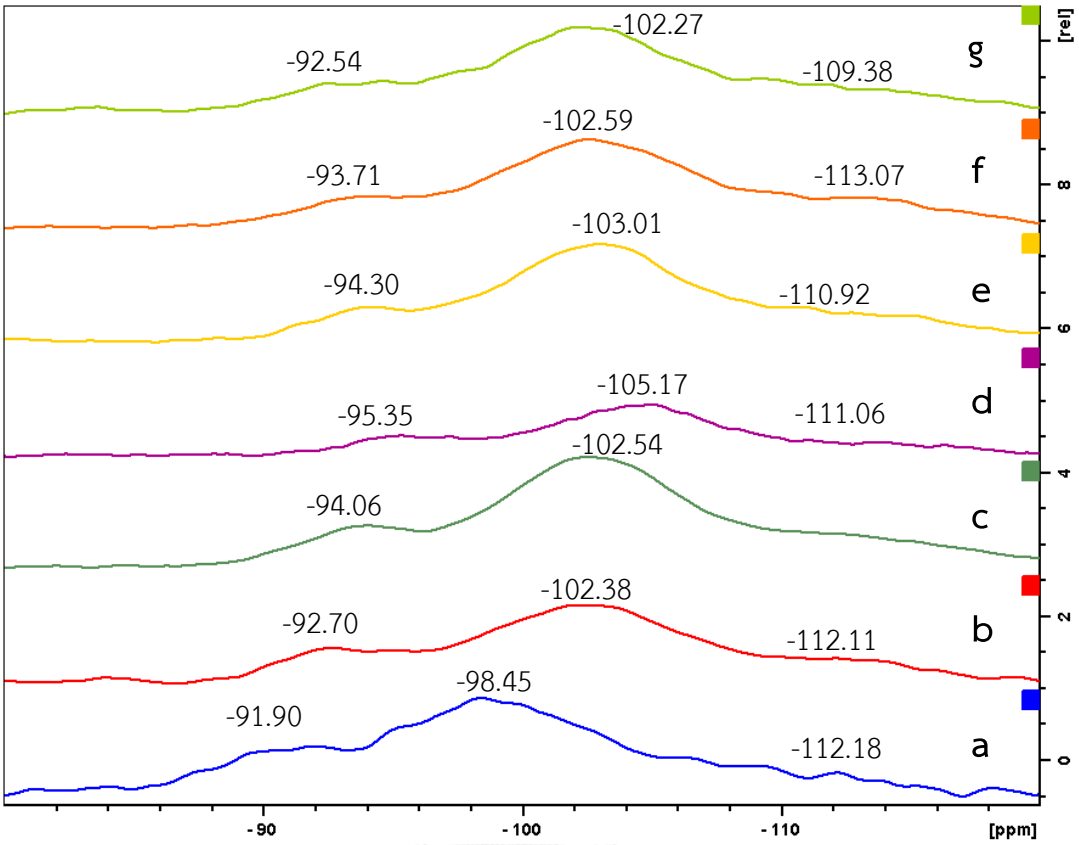

Figure VI-3 ^{29}Si CP MAS NMR spectra of untreated CSD (a), CSD processed with water (b), dried spheronized CSD made with 0.1% w/w HCO-40 (c), CSD pellets made with HCO-40 solution at concentration 0.5% w/w (d), 1% w/w (e), 1.5% w/w (f), 2% w/w (g)

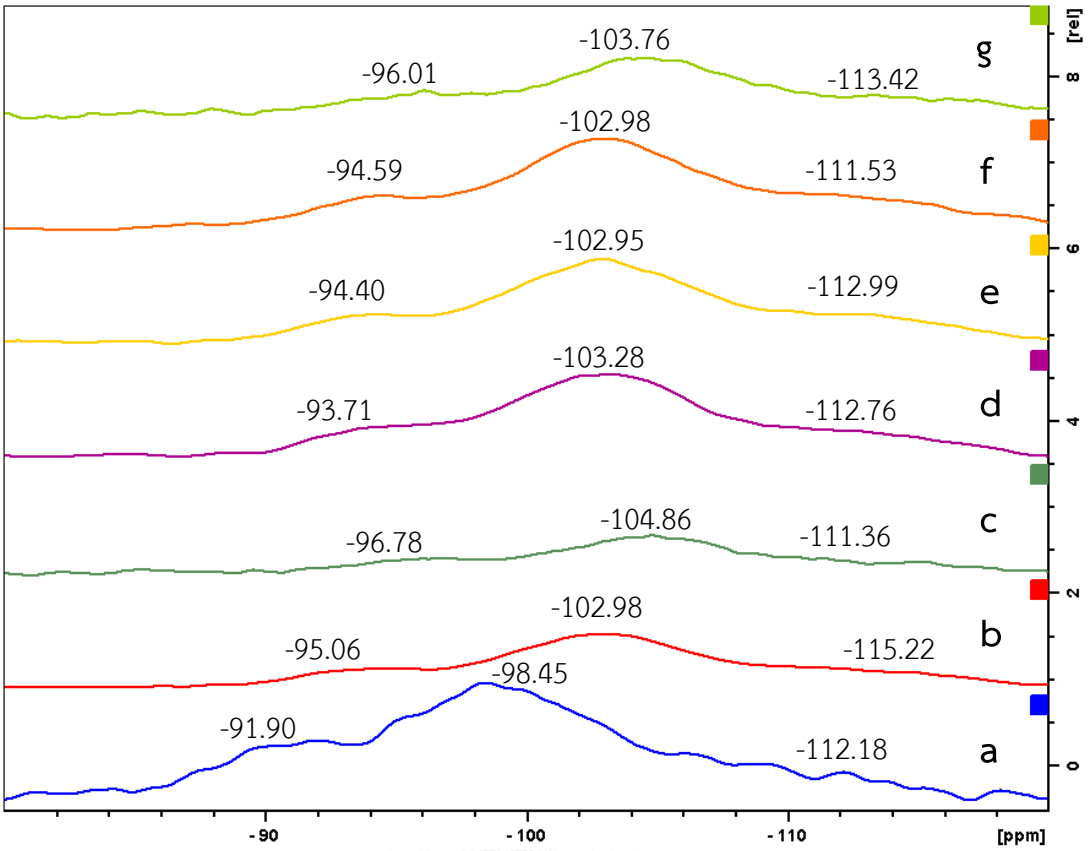

Figure VI-4 ^{29}Si CP MAS NMR spectra of untreated CSD (a), CSD pellets made with HCO-40 solution at concentration 2.5% w/w (b), 3% w/w (c), 5% w/w (d), 7.5% w/w (e), 10% w/w (f), 12.5% w/w (g)

VITA

Sanpeth Limpakomon was born on March 18, 1982 in Suphanburi, Thailand. He received his Bachelor of Science in Pharmacy from the Faculty of Pharmaceutical Sciences, Chulalongkorn University, Bangkok, Thailand, in 2004. He also obtained the Bachelor of Engineering (Mechanical Engineering) from Faculty of Engineering, Pathumwan Institute of Technology, Bangkok, Thailand, in 2012. He worked as a production pharmacist at the Government Pharmaceutical Organization for 5 years during 2004 - 2009 and spent another year at Interthai Pharmaceutical Manufacturing Limited during 2009 - 2010.